CALIFORNIA INSTITUTE OF TECHNOLOGY

SOIL MECHANICS LABORATORY

APPLICATION OF PLASTICITY THEORY TO SOIL BEHAVIOR: A NEW SAND MODEL

by

J.P. Bardet

SML 83-01

A Report on Research Conducted under a Grant
from the National Science Foundation
and support from the
Earthquake Research Affiliates Program
of the California Institute of Technology

Pasadena, California
September, 1983

This investigation was partially sponsored by Grant No. CME-7913822 from the National Science Foundation, Geotechnical Engineering Program, under the supervision of R.F. Scott. Any opinions, findings, and conclusions or recommendations expressed in this publication are those of the author and do not necessarily reflect the views of the National Science Foundation.

APPLICATION OF PLASTICITY THEORY TO SOIL BEHAVIOR: A NEW SAND MODEL

Thesis by

J. P. Bardet

In Partial Fulfillment of the Requirements
for the Degree of Doctor of Philosophy

California Institute of Technology
Pasadena, California

1983

(Submitted September 27, 1983)

A mes parents

(To my parents)

ABSTRACT

The representation of rheological soil behavior by constitutive equations is a new branch of soil mechanics which has been expanding for 30 years. Based on continuum mechanics, numerical methods (finite elements) and experimental techniques, this new discipline allows practicing engineers to solve complex geotechnical problems. Although all soils are constituted of discrete mineral particles, forces and displacements within them are represented by continuous stresses and strains. Most stress-strain relationships, which describe the soil behavior, are derived from plasticity theory. Originated for metals, the conventional plasticity is presented and illustrated simultaneously with a metal and a soil model. Each plasticity concept may be criticized when applied to soil. A recent theory, called "bounding surface plasticity," generalizes the conventional plasticity and describes more accurately the cyclic responses of metals and clays. This new theory is first presented and linked with the conventional plasticity, then applied to a new material, sand. Step by step a new sand model is constructed, mainly from data analysis with an interactive computer code. In its present development, only monotonic loadings are investigated. In order to verify the model ability to describe sand responses, isotropic, drained and undrained tests on the dense Sacramento River sand are simulated numerically and compared with real test results and predictions with another model. Finally the new constitutive equation, which was formulated in the p-q space for

axisymmetric loadings, is generalized in the six-dimensional stress state with the assumption of isotropy and a particular Lode's angle contribution. This new model is ready to be used in finite element codes to represent a sand behavior.

ACKNOWLEDGMENTS

I would like to express my sincere appreciation to my advisor, Professor R.F. Scott, for his patience, guidance and financial support during my studies and researches at the California Institute of Technology. I am particularly indebted to him for letting me teach a term of his graduate soil mechanics course.

My gratitude is also extended to Mrs. Sharon Beckenbach and Mrs. Gloria Jackson for their accomplished typing of the manuscript

TABLE OF CONTENTS

CHAPTER I

INTRODUCTION

Soil Mechanics is an old discipline in Arts and Sciences. From the earliest times, when people started to build, it was necessary to construct appropriate foundations. Designed with empirical, but nevertheless adequate techniques, some foundations still support their structures, after hundreds to thousands of years. The Egyptians knew how to make a wide horizontal plane almost perfect to start their pyramids, without the help of optical devices: they covered the foundation area with water and leveled off the emerging ground. The Romans constructed roads with pavement and a base composed of different types of aggregates. As in most sciences, the knowledge that Greeks and Romans accumulated was lost during the Middle Ages and recovered during the Renaissance. In Italy, successful wooden pile foundations were applied in the Lagoon of Venice; less successful were the foundations at Pisa, but still to our day adequate. In the eighteenth century, military engineers such as Coulomb (1736-1806) applied his friction theory to obtain the pressures acting on retaining walls. The major development of foundation techniques came later with the expansion of the railways owing much to famous contributors such as Rankine (1820-1872) and Winkler (1835-1888). Up to the beginning of the twentieth century, foundation engineering was not disassociated from structural engineering. Terzaghi (1883-1963) caused Soil Mechanics to gain its

independence and to be recognized as a particularly important discipline in Civil Engineering. Since that time, sub-disciplines have emerged in Soil Mechanics.

From about 1955, a new branch in soil mechanics has been steadily increasing: the constitutive modeling of soil behavior. By definition, it describes the soil behavior with constitutive equations using the framework of continuum mechanics. Relations between strain and stress are used eventually in finite element programs to solve engineering problems formulated as boundary-value problems. The soil is treated as an engineering material in the same way as steel, concrete or polymers.

The development of this new branch may be appreciated in Fig. 1.1a by the number of publications in two soils mechanics journals: a British Journal, "Geotechnique," and an American one, "the Geotechnical Engineering Division Journal of the American Society of Civil Engineers." These two journals of steady popularity for many years in soil mechanics capture the increasing interest in this new field. However, they greatly underestimate the total production of papers since the recent creation of specialized magazines such as the "International Journal for Numerical and Analytical Methods in Geomechanics," "Mechanics of Materials," "Numerical Journal for Geomechanics," etc.

The different peaks observed in Fig. 1.1a correspond to significant events of the new branch history. Prior to 1940, the soil behavior was represented by elasticity theory. The plasticity theory, initiated in

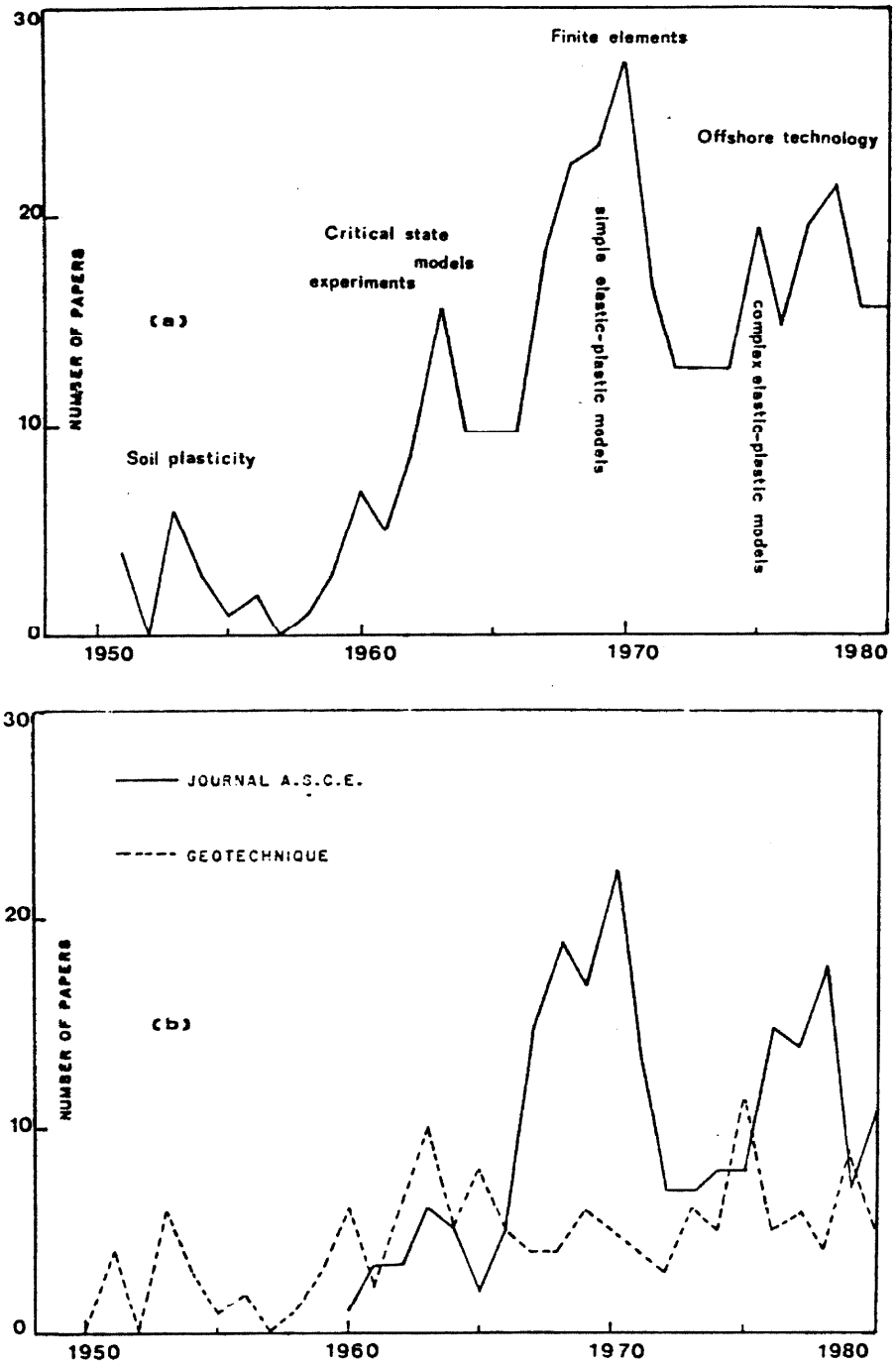

Fig. 1.1. Number of papers on soil properties and soil constitutive equations published in two journals of steady popularity in soil mechanics: a British journal, "Geotechnique," and an American one, "The Geotechnical Engineering Division Journal of the American Society of Civil Engineers,"

a) accumulated publications of both journals
b) separate publications of each journal.

1868 by Tresca and Saint Venant was only applied to metal. Later, about 1945, soil plasticity at its beginning was strictly derived from metal plasticity. But soil, compared to metal, has a different rheological behavior, which depends mainly on mean pressure and density. The first soil models derived from metal plasticity could not describe the difference and were not successful in soil mechanics. In 1955, Drucker, Gibson and Henkel [1.11] compensated for this deficiency and proposed the first original soil model which disassociated soil from metal plasticity. In 1956 an important series of experimental data on clays was produced by Parry [1.19] in Great Britain. A few years later, this abundant collection of tests, drained and undrained at different confining pressures, were interpreted by Roscoe, Schofield and Wroth [1.24]. These researchers introduced the concept of "critical state" into the plasticity theory to create a clay model, satisfactory over a wide range of tests and overconsolidation ratios.

In the 1950's, the soil models were only considered as a unifying approach to explain the soil response during various laboratory tests and for different initial density. In particular Roscoe, Schofield, and Wroth [1.24] correlated normally and overconsolidated clay behaviors during drained and undrained tests. However, the soil models could not be used to solve practical engineering problems. If these problems were formulated as boundary value problems, the nonlinear stress-strain relationships were leading to nonlinear partial differential equations, which could not be solved with the existing techniques, i.e., with

analytical or graphical methods. About 1965, the development of computer facilities and numerical methods was a turning point in soil modeling. Most practical and complex geotechnical problems, which had been approached until then with empirical methods, could be solved as boundary value problems with the help of accurate and rigorous numerical techniques. Finite element and finite difference methods offered the solution to nonlinear partial differential equations with complex boundary conditions and geometries. Simple soil models started to be used in finite element codes, mostly derived from nonlinear elasticity or metal-plasticity. They attempted to describe the nonlinear and nonreversible soil behavior as simply as possible with a minimum number of parameters. Simultaneously, with the theoretical development of soil models, the testing technique evolved. The standard triaxial test became more refined. Although originated in 1936 by Kjellman [1.14], the true triaxial tests were applied to cubical soil samples in order to investigate the influence of the intermediate principal stress (e.g., Ko and Scott [1.15]). In 1975, soil modeling was reanimated, mainly due to the growth of offshore oil production technology. The main challenge in this area is to describe inelastic cyclic soil behavior occurring around foundations or piles during periodic wave or earthquake loading. The soil models are founded not only on plasticity theory, but also on different constitutive theories such as rate-type equations. Their formulation becomes very theoretical and involves more and more material constants. The testing techniques also become more sophisticated. For illustration, in order to define the strain field within a sand sample,

X-ray pictures are taken to measure the displacement of lead shots located within the sample. The testing effort is now oriented towards the effect of rotation of principal stresses either with the hollow cylinder apparatus (e.g. Symes et al. [1.27]) or with triaxial apparatus (e.g. Arthur et al. [1.3]).

Recently, as a response to this increase in the number of models and to demands from industry, international conferences have taken place all over the world: Montreal (1980), Delft (1981), Zurich (1982), Grenoble (1982), and Tucson (1983) are examples. In these forums of material modeling, so many different and contradictory opinions have been formulated concerning the reliability and capability of existing models that an attempt at a unifying approach becomes necessary.

As a supplement to Fig. 1.1a, Fig. 1.1b illustrates the difference of activity between Europe and the United States. The British publications are steadily increasing while the American ones follow the rule of the free market: demand and supply.

Although the soil models are too numerous to be described in detail, the basic theories, on which they are founded, are more limited in quantity. To our knowledge, eight main divisions may be distinguished in the representation of the rate-independent behavior of soil.

- Elasticity
- Plasticity (single yield surface)
- Plasticity (multiple yield surfaces)
- Plasticity (bounding surface)
- Endochronic
- Rate-type
- Nonlinear incremental
- Empirical model

Theories such as the above have been applied to all kinds of materials. In this respect, soil has become an engineering material such as steel or concrete.

For each class of theory, a few examples are given in Table 1.1. No attempt at an exhaustive presentation has been made; only models believed to be mostly significant are present. From this table different information may be extracted:

- Age of the model
- Type of soil it is best qualified to describe, e.g., normally consolidated clays, sand, etc.
- Number of material constants which need to be specified by experiment to fully characterize the soil behavior. In the same way that isotropic linear elasticity needs two constants, E Young's modulus and ν Poisson's ratio, all models require similar constants different for every material. The number of constants is a sign of complexity, not only regarding the

TABLE 1.1 PRINCIPAL MODELS IN SOIL MECHANICS

General Framework	Authors	Date of Publication	Material Type	Number of Parameters	Comments	Refs.
Plasticity Single Yield Surface	Schofield Wroth	1968	Normally and overconsolidated clay. Isotropic	3	One of the first models for clay. Large elastic domain for overconsolidated clay.	26
	Roscoe Burland	1968	Normally and overconsolidated clay. Isotropic	4	Similar to Schofield-Wroth model but different shape for yield surface.	23
	DiMaggio Sandler Baladi	1971 1977	Sands		Applied for high confining pressure (nuclear blast).	10 25
	Lade	1975 1977	Sands	9 or 14	2 models for medium range pressure. First model with three-dimensional failure surface.	16 17
	Pender	1978	Normally and overconsolidated clay. K_0 consolidated	4	Attempt to describe the overconsolidated clay behavior.	20
Plasticity Multiple Yield Surfaces	Mroz	1983	Clay - K_0 overconsolidated	7	2 models, infinite number of yield surfaces (INS), or only 2 surfaces.	18
	Prevost	1978	Clays Sand	Depending on number on YS.	2 models with nested yield surfaces, cylinders or ellipsoids.	21 22
Bounding Surface (B.S.) Plasticity	Dafalias Herrmann	1980	Normally and overconsolidated clay.	8	Adaptation of Roscoe Burland into B.S. framework.	7
	Aboim	1982	Sands	8	A simple B.S. model for sand.	1
	Bardet	1983	Sands	13	Adaptation of B.S. theory to sand.	
Endochronic Theory	Valanis Read	1982	Sands	?	Application to sand of new intrinsic time measure (critical state).	28
	Bazant	1976	Clays Sands	?	Several models with adapted endochronic theory.	2,4 5,6
	Wu-Wang	1980	Sands	11	Another application of new intrinsic time measure.	29 30
Rate Type	Davis Mullenger	1978	Clays	12	Application of hypoelasticity to clay	9
	Gudehus Kolymbas	1979	Sands		A rate-type model from Germany.	12
Non-linear Incremental	Darve	1982	Sands & clays	14	Different from all other theories. This model is based on combination of triaxial paths to simulate the material memory. All the theoretical framework has been initiated for soil, but it is applied at present to concrete.	8

theoretical notions, but also in the experimental processes required to establish the constants for a particular theory or model.

CHAPTER II

THE MATERIAL SOIL AS A CONTINUUM

2.1 APPLICATION OF CONTINUUM MECHANICS TO ASSEMBLY OF DISCRETE PARTICLES

All soils (sands, silts or clays) consist of an assemblage of many individual particles with air and/or liquid filling the void between particles. A sand is composed of approximately rotund particles with sharp or rounded corners and size varying from 0.06 to 2 millimeters as usually defined. Silts have particle sizes ranging from 0.06 to 0.002 millimeters. A variety of minerals such as quartz and feldspars may be found in both materials. The interaction relation between grains is frictional. Clays consist of small plates with size from 0.002 to 10^{-6} millimeters held together by short-range interaction forces. Clay minerals, kaolinite, illite, montmorillonite, etc., are different from those in sands and silts. A better description of soils constitution may be found in most soil mechanics textbooks, e.g., Lambe and Whitman [2.10]. According to their size, the grains of sands and silts may be observed with the naked eye or a magnifying lens; clay particles can only be examined with a powerful microscope or electron-microscope. Since their physical constitution is more easily observable, our attention is drawn particularly to the coarser granular media.

When external loadings, composed of prescribed displacement and/or forces, are applied to a granular mass as shown in Fig. 2.1a, redistribution of forces and displacement occurs inside the material volume. Looking closely in the neighborhood of a given particle, neighbor particles form contacts as shown in Fig. 2.1b. Each contact action, which is distributed over a small area of a grain, may be represented by a resultant force and a torque, located at the contact position. In most microscopic studies, this torque is neglected according to the small size of contact area. The positions of contact forces change during application of loading; eventually the contacts may be deleted, or relocated. Each grain, which is generally represented by a rigid body, has a displacement which is characterized by the translation and the rotation of the centroid. The global mass deformation results from relative particle motions, slippage of contacts and reorganization of local structure, i.e., from microscopic changes in forces and displacements.

Although it corresponds to reality, this description of the physics of a granular material cannot be applied to solve engineering problems practically for various reasons: It is impossible to define exactly the geometry of each grain, corner, edge, etc., for the volume of material considered in a geotechnical problem. But even for well-defined grain geometry such as a regular assembly of uniform spheres, the number of unknowns constitutes a barrier to any analysis. For illustration purposes, a cubic meter contains approximately 2.10^9 to 3.10^9 spheres of

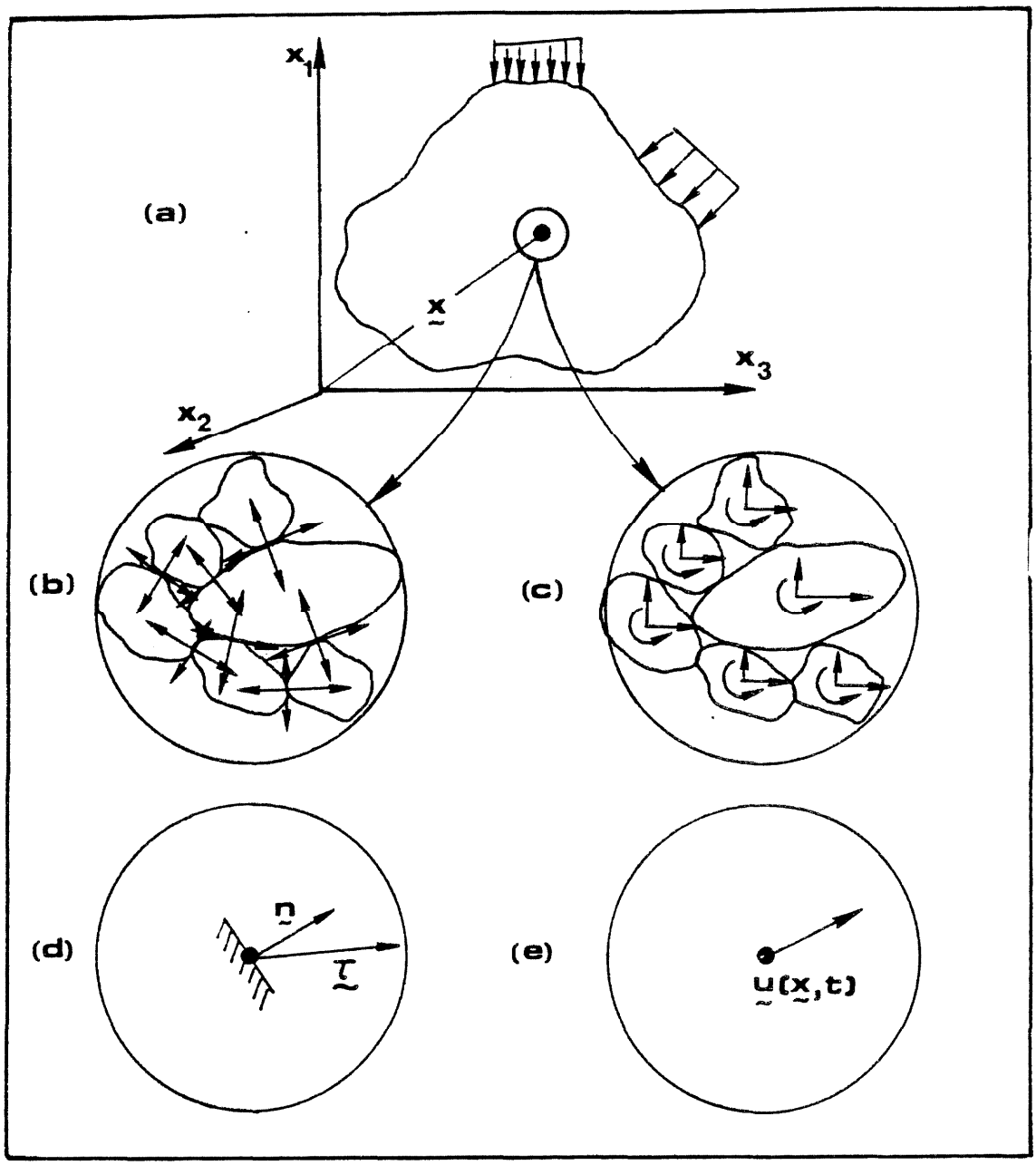

Fig. 2.1. Transition from an assembly of discrete particles to a continuous medium.

(a) Volume of granular material subjected along its boundary to prescribed forces and/or displacements.
(b) Normal and tangential forces acting on grain contacts at a microscopic level.
(c) Translation and rotation of each grain at a microscopic level.
(d) Approximation of the discrete system of contact forces in (b) by a continuous distribution of traction vector.
(e) Representation of displacement of each grain in (c) by a continuous displacement field.

1 mm in radius, depending on whether they are organized in uniform simple cubic or closed hexagonal packing (after Deresiewicz [2.8]). Since each sphere and each contact (force-position) possesses 6 degrees of freedom, the total number of unknown quantities may reach 4.10^{10} which is still a prohibitive number for all present analyses, theoretical, experimental or numerical.

An alternative way to solve the problem of Fig. 2.1a is to assume that the discrete distribution of forces and displacement in the granular mass may be represented by continuous quantities. The displacement of particles in the neighborhood of a particle, at initial position xtilde in a reference frame, is smoothed by a continuous displacement field denoted utilde(xtilde,t) depending on initial position xtilde and time t (Fig. 2.1e). In a similar way, the contact forces are averaged by a continuous distribution of stress vectors, sometimes called traction vectors (Fig. 2.1d). Each vector depends only on the position at time t of a particle initially at position $\underline{x}$, and on the unit vector $\underline{n}$ to some unit area surface on which it is acting. The stress vector is denoted tautilde. It is assumed to depend only on the direction of the contact surface where it acts, not on its curvature.

These assumptions of continuity for the displacements and acting forces within a granular mass raise a few interesting questions which seem to be regaining favor recently in material modeling. These hypotheses may be examined with three different approaches; experimental techniques is one of them. In such an approach, discrete quantities

such as the displacement of individual particles and forces at the contacts can be measured on some simpler physical material model. Examples are assemblies of optically sensitive disks. Forces at contacts are obtained from photoelasticity effects; displacements are found by comparison of photographs made at various stages of the experiment. This method was used by Dantu [2.6], De Josselin de Jong and Verruijt [2.7], and Van der Kogel [2.18]. In a recent experiment, Luong [2.11] used infrared thermography to detect localization of energy dissipation by friction in real sand samples.

Complementing the experimental approach on simplified material Cundall and Strack [2.3] and Scott and Craig [2.16] propose to use computers to simulate two-dimensional material behavior. Numerical and real experiments on idealized material consisting of two-dimensional assembly of disks were compared by Cundall et al. [2.5].

The third approach involved general theoretical work, starting from microscopic behavior to obtain macroscopic response. Such attempts have given some useful results in terms of physics of material behavior such as the stress-dilatancy theory, which was originally formulated in 1962 by Rowe [2.15] and mathematically founded in 1965 by Horne [2.9] for spheres. The stress-dilatancy theory was able to explain qualitatively and quantitatively how sands dilate when subjected to shearing stresses.

In 1982, recent works, such as Nemat-Nasser [2.13,2.2] and Oda and Konishi [2.14], prove that the microscopic is regaining favor in

material modeling, and is especially justified in view of the increasing complexity of constitutive equations for soils.

All the above approaches, experimental, numerical or theoretical, give results on discrete quantities. Since they are founded on real physics of materials, their outcome, may be interpreted significantly in terms of continuous quantities. All transitions from discrete to continuous involve averaging processes, generally performed on some finite material volume. For illustration, Cundall et al. [2.5] defines the deformation gradient (which characterizes ultimately the strains), in an assembly of discrete disks, in the following way: First, the equivalent continuous displacement field, at any point xtilde of the continuum, is defined either by the real displacement of a disk particle or by the imaginary continuous displacement which extrapolates the motion of particles surrounding the insterstitial space; this choice depends on whether or not the point xtilde lies on a disk.

The average displacement gradient tensor with Cartesian component $\bar{u}_{i,j}$ may be defined as

$$\bar{u}_{i,j} = \frac{1}{V} \int_V \frac{\partial u_i}{\partial x_j} \, dV \qquad (i,j=1,2,3) \tag{2.1}$$

where u_i is the i^{th} component of the equivalent continuous displacement field, $\frac{\partial u_i}{\partial x_j}$ is the gradient of continuous displacement field, and V is a

material volume selected large enough to yield significant continuous results.

It is not certain that all discrete quantities may be averaged without losing some significant physics of the material behavior. For instance, the averaging process for the deformation gradient may hide discontinuities in the displacement field, such as localized shear band. Such discontinuities, not always easy to characterize within a discrete system, make meaningless the transition from discrete to continuous. It will be interesting to establish criteria for such transitions; they could yield instructive data on how discontinuities emerge and stress-localization appears. In a continuum mechanics context, these results would be useful with bifurcation methods applied to boundary value problems.

However, disregarding the microscopic aspect of material behavior, the general attitude in soil modeling is more pragmatic. Generally urged by immediate concerns, practicing engineers do not question the validity of the continuity assumption to represent soil behavior. This short-term attitude is quite justified by the combined power of continuum mechanics and of numerical techniques coupled with computers. The material behavior described in terms of mathematical constitutive equations is compatible with numerical methods such as finite elements. Most engineering problems with complex geometries and sophisticated materials become solvable as boundary value problems.

Once the continuity assumption has been selected to describe a soil, all continuum mechanics results may be applied. The first step is to define the kinematics of the material, i.e., the motion within it in terms of displacement, velocity and acceleration and the kinetics acting, i.e., the forces developed compatible with the motion.

2.2 DESCRIPTION OF KINEMATICS

Only the necessary concepts for this presentation are defined. A more general description of the kinematics in a continuum may be found in various textbooks on continuum mechanics (e.g., Malvern [2.12], Truesdell and Toupin [2.17]).

In a conventional way, for simplicity, only small displacements are considered. The deformations are characterized by the infinitesimal symmetric strain tensor epsilont with Cartesian components ε_{ij} such that

$$\varepsilon_{ij} = \frac{1}{2}\left[\frac{\partial u_i}{\partial x_j} + \frac{\partial u_j}{\partial x_i}\right] \qquad (i,j=1,2,3) \qquad (2.2)$$

where u_i(xtilde,t) are the Cartesian components of the displacement field at time t of a material point initially at position xtilde and $\frac{\partial u_i}{\partial x_j}$ are partial derivatives of the i^{th} displacement field coordinate with respect to the j^{th} position coordinate.

From this total strain, which describes a state of deformation within a material, an incremental quantity may be defined as Biot [2.1],

to represent changes about this state. Between time t and infinitely close time t+dt increments of strains are defined by substituting the incremental displacement field between time t and time t+dt in relation (2.2). Another approach, commonly used in solid mechanics, is to employ rate instead of increment. Within our presentation both descriptions are equivalent, since any increment (displacement or other) is a rate multiplied by an increment of time dt. Increments are used here since we are only concerned with rate-independent material.

The principal values of the strain tensor are denoted $\varepsilon_1, \varepsilon_2, \varepsilon_3$.

For the special axisymmetric conditions, defined by:

$$\varepsilon_{22} = \varepsilon_{33} = \varepsilon_2 = \varepsilon_3 \quad ; \tag{2.3a}$$

$$\varepsilon_{ij} = 0 \quad \text{when} \quad i \neq j \qquad (i,j=1,2,3) \tag{2.3b}$$

two new coordinates are introduced ε_v and ε_q; they are related to principal components in the following way:

$$\varepsilon_v = \varepsilon_1 + 2\varepsilon_3 \tag{2.4a}$$

$$\varepsilon_q = \frac{2}{3}(\varepsilon_1 - \varepsilon_3) \tag{2.4b}$$

These last definitions have been commonly used in soil mechanics for axisymmetric states since the early soil models were developed in 1960. As a common convention in soil mechanics, all compressive strains are

taken positive, and tensile strains negative, i.e., they have the opposite sign to the usual solid mechanics convention.

2.3 DESCRIPTION OF KINETICS

The forces inside a material are represented by the Cauchy stress tensor sigmat with Cartesian coordinates σ_{ij} at position xtilde and time t. The increment of stress between time t and t+dt is described by the incremental stress tensor dsigmat with components $d\sigma_{ij}$.

The principal values of the stress tensor are denoted $\sigma_1, \sigma_2, \sigma_3$. For axisymmetric loading, i.e.,

$$\sigma_{22} = \sigma_{33} = \sigma_2 = \sigma_3 \tag{2.5a}$$

$$\sigma_{ij} = 0, \quad \text{when} \quad i \neq j \qquad (i,j=1,2,3) \tag{2.5b}$$

only two stress components are necessary: p and q defined as:

$$p = \frac{1}{3}(\sigma_1 + 2\sigma_3) \tag{2.6a}$$

$$q = \sigma_1 - \sigma_3 \tag{2.6b}$$

As for strains, all compressive stresses are positive, tensile stresses negative. Now, the coefficient $\frac{2}{3}$ entering the definition of ε_q in relation (2.4b) may be justified; it was selected in order to conserve a simple form for the incremental work dW defined as

$$dW = \sigma_{ij} d\varepsilon_{ij} \qquad \text{(sum on i,j=1,2,3)} \tag{2.7a}$$

By calculation, using the axisymmetric condition specified in relations (2.5) and (2.3)

$$dW = p d\varepsilon_v + q d\varepsilon_q \tag{2.7b}$$

It should be kept in mind that this representation of stresses and strains with p, q, ε_v, ε_q is restricted to axisymmetric loading; its convenience in studying soil behavior in the standard triaxial apparatus justifies its use.

CHAPTER III

CLASSICAL PLASTICITY THEORY

The plasticity theory started in 1868 when Tresca presented two notes dealing with the flow of metals under great pressures to the French Academy. Saint-Venant (1797-1886), who had to prepare a report on that work as member of the Academy, became interested in this subject. He was the first to set up the fundamental equations of plasticity and to use them in practical problems. Around 1950, famous contributors like Hill [3.4] completed the mathematical structure of plasticity.

Originally concerned with yielding of metal, this theory was only applied to soil around 1960. Its fundamental basis lies in observations made from the simplest testing on material: the uniaxial test. All the physical observations, obtained for the simple unidimensional state, have been generalized to the combined state of stress (six-dimensional) in a tensorial form with the help of geometrical considerations.

3.1 FUNDAMENTAL PLASTICITY CONCEPTS FROM UNIAXIAL TESTS

A typical stress-strain curve obtained in a uniaxial test of most material (metal, soil, etc.) is shown in Fig. 3.1a. Only the axial component of stress and strain is recorded; both are assumed to be uniformly distributed in the sample. In the particular example of Fig. 3.1a, three cycles of loading-reloading are performed. In order to be

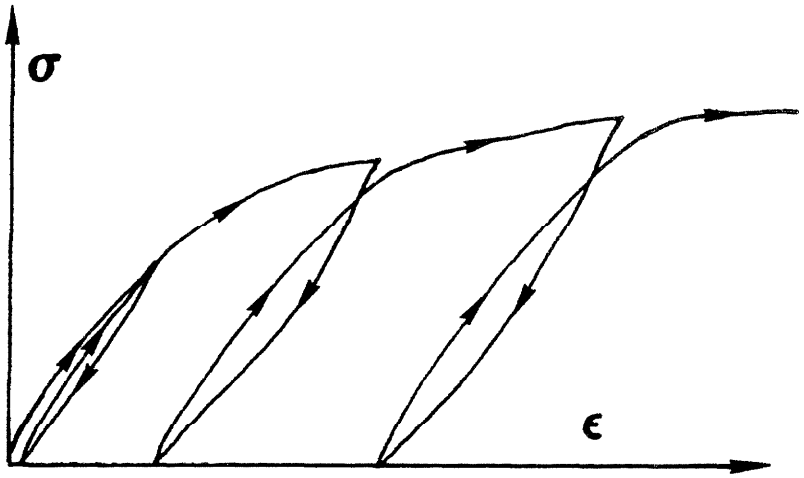

Fig. 3.1a. Typical stress-strain curve in uniaxial test performed on a real material.

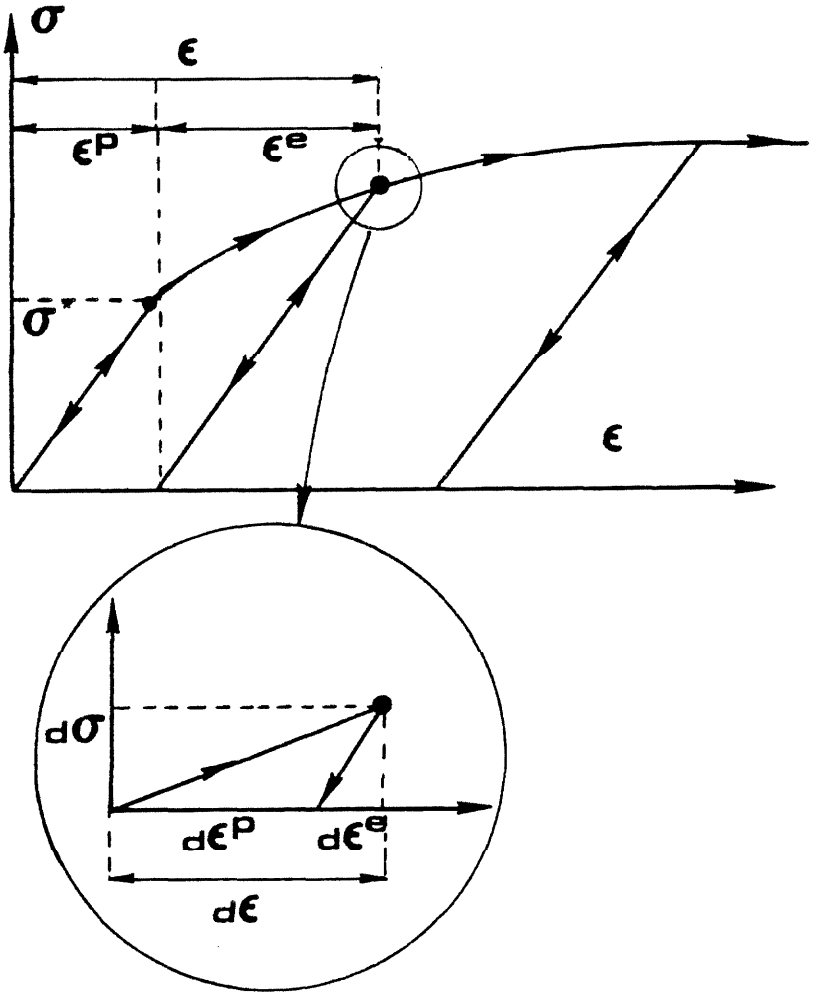

Fig. 3.1b. Idealized global and incremental material responses for development of plasticity theory.

described with mathematical terms, this complex nonlinear and irreversible behavior must be approximated without losing significant features. Such a schematic material response is shown in Fig. 3.1b and may be described by the following remarks:

1. The response is reversible around the origin; it may be represented by an isotropic linearly elastic behavior to a first approximation.
2. A threshold for reversibility is reached when the stress exceeds a "yield shear" or elastic limit. Beyond this limit, denoted σ^*, irreversibility is characterized by permanent or unrecoverable deformation after a stress removal (Fig. 3.1b).
3. Following yielding, more apparent nonlinear effects manifest themselves: the stress-strain curve bends towards the strain axis.
4. During unloading and reloading, the response is almost parallel to the initial response about the origin (if the hysteretic phenomenon is ignored).
5. At the end of a reloading, the strain ε is the sum of an unrecoverable strain ε^p and a recoverable strain ε^e (Fig. 3.1b):

$$\varepsilon = \varepsilon^e + \varepsilon^p \tag{3.1}$$

6. The response during a reloading phase is reversible until the stress exceeds a new yield stress: the previous yielding stress has increased its value to the highest value taken by

the stress state during the loading history. The material looks harder than it was originally; this phenomenon is known as "strain hardening." This remark also applies for successive unloading–reloading processes.

7. The material exhibits some memory of its previous loading history. This remembrance ability may be captured by the yield stress value. Other variables called "internal variables," may be defined to characterize this memory. This terminology comes from irreversible thermodynamics. In order to fully characterize an irreversible thermodynamic state, the "observed" or "external" variables such as temperature and stress are insufficient; new variables, called "hidden" or "internal" must also be defined.
8. The material fails when the stress reaches a final failure stress. This failure stress, the limit of the possible stress for a material, differs from the yield stress which is the threshold for irreversible strain.

In a different system of coordinates, stress–plastic strain, (the reversible strain is removed from the total strain) the material response of Fig. 3.1b is shown in Fig. 3.1c.

At an incremental level, i.e., for an infinitesimal increment of stress, $d\sigma$, as shown in Fig. 3.1b, the above remarks also pertain.

The incremental strain $d\varepsilon$, corresponding to a stress increment $d\sigma$, from a state σ, is equal to:

a) only the elastic strain increment $d\varepsilon^e$, i.e.:

$$d\varepsilon = d\varepsilon^e \quad , \quad d\varepsilon^p = 0 \tag{3.2}$$

if the stress state σ is less than the yield stress σ^* or if the stress increment $d\sigma$ is negative.

b) the sum of elastic and plastic incremental strain respectively $d\varepsilon^e$ and $d\varepsilon^p$, i.e.:

$$d\varepsilon = d\varepsilon^e + d\varepsilon^p \tag{3.3}$$

if the stress state σ is equal to the yield stress σ^* and the stress increment $d\sigma$ is positive.

In contrast to most materials, which strain-harden in uniaxial tests as indicated in Fig. 3.1a, soils, under some circumstances, present a more complex behavior, known as "strain-softening," represented in Fig. 3.1d. Obtained with strain-controlled testing devices, the stress is observed to decay as the strain exceeds some value. Although the stress σ decreases, this behavior is different from unloading as shown in Fig. 3.1d. During unloading both strain and stress increments are negative, while during strain-softening these increments have opposite signs. These two different processes are distinguished by the sign $\frac{1}{S} d\sigma$, where S is the slope of the stress-strain curve at stress σ. For unloading

$\frac{1}{S}\, d\sigma$ is negative, whereas for loading, with or without strain-softening, $\frac{1}{S}\, d\sigma$ is positive.

3.2 GENERALIZATION TO SIX-DIMENSIONAL STRESS SPACE

All fundamental concepts, introduced for the simple unidimensional state of stress and strain, need to be generalized for every possible combined state in the space of the symmetric Cauchy stress tensor and of the infinitesimal strain tensor. A conventional stress formulation has been preferred to a strain formulation (Naghdi and Trapp [3.7], Yoder [3.13]). All generalizations to the six-dimensional stress space are performed in Cartesian tensorial form, with the help of Euclidean geometrical considerations. Two particular simple models, one applied to metal, the other to soil, illustrate step-by-step the presentation of each new plasticity concept.

The stress state is represented by the Cauchy stress tensor $\underline{\sigma}$, with six independent Cartesian components σ_{ij}, $(i,j = 1,2,3)$. The increment of stress is described by the incremental stress tensor $d\underline{\sigma}$ with components $d\sigma_{ij}$ $(i,j = 1,2,3)$. The strains, corresponding to $\varepsilon, \varepsilon^e, \varepsilon^p$ in the unidimensional case, are represented by the following quantities:

$\underline{\varepsilon}$ (total) strain state with components ε_{ij}, $(i,j=1,2,3)$

$\underline{\varepsilon}^e$ elastic strain state with components ε^e_{ij}, $(i,j=1,2,3)$

$\underline{\varepsilon}^p$ plastic strain state with components ε_{ij}^p , (i,j=1,2,3)

The increments of strains, total, elastic or plastic are denoted by:

$d\underline{\varepsilon}$ increment of total strain with components $d\varepsilon_{ij}$, (i,j=1,2,3)

$d\underline{\varepsilon}^e$ increment of elastic strain with components $d\varepsilon_{ij}^e$, (i,j=1,2,3)

$d\underline{\varepsilon}^p$ increment of plastic strain with components $d\varepsilon_{ij}^p$, (i,j=1,2,3)

The description of total strain into elastic and plastic strain is still assumed to be valid in the six-dimensional strain space

$$\underline{\varepsilon} = \underline{\varepsilon}^e + \underline{\varepsilon}^p \tag{3.4a}$$

or in terms of components

$$\varepsilon_{ij} = \varepsilon_{ij}^e + \varepsilon_{ij}^p \quad , \qquad (i,j=1,2,3) \tag{3.4b}$$

For increments, the same assumption holds:

$$d\underline{\varepsilon} = d\underline{\varepsilon}^e + d\underline{\varepsilon}^p \tag{3.5a}$$

or

$$d\varepsilon_{ij} = d\varepsilon_{ij}^e + d\varepsilon_{ij}^p \quad , \qquad (i,j=1,2,3) \tag{3.5b}$$

The increment $d\underline{\varepsilon}$ is fully characterized by its Euclidean norm and its direction. The norm, denoted $||d\underline{\varepsilon}||$, is defined such that:

$$||d\underline{\varepsilon}|| = (d\varepsilon_{11}^2 + d\varepsilon_{22}^2 + d\varepsilon_{33}^2 + 2d\varepsilon_{12}^2 + 2d\varepsilon_{23}^2 + 2d\varepsilon_{31}^2)^{1/2} \quad (3.6a)$$

The factor 2 in front of the shear strain, $d\varepsilon_{ij}$, where i is different from j, takes into account the symmetry of the infinitesimal strain tensor $d\underline{\varepsilon}$. This last definition may be contracted using Einstein's implied sum notation:

$$||d\underline{\varepsilon}|| = (d\varepsilon_{ij} \cdot d\varepsilon_{ij})^{1/2} \quad , \qquad (\text{sum on } i,j=1,2,3) \qquad (3.6b)$$

The implied sum convention is an attractive way to condense equations and is used frequently in the rest of this presentation. The direction of $d\underline{\varepsilon}$ is defined by the unit vector $\underline{m}$ with the same direction and the following components:

$$m_{ij} = \frac{d\varepsilon_{ij}}{||d\underline{\varepsilon}||} \quad , \qquad (i,j=1,2,3) \qquad (3.7)$$

The definitions (3.6) and (3.7) apply to any increments, in particular to plastic and elastic strain increments $d\underline{\varepsilon}^p$ and $d\underline{\varepsilon}^e$. To define $d\underline{\varepsilon}$ resulting from an increment of stress $d\underline{\sigma}$ at a state $\underline{\sigma}$, $d\underline{\varepsilon}^e$ and $d\underline{\varepsilon}^p$ need to be determined. $d\underline{\varepsilon}^e$ is found by using an elastic model, whereas to fully characterize $d\underline{\varepsilon}^p$, three points remain to be examined: 1) existence, 2) direction and 3) amplitude. These aspects refer in turn to the yield criterion, the flow rule and the hardening rules, which are described as follows.

3.2.1 Existence of Unrecoverable Strain (Yield Criterion)

The yield point σ^* defined in the uniaxial test, is generalized into a hypersurface in the six-dimensional stress space, called the "Yield Surface" (the prefix "hyper" is usually omitted). By definition, the yield surface encloses a domain in stress space in which any infinitésimal stress change produces only recoverable strain. This surface is represented by a general equation:

$$f(\underline{\sigma},\underline{r}) = 0 \tag{3.8a}$$

or explicitly

$$f(\sigma_{11},\sigma_{22},\sigma_{33},\sigma_{12},\sigma_{23},\sigma_{31},r_1,r_2,\ldots,r_n) = 0 \tag{3.8b}$$

where $\underline{r}$ or $r_1,r_2,\ldots,r_n$ refer to the parameters controlling the size, shape, etc., of the yield surface. Once the yield surface has been defined, the presence or absence of unrecoverable strain, at some stress state, is characterized by the "yield criterion".

Yield criterion:

a) $f(\underline{\sigma},\underline{r}) < 0$, the stress state $\underline{\sigma}$ lies inside the yield surface; any increment of stress creates only incremental elastic strain $d\underline{\varepsilon}^e$, i.e., $d\underline{\varepsilon}^p = \underline{0}$.

b) $f(\underline{\sigma},\underline{r}) = 0$, the stress state $\underline{\sigma}$ lies on the yield surface. If $d\underline{\sigma}$ is

oriented outwards (loading), irreversible strain results, i.e. $d\underline{\varepsilon}^p \neq \underline{0}$; if $d\underline{\sigma}$ points inwards (unloading) or is tangent to the yield surface, only elastic strain develops, i.e. $d\underline{\varepsilon}^p = \underline{0}$.

c) The case $\dot{f}(\underline{\sigma},\underline{x}) > 0$ is impossible.

This impossibility is justified by invoking the following argument: if a state of stress $\underline{\sigma}$ is allowed to exist outside the yield surface, then for any increment of stress from this state $\underline{\sigma}$, irreversible deformation would occur. No unloading with reversible response would be possible, which is contradictory to the previous uniaxial concept defined from uniaxial tests shown in Fig. 3.1a. Therefore the yield surface must change its position, or deform in order to follow the stress state when plastic flow occurs, so that the stress state $\underline{\sigma}$ lies on or within the yield surface. This condition is known as the "consistency condition."

A more precise definition of loading and unloading entering the yield criterion may be given with the help of the unit vector normal and pointing outwards from the yield surface at $\underline{\sigma}$ (see Fig. 3.2). Denoted $\underline{n}$, this unit vector has its components n_{ij} such that:

$$n_{ij} = \left[\frac{\partial f}{\partial \sigma_{k\ell}} \cdot \frac{\partial f}{\partial \sigma_{k\ell}}\right]^{-\frac{1}{2}} \cdot \frac{\partial f}{\partial \sigma_{ij}} \qquad \begin{matrix}(i,j=1,2,3)\\ (\text{sum on } k,\ell=1,2,3)\end{matrix} \qquad (3.9)$$

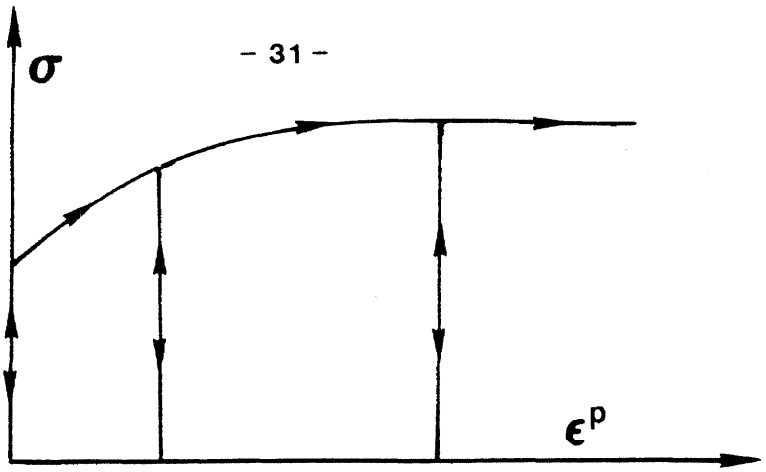

Fig. 3.1c. Idealized material response after subtracting the elastic strain.

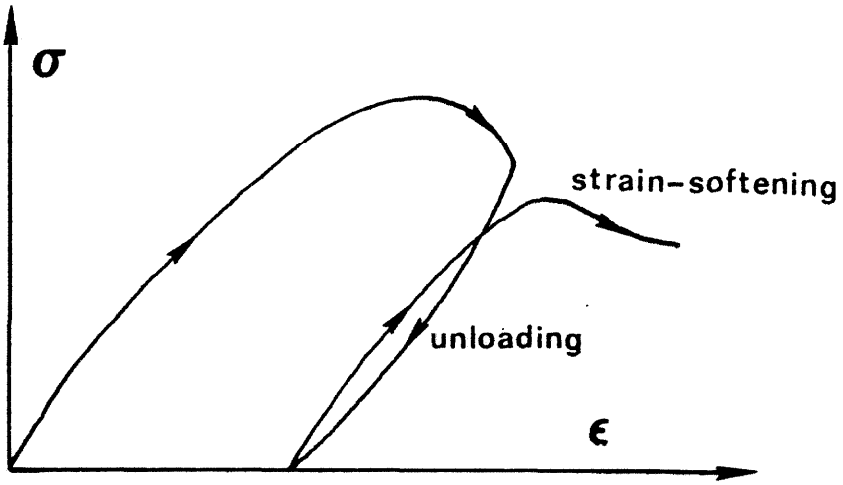

Fig. 3.1d. Typical stress-strain curve in uniaxial test on a strain-softening soil.

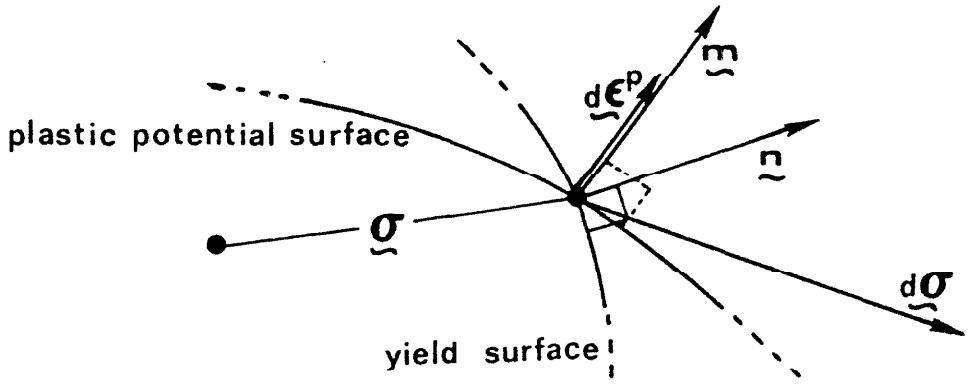

Fig. 3.2. Yield surface and plastic potential surface in stress space.

where $\frac{\partial f}{\partial \sigma_{ij}}$ is the partial derivative of $f(\underline{\sigma},\underline{\kappa})$ with respect to the stress component σ_{ij}. After characterizing the scalar product between $\underline{n}$ and $d\underline{\sigma}$ in the following way:

$$\underline{n}^{*}d\underline{\sigma} = n_{ij}d\sigma_{ij} \qquad \text{(sum on i,j=1,2,3)} \tag{3.10}$$

the loading and unloading, which indicate if the stress increment points outwards or inwards to the yield surface, may be redefined in the following way:

$$\text{loading} \qquad \underline{n}^{*}d\underline{\sigma} > 0 \tag{3.11a}$$

$$\text{neutral loading} \qquad \underline{n}^{*}d\underline{\sigma} = 0 \tag{3.11b}$$

$$\text{unloading} \qquad \underline{n}\,d\underline{\sigma} < 0 \tag{3.11c}$$

Example 1:

The simplest elastic–plastic model, applied to metal, is certainly the von Mises' model. The yield surface is a cylinder in the principal stress space, the axis of which is parallel to the hydrostatic axis, as represented in Fig. 3.3. The equation of such a surface is obtained by stating that the distance to any point on this surface to its axis is equal to the radius denoted R, i.e.

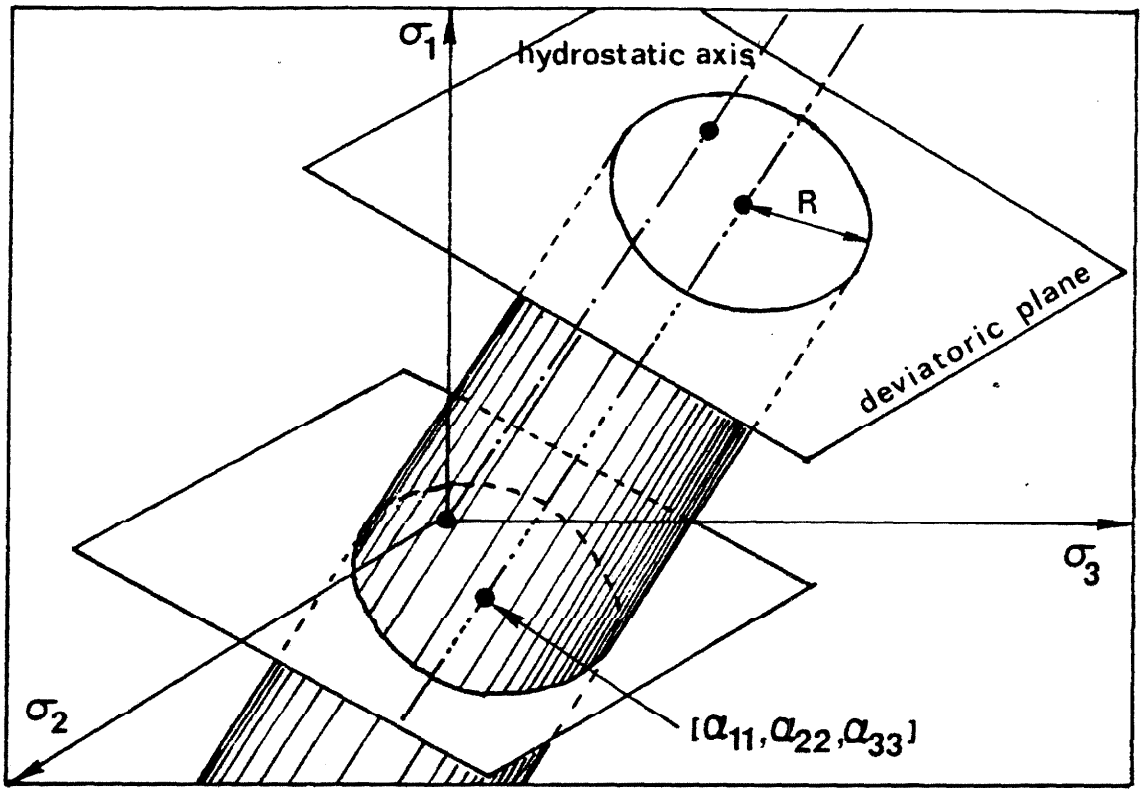

Fig. 3.3. von Mises' yield surface in principal stress space.

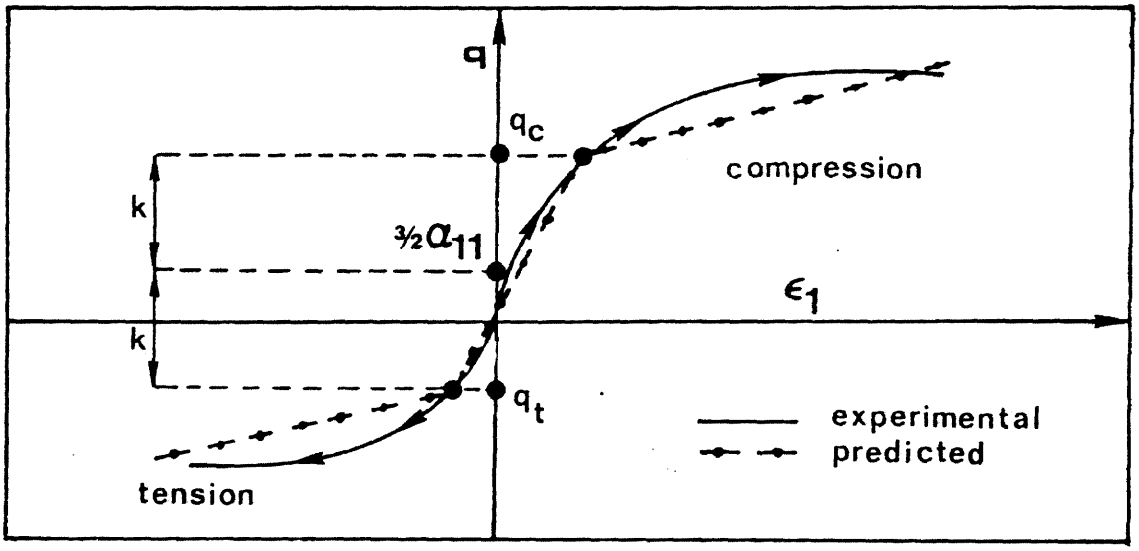

Fig. 3.4. Typical experimental response curves of a real material and predicted response curves by von Mises' model during two uniaxial tests (compression and tension).

$$(\sigma_{ij}-p\delta_{ij}-\alpha_{ij})(\sigma_{ij}-p\delta_{ij}-\alpha_{ij}) = R^2 \quad \text{(sum on i,j=1,2,3)} \tag{3.12}$$

where δ_{ij} is the Kronecker symbol defined such as

$$\delta_{ij} = \begin{array}{l} 0 \text{ if } i\neq j, \ (i,j=1,2,3) \\ 1 \text{ if } i=j, \ (i,j=1,2,3) \end{array} \tag{3.13}$$

and p is the mean pressure defined such that:

$$p = \frac{1}{3}(\sigma_{11} + \sigma_{22} + \sigma_{33}) \tag{3.14}$$

and α_{ij}'s are components of a point of the yield surface axis (see Fig. 3.3) such that

$$\alpha_{11} + \alpha_{22} + \alpha_{33} = 0 \tag{3.15}$$

Introducing the deviatoric stress tensor $\underline{s}$ with Cartesian components s_{ij} such that

$$s_{ij} = \sigma_{ij} - p\delta_{ij} \qquad (i,j=1,2,3) \tag{3.16}$$

equation (3.12) becomes

$$(s_{ij}-\alpha_{ij})(s_{ij}-\alpha_{ij}) = R^2 \qquad \text{(sum on i,j=1,2,3)} \tag{3.17}$$

For convenience, equation (3.17) becomes

$$\frac{3}{2}(s_{ij}-\alpha_{ij})(s_{ij}-\alpha_{ij}) - k^2 = 0 \qquad \text{(sum on i,j=1,2,3)} \qquad (3.18)$$

where k is defined such as

$$k = \left[\frac{3}{2}\right]^{1/2} R \qquad (3.19)$$

The values of α_{ij}'s and k may be calculated from the uniaxial loading, which was specified in (2.5). For this particular loading the deviatoric stress components are such that

$$s_{11} = \frac{2}{3} q \qquad (3.20a)$$

$$s_{22} = s_{33} = -\frac{q}{3} \qquad (3.20b)$$

$$s_{ij} = 0 \quad , \quad i \neq j \quad , \quad (i \neq j = 1,2,3) \qquad (3.20c)$$

For convenience, assume that the α_{ij}'s satisfy the following relations:

$$\alpha_{22} = \alpha_{33} \qquad (3.21a)$$

$$\alpha_{ij} = 0 \quad , \quad i \neq j \quad , \quad (i,j=1,2,3) \qquad (3.21b)$$

Using relations (3.15), (3.20), (3.21), relation (3.18) becomes:

$$q = \frac{3}{2} \alpha_{11} \pm k \qquad (3.22)$$

If two different uniaxial tests, one in compression and another in tension, are available, two yield stresses may be chosen such as shown in Fig. 3.4. The yield stresses in the compressive and tensile tests

are respectively denoted q_c and q_t. Since q_c and q_t satisfy relation (3.22) for different signs, α_{11} and k are such that

$$\alpha_{11} = \frac{q_c + q_t}{3} \tag{3.23a}$$

$$k = \frac{q_c - q_t}{2} \tag{3.23b}$$

All other components α_{ij} are generated from (3.21) and (3.15). The unit vector $\underline{n}$ to the yield surface may also be calculated. From relation (3.18) is obtained:

$$\frac{\partial f}{\partial \sigma_{ij}} = 3(s_{ij}-\alpha_{ij}) \qquad (i,j=1,2,3) \tag{3.24}$$

From (3.9), (3.18) and (3.24), it is concluded that

$$n_{ij} = \left[\frac{3}{2}\right]^{1/2} \frac{s_{ij}-\alpha_{ij}}{k} \qquad (i,j=1,2,3) \tag{3.25}$$

The yield criterion, and specifically relations (3.11), may be simplified for the uniaxial test, such that

$$n_{k\ell} \cdot d\sigma_{k\ell} = \left[\frac{2}{3}\right]^{1/2} \frac{1}{k} \left[q - \frac{3}{2}\alpha_{11}\right] d\sigma_{11} \quad (\text{sum on } k,\ell=1,2,3) \tag{3.26}$$

If q is greater than q_t and less than q_c, only elastic strain is possible for any stress increment. If q is equal to q_t or q_c, then plastic strain exists dependent on the sign of the terms in relation (3.26). If these terms are positive, there is plastic strain; if they are negative,

only elastic strain occurs.

Example 2:

Lade's first soil model [3.5] follows closely the concepts of metal plasticity, but also exhibits some characteristic features of soil behavior. This model is presented in parallel with von Mises' model.

The yield surface has for equation:

$$f(\underline{\sigma},\chi) = I^3 - \chi I_3 = 0 \qquad (3.27)$$

where χ is the only parameter which controls the yield surface shape (i.e., χ is equal to r_1) and I, I_3 are stress invariants defined in the following way.

$$I = \sigma_{kk} = \sigma_{11} + \sigma_{22} + \sigma_{33} \quad (\text{sum on } k=1,2,3) \qquad (3.28a)$$

$$I_3 = \det|\underline{\sigma}| = \sigma_{11}\sigma_{22}\sigma_{33} + 2\sigma_{12}\sigma_{23}\sigma_{31} - \left[\sigma_{11}\sigma_{23}^2+\sigma_{22}\sigma_{31}^2+\sigma_{33}\sigma_{12}^2\right] \qquad (3.28b)$$

Such a surface (Eq. 3.27) is a cone, centered on the hydrostatic axis, with its tip at the origin of stress as shown in Figs. 3.5. The elastic domain, bounded by this surface, depends on the mean pressure p, i.e., on I. Since the unit vector $\underline{n}$ is lengthy to work out, only the partial derivatives are given in the following relations:

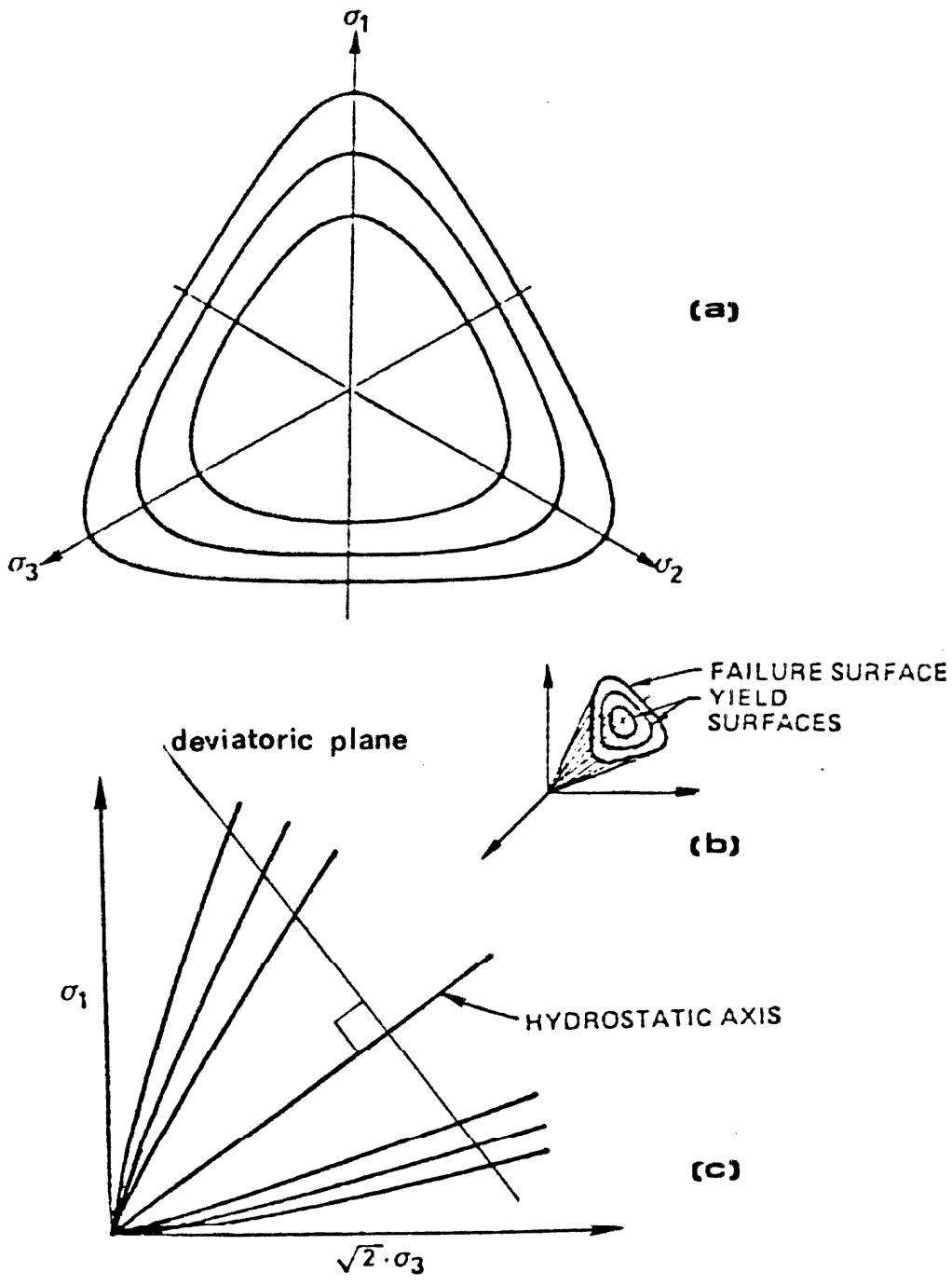

Fig. 3.5. Failure surface and two successive positions of yield surface of Lade's model.

a) in deviatoric plane
b) in principal stress space
c) in plane $\sigma_2=\sigma_3$

$$\frac{\partial f}{\partial \sigma_{ij}} = 3I^2\delta_{ij} - \chi \frac{\partial I_3}{\partial \sigma_{ij}} \qquad (i,j=1,2,3) \qquad (3.29)$$

where all components $\frac{\partial I_3}{\partial \sigma_{ij}}$ are generated, by permutation of indices, using the following relations

$$\frac{\partial I_3}{\partial \sigma_{11}} = \sigma_{22}\sigma_{33} - \sigma_{23}^2 \qquad (3.30a)$$

$$\frac{\partial I_3}{\partial \sigma_{12}} = \sigma_{23}\sigma_{31} - \sigma_{12}\sigma_{33} \qquad (3.30b)$$

3.2.2 Direction of Plastic Flow: Flow Rule

Obviously defined uniquely in the case of any unidimensional state, the plastic flow direction must be characterized in a multidimensional stress space by a "flow rule." From experimental observations, contrary to what elasticity theory predicts (see Section 3.5.4), the plastic flow direction is related to the total stress state and is independent of the stress increment. Analogously to irrotational fluid flow, which is normal to the potential lines in fluid mechanics, for all the stress states and stress increments creating plastic strain (as specified by the yield criterion), the plastic flow direction is collinear to the gradient of a function, called the "plastic potential," and denoted $g(\underline{\sigma},\underline{s})$ or explicitly $g(\sigma_{11},\sigma_{22},\sigma_{33},\sigma_{12},\sigma_{23},\sigma_{31},s_1,\ldots,s_m)$. $\underline{s}$ with components s_k's, k varying from 1 to m, represents the variables that describe the changes in the function g resulting from plastic flow.

The gradient direction is characterized by the unit vector normal to the plastic potential surface passing through the stress state, and pointing outwards from this surface. Denoted by $\underline{m}$, the components m_{ij} of this vector are given by an expression similar to (3.9), where g is substituted for f.

The incremental plastic strain $d\underline{\varepsilon}^p$ is collinear to $\underline{m}$ (Fig. 3.2), which is expressed in the following way:

$$d\underline{\varepsilon}^p = ||d\underline{\varepsilon}^p||\underline{m} \tag{3.31a}$$

$$d\varepsilon_{ij}^p = ||d\underline{\varepsilon}^p||m_{ij} \quad , \qquad (i,j=1,2,3) \tag{3.31b}$$

where $||d\underline{\varepsilon}^p||$, amplitude of $d\underline{\varepsilon}^p$, is a positive scalar.

For convenience, it is often assumed that the potential surface and yield surface are coincident. In this case the flow rule is said to be associative; if they are not coincident, it is termed nonassociative.

Example 1: von Mises' Model

From observations on metal, an associative rule is selected. The unit vector $\underline{m}$, which represents the plastic flow direction, is coincident with the unit vector $\underline{n}$, which represents the normal to the yield surface.

The plastic volumetric strain $d\varepsilon_v^p$ is given by the relation:

$$d\varepsilon_v^p = d\varepsilon_{11}^p + d\varepsilon_{22}^p + d\varepsilon_{33}^p \qquad (3.32)$$

Since the vector $\underline{m}$ is given by (3.25) and since the deviatoric stresses also verify the relation (3.15), it can be shown that the plastic volumetric is zero so that von Mises' model predicts no plastic volumetric change.

Example 2: Lade's Model

Lade's model is nonassociative; the plastic potential surface is defined as follows:

$$g(\underline{\sigma},\xi) = I^3 - K_2 I_3 - \xi = 0 \qquad (3.33)$$

where the scalar ξ is defined so that the potential surface goes through the stress state and where K_2 is related to the yield surface (relation 3.7) by the following expression.

$$K_2 = A\chi + 27(1-A) \qquad (3.34)$$

in which A is a material constant.

In Fig. 3.6 the failure, yield and plastic potential surfaces have been compared in the p-q space (Section 2.3) for a special stress state and a particular sand (Monterey No. 0 sand).

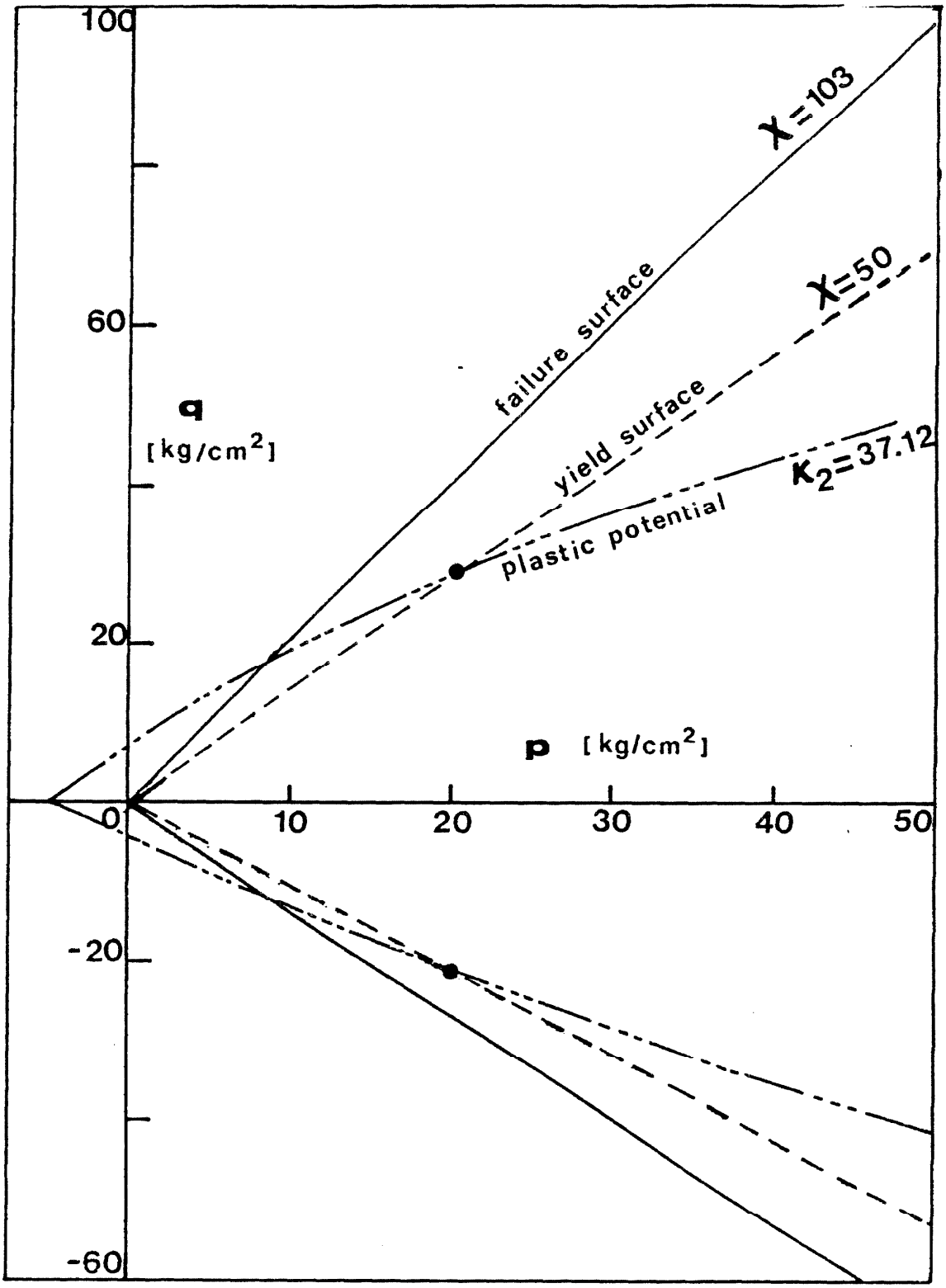

Fig. 3.6. Failure, yield and plastic potential surface for Lade's model (dense Monterey No. 0 sand).

3.2.3 Amplitude of Plastic Flow, Hardening Rules

The amplitude of the plastic increment is the last point which needs to be specified; it is calculated from the motion of the yield surface by invoking the consistency condition. In order to follow the stress state during plastic flow, the yield surface must be able to alter its shape, position, etc. All these changes are accomplished by modifying the parameters $r_1,\ldots,r_m$ of Equation (3.8). All the parameters r_k (e.g., radius and center position for von Mises' model) themselves depend upon some different, more fundamental, quantities; that is, the "internal" or hidden variables. If the evolution law (i.e., the relation between the parameters r_k and the internal variables) is specified, then all changes in yield surface are described. The concept of internal variables, formulated recently for plasticity by Lubliner [3.6] is based on the idea of state variables in irreversible thermodynamics. Since the material exhibits an irreversible behavior, the state of a body is described at each material point not only by the values of "observed" or "external" variables (such as deformation or stress), but also by values of "hidden" or "internal" variables. These variables are usually taken to be scalars or components of a properly invariant second order tensor; the plastic strain tensor $\underline{\varepsilon}^p$ is usually selected as the internal variable. The external variables are the stresses, since the plasticity theory is formulated in a stress space. For strain-plasticity (Naghdi and Trapp [3.7], Yoder [3.13]) the strains are selected. From the consistency condition, applied for the infinitesimal stress increments creating plastic strains, the following

relation must hold:

$$\frac{\partial f}{\partial \sigma_{k\ell}} d\sigma_{k\ell} + \frac{\partial f}{\partial \varepsilon^p_{k\ell}} d\varepsilon^p_{k\ell} = 0 \qquad \text{(sum on } k,\ell=1,2,3) \qquad (3.35)$$

Substituting relation (3.31b) into (3.35) and using (3.9), the amplitude of the plastic strain is such that:

$$||d\underline{\varepsilon}^p|| = -\left[\frac{\partial f}{\partial \sigma_{k\ell}} \cdot \frac{\partial f}{\partial \sigma_{k\ell}}\right]^{1/2} \frac{n_{ij} \cdot d\sigma_{ij}}{\frac{\partial f}{\partial \varepsilon^p_{pq}} \cdot m_{pq}} \qquad (3.36)$$

$$\text{(sum on } i,j,k,\ell,p,q=1,2,3)$$

By definition, the plastic modulus, denoted H, is:

$$H = -\left[\frac{\partial f}{\partial \sigma_{k\ell}} \cdot \frac{\partial f}{\partial \sigma_{k\ell}}\right]^{1/2} \frac{\partial f}{\partial \varepsilon^p_{pq}} \cdot m_{pq} \qquad \text{(sum on } k,\ell,p,q=1,2,3) \qquad (3.37)$$

With (3.31b), (3.36) and (3.37) the plastic strain increment becomes

$$d\varepsilon^p_{ij} = \frac{1}{H} m_{ij}(n_{rs} d\sigma_{rs}) \qquad \begin{matrix}(i,j=1,2,3)\\ \text{(sum on } r,s=1,2,3)\end{matrix} \qquad (3.38)$$

The Macaulay's bracket, denoted $\langle\ \rangle$, is defined

$$\langle x \rangle = x \cdot H_e(x) \tag{3.39}$$

where H_e is the Heaviside function. The relation (3.38) may be rewritten with a built-in yield criterion,

$$d\varepsilon^p_{ij} = m_{ij} \frac{1}{H} \langle n_{rs} d\sigma_{rs} \rangle \qquad \begin{matrix}(i,j=1,2,3)\\(\text{sum on } r,s=1,2,3)\end{matrix} \tag{3.40}$$

During strain softening, H and the scalar product $\underline{n} \cdot d\underline{\sigma}$ are both negative. Strain-softening alters relation (3.40) in the following way:

$$d\varepsilon^p_{ij} = m_{ij} \langle \frac{1}{H} n_{rs} d\sigma_{rs} \rangle \qquad \begin{matrix}(i,j=1,2,3)\\(\text{sum on } r,s=1,2,3)\end{matrix} \tag{3.41}$$

Example 1: von Mises' Model

Two different hardening rules are presented successively: isotropic and kinematic.

a) Isotropic hardening (Fig. 3.7a)

The yield surface expands radially about its fixed axis. By applying the consistency condition to the yield surface defined in (3.18), there results

$$3(s_{ij} - \alpha_{ij}) ds_{ij} = 2k dk \qquad (\text{sum on } ij=1,2,3) \tag{3.42}$$

As a result of a stress change, the radius k is altered such that

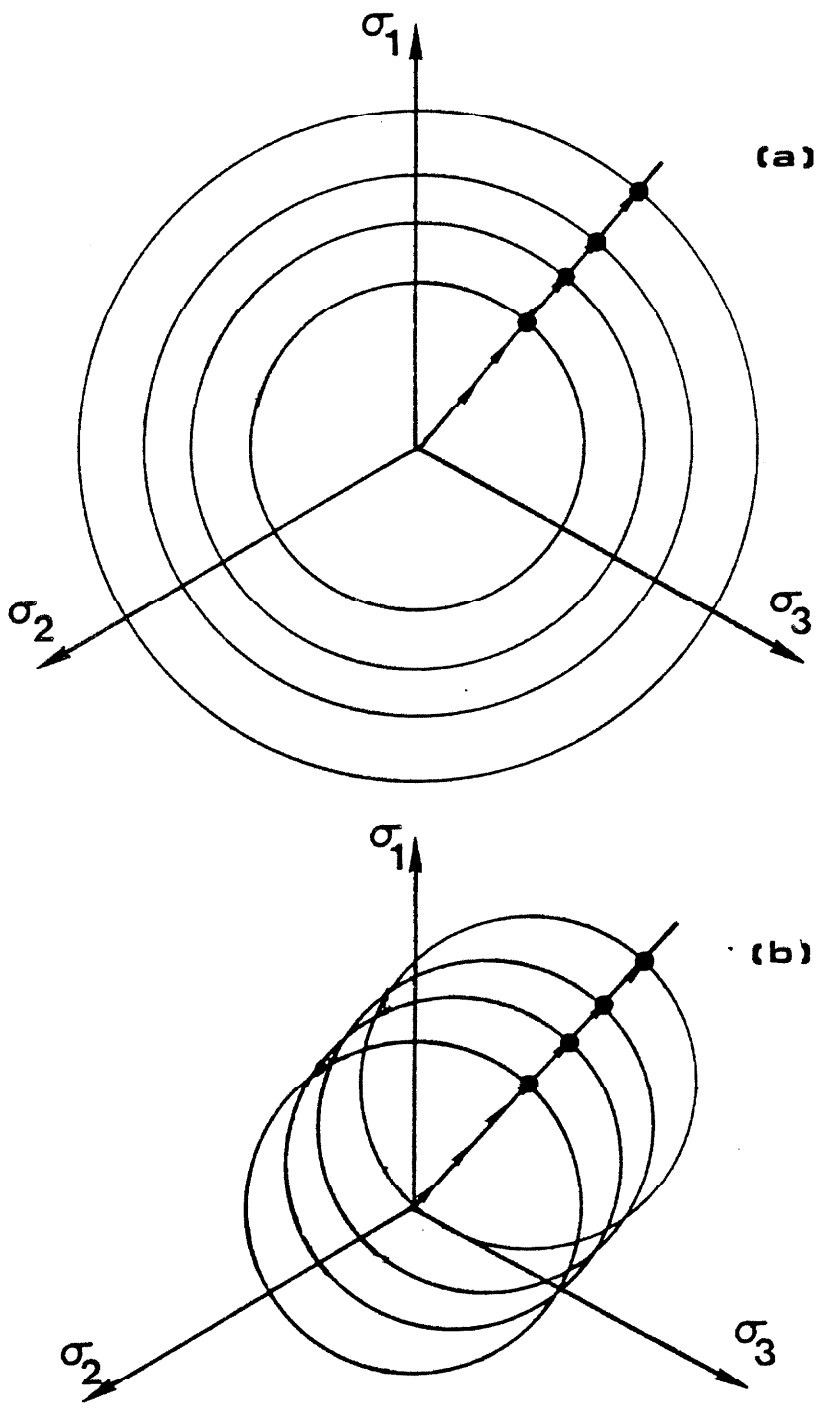

Fig. 3.7. Four successive positions of von Mises' yield surface in a deviatoric plane with different hardening rules, and the same loading path:

a) isotropic hardening
b) kinematic hardening

$$dk = \frac{3}{2}\frac{(s_{ij}-\alpha_{ij})ds_{ij}}{k} \qquad \text{(sum on ij=1,2,3)} \qquad (3.43)$$

b) Kinematic hardening (Fig. 3.7b)

The yield surface is translated without changing its radius. The consistency condition implies that

$$(s_{ij}-\alpha_{ij})ds_{ij} = (s_{kl}-\alpha_{kl})d\alpha_{kl} \qquad (3.44)$$

(sum on i,j,k,l=1,2,3)

The unique relation (3.44) is not sufficient to define all six $d\alpha_{ij}$'s. The direction of the incremental center displacement $d\alpha_{ij}$ is supposed to be collinear to the plastic strain increment, i.e., there exists a scalar λ such that

$$d\alpha_j = \lambda d\varepsilon^p_{ij} \qquad (i,j=1,2,3) \qquad (3.45)$$

Using relation (3.44), λ is found such that

$$\lambda = \frac{(s_{ij}-\alpha_{ij})ds_{ij}}{(s_{kl}-\alpha_{kl})d\varepsilon^p_{kl}} \qquad \text{(sum on i,j,k,l=1,2,3)} \qquad (3.46)$$

Related to the hardening rule (isotropic or kinematic), the plastic modulus H depends on the evolution of k or α_{ij}'s w.r.t. to ε^p_{ij}. The amplitude of the plastic strain increment from (3.6b), (3.25) and (3.38) satisfies the following relation:

$$||d\varepsilon^p|| = \frac{1}{H}\,\frac{3}{2}\,\frac{(s_{ij}-\alpha_{ij})}{k}\,ds_{ij} \tag{3.47}$$

(sum on i,j=1,2,3)

therefore, for isotropic hardening, the plastic modulus is such that

$$H = \left[\frac{3}{2}\right]^{3/2}\frac{dk}{||d\varepsilon^p||} \tag{3.48}$$

Whereas for kinematic hardening, since

$$(s_{k\ell}-\alpha_{k\ell})d\varepsilon_{k\ell} = \frac{1}{H}(s_{rs}-\alpha_{rs})ds_{rs} \tag{3.49}$$

(sum on k,ℓ,r,s=1,2,3)

therefore the plastic modulus is expressed

$$H = \frac{d\alpha_{ij}}{d\varepsilon^p_{ij}} = \frac{||d\alpha||}{||d\varepsilon^p||} \tag{3.50}$$

A common alternate way, particularly for the von Mises' material, is to fix the plastic modulus H to be constant: the hardening is said to be linear. The motion is consequently specified for each hardening rule by relation (3.48) or (3.50).

Example 2: Lade's Model

Only one internal variable is selected to characterize the material memory: the plastic work, denoted W_p, and defined by integration of an increment of plastic work dW_p. dW_p is such that

$$dW_p = \sigma_{ij} \cdot d\varepsilon^p_{ij} \qquad (sum\ on\ i,j=1,2,3) \tag{3.51}$$

Lade found that the motion of the yield surface is related to the evolution of the internal variable W_p in the following way:

$$\chi - f_t = \frac{W_p}{a + d\, W_p} \tag{3.52a}$$

where

$$d = \frac{1}{r_f} (K_1 - f_t) \tag{3.52b}$$

and

$$a = M p_a \left[\frac{\sigma_3}{p_a}\right]^f \tag{3.52c}$$

where r_f, K_1, f_t, M, f are material constants, p_a the atmospheric pressure (selected as a reference value) and σ_3 the minor effective principal stress.

As plastic work is dissipated, the yield surface expands about the hydrostatic axis. From (3.52a) the incremental change in yield surface

χ and in internal variable W_p are related as follows

$$dW_p = \frac{a\,d\chi}{\left[1 - r_f \frac{\chi - f_t}{K_1 - f_t}\right]^2} \tag{3.53}$$

The plastic modulus is derived from relation (3.37). Since the following relations hold [from (3.51) and (3.52a)]

$$\frac{\partial f}{\partial \varepsilon^p_{ij}} = \frac{\partial \chi}{\partial W_p} \sigma_{ij} \qquad (i,j=1,2,3) \tag{3.54}$$

the plastic modulus H is:

$$H = -\frac{1}{a}\left[1 - r_f \frac{\chi - f_t}{K_1 - f_t}\right]^2 m_{ij}\sigma_{ij}\left[\frac{\partial f}{\partial \sigma_{k\ell}} \frac{\partial f}{\partial \sigma_{k\ell}}\right]^{1/2} \tag{3.55}$$

(sum on $i,j,k,\ell=1,2,3$)

3.3 FORMULATION OF ELASTIC-PLASTIC RELATIONS FOR AXISYMMETRIC LOADING

The formulation of elastic-plastic constitutive equations has been performed in the most general combined state of stress, i.e., in the six-dimensional space of the Cauchy stress tensor. For some specific loadings, where only a few components of the stress tensor vary, the general tensorial formulation becomes redundant and must be simplified.

For instance, in soil mechanics, soil behaviors are mainly extracted from conventional triaxial tests. During these particular tests, only the axisymmetric stress states defined by relation (2.5) are

possible. Since the two-dimensional p-q space represents any axisymmetric stress states, it may be selected as the new simplified stress space to reformulate the elastic-plastic theories during axisymmetric loading. Both the yield and potential surfaces, originally hypersurfaces defined in a six-dimensional space, are projected in the p-q space. The yield surface projection satisfies the following equations

$$f^*(p,q,\xi) = f(\sigma_{11},\sigma_{33},\sigma_{33},0,0,0,\xi) = 0 \tag{3.56}$$

The unit vector normal to this new yield surface has for component n_p, n_q in the p-q space such that

$$n_p = \frac{\partial f^*}{\partial p} \cdot \left[\frac{\partial f^*}{\partial p}^2 + \frac{\partial f^*}{\partial q}^2 \right]^{-1/2} \tag{3.57a}$$

$$n_q = \frac{\partial f^*}{\partial q} \cdot \left[\frac{\partial f^*}{\partial p}^2 + \frac{\partial f^*}{\partial q}^2 \right]^{-1/2} \tag{3.57b}$$

The terms $\frac{\partial f^*}{\partial p}$ and $\frac{\partial f^*}{\partial q}$, partial derivatives of the yield function $f^*(p,q,\xi)$ w.r.t. p and q, are calculated by the chain rule from (3.56) and (2.6) so that

$$\frac{\partial f^*}{\partial p} = \frac{1}{3}\frac{\partial f}{\partial \sigma_{11}} + \frac{2}{3}\frac{\partial f}{\partial \sigma_{33}} \tag{3.58a}$$

$$\frac{\partial f^*}{\partial q} = \frac{\partial f}{\partial \sigma_{11}} - 2\,\frac{\partial f}{\partial \sigma_{33}} \qquad (3.58b)$$

Similar definitions apply to a new potential function $g^*(p,q,\xi)$ and its normal unit vector with components m_p, m_q in the p–q space.

Corresponding to the new simplified stress space, a new strain space is selected with the following restriction: it must not only contain any strain predicted by the model, but also preserve the normality rule between stress and strain. For instance, the ε_v–ε_q space, defined in relations (2.4), is appropriate only for models which predict axisymmetric strains obeying relations (2.3). All other models predicting strains outside of the ε_v–ε_q space cannot be formulated in the p–q space. The normality rule between the new stress and strain is preserved by relation (2.7). The unit vector (m_p, m_q) normal to the projected plastic potential in the p–q space is still collinear with the plastic strain increment $(d\varepsilon_v^p, d\varepsilon_q^p)$ in the ε_v–ε_q space. In summary, only for elastic–plastic models that predict axisymmetric strains during axisymmetric stress loadings, may the relations (3.41) be rewritten in the form:

$$d\varepsilon_v^p = m_p \left\langle \frac{1}{H^*} (n_p dp + n_q dq) \right\rangle \qquad (3.59a)$$

$$d\varepsilon_q^p = m_q \left\langle \frac{1}{H^*} (n_p dp + n_q dq) \right\rangle \qquad (3.59b)$$

where H^* is the plastic modulus for axisymmetric loading. H^* is different but related to H defined by relation (3.37). Following the same approach, which leads to the definition of the plastic modulus H in

(3.37), H* is defined by the following relation:

$$H^* = -\left[\frac{\partial f^*}{\partial p}^2 + \frac{\partial f^*}{\partial q}^2 \right]^{1/2} \left[\frac{\partial f^*}{\partial \varepsilon_v^p} m_p + \frac{\partial f^*}{\partial \varepsilon_q^p} m_q \right] \qquad (3.60)$$

When no ambiguity exists, the superscript "*" is omitted to avoid an excess of notation.

3.4 ISOTROPIC ELASTIC PLASTIC CONSTITUTIVE EQUATIONS

In their most general expression, the yield and potential functions depend on the six independent coordinates of the symmetric Cauchy stress tensor. These six components are represented by three principal values denoted σ_1, σ_2 and σ_3 in a principal stress frame. The three additional degrees of freedom define the rotation between the principal and the fixed frames.

Since a function with six variables is difficult to define, most constitutive laws include hypotheses to simplify the dependence of variables. As a common assumption, the rotation of principal stresses is neglected: the three variables, which describe the rotation of the principal stress frame w.r.t. to the fixed frame, may be disregarded. The model may then be formulated completely in the three dimensional principal stress space. Recently, experimental investigations on soils have been carried out to check this assumption. Using new laboratory equipment such as the hollow cylinder torsion apparatus (Symes et al. [3.10]) or the true triaxial apparatus with application of shear stress

along the boundaries (Arthur et al. [3.1]), the effect of principal stress rotation has not been found to be negligible. Eventually, when sufficient and reliable data are available, this phenomenon will be taken into account in soil models.

3.4.1 Isotropic Elastic-Plastic Models

A more drastic hypothesis to simplify the dependence of yield and potential functions upon stress components, is to assume that the material response is isotropic: not only the principal stress rotations are neglected but also the yield and potential functions are taken to depend only on the stress invariants, i.e., are symmetric functions of the principal stresses. (By definition, a symmetric function has its value unchanged by any permutation of its variables.) The stress invariants, which are commonly used in soil mechanics, are denoted I, J, and S and are defined here in the following way:

$$I = \sigma_{kk} \qquad \text{(sum on } k=1,2,3) \qquad (3.61a)$$

$$J = (\tfrac{1}{2}\, s_{ij} s_{ij})^{\frac{1}{2}} \qquad \text{(sum on } i,j=1,2,3) \qquad (3.61b)$$

$$S = (\tfrac{1}{3}\, s_{ij} s_{jk} s_{ki})^{\frac{1}{3}} \qquad \text{(sum on } i,j,k=1,2,3) \qquad (3.61c)$$

where the s_{ij}'s are components of the deviatoric stress tensor defined in relation (3.16).

Sometimes instead of using the third invariant S, a new quantity, called Lode's angle and denoted θ, is preferred. This angle is defined

$$\theta = \frac{1}{3} \sin^{-1} \left[\frac{3}{2} 3^{3/2} \left[\frac{S}{J} \right]^3 \right] \qquad (3.61d)$$

The invariants I and J have a representation in a principal stress frame (Fig. 3.8). If O, M, and m represent successively the stress origin, the stress state and its projection on the hydrostatic axis, the following relations hold:

$$OM = I/3^{3/2} \qquad (3.62a)$$

$$mM = \frac{2}{3^{3/2}} J \qquad (3.62b)$$

Lode's angle, defined between $-\frac{\pi}{6}$ and $\frac{\pi}{6}$, is represented in Fig. 3.8b. Since all stress invariants are symmetric functions of the principal stress values σ_1, σ_2 and σ_3, there are six different stress states, obtained by permutation of σ_1, σ_2 and σ_3 with the same stress invariant values.

Example

Lade's model is an isotropic model; both yield and potential surfaces are expressed in terms of stress invariants. However, von Mises' model may be nonisotropic: when the yield surface is not centered on the hydrostatic axis, its equation (3.18) is not symmetric w.r.t. to the principal stress values.

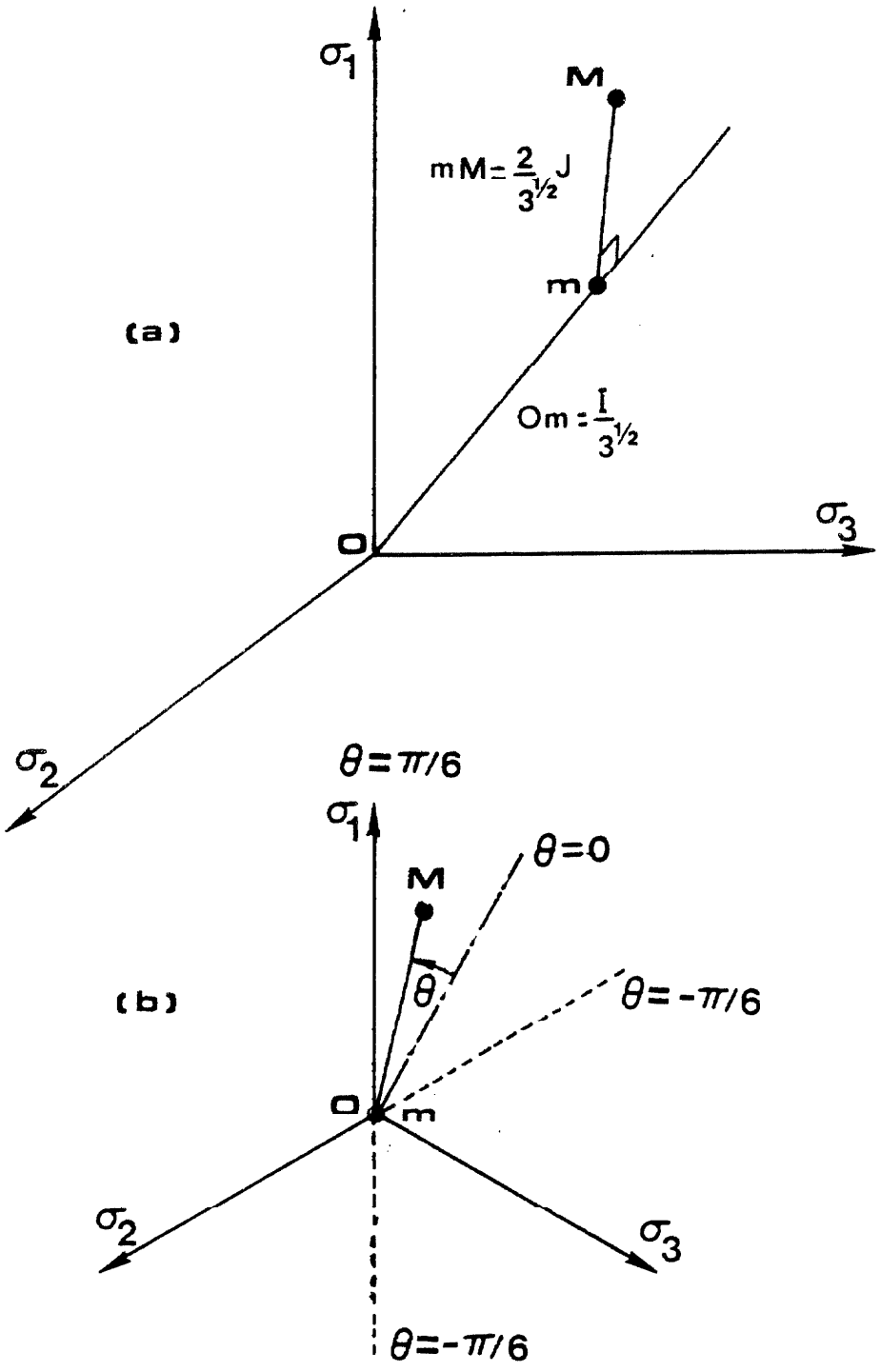

Fig. 3.8. Representation of stress invariants:

(a) I,J in principal stress space
(b) Lode's angle θ in a deviatoric plane

Because of the simple dependence of yield and potential functions on only variables I, J, S (or θ), the isotropic elastic-plastic constitutive relation presents an attractive formulation. The partial derivatives of yield and potential functions w.r.t. stress σ_{ij} may be expressed as a function of their derivatives w.r.t. I, J and S (or θ) by using the chain rule, e.g., the partial derivatives of the yield function become

$$\frac{\partial f}{\partial \sigma_{ij}} = \frac{\partial f}{\partial I}\frac{\partial I}{\partial \sigma_{ij}} + \frac{\partial f}{\partial J}\frac{\partial J}{\partial \sigma_{ij}} + \frac{\partial f}{\partial S}\frac{\partial S}{\partial \sigma_{ij}} \qquad (i,j=1,2,3) \qquad (3.63)$$

(if θ is used instead of S, the last term becomes $\frac{\partial f}{\partial \theta}\frac{\partial \theta}{\partial \sigma_{ij}}$)

where the following derivatives $\frac{\partial I}{\partial \sigma_{ij}}$, $\frac{\partial J}{\partial \sigma_{ij}}$, $\frac{\partial S}{\partial \sigma_{ij}}$ and $\frac{\partial \theta}{\partial \sigma_{ij}}$ are calculated from relations (3.61) to yield the following values

$$\frac{\partial I}{\partial \sigma_{ij}} = \delta_{ij} \qquad (i,j=1,2,3) \qquad (3.64a)$$

$$\frac{\partial J}{\partial \sigma_{ij}} = \frac{s_{ij}}{2J} \qquad (i,j=1,2,3) \qquad (3.64b)$$

$$\frac{\partial \theta}{\partial \sigma_{ij}} = -\frac{1}{2J^2}\tan(3\theta)s_{ij} + \frac{3^{1/2}}{2J\cos(3\theta)}\left[\frac{s_{ik}s_{kj}}{J^2} - \frac{2}{3}\delta_{ij}\right] \qquad (i,j=1,2,3) \qquad (3.64c)$$

$$\frac{\partial S}{\partial \sigma_{ij}} = \frac{1}{3}\left[\frac{s_{ik}s_{kj}}{S^2} - \frac{2}{3}\left[\frac{J}{S}\right]^2\delta_{ij}\right] \qquad (i,j=1,2,3) \qquad (3.64d)$$

3.4.2 Isotropic Models in the p-q Space

The isotropic elastic-plastic constitutive relations can always be written in the p-q space for axisymmetric stress loading. For this special loading, the stress invariants of (3.61) can be calculated

$$I = 3p \tag{3.65a}$$

$$J = 3^{-\frac{1}{2}} |q| \tag{3.65b}$$

$$\theta = \frac{\pi}{6} \ , \ q \geq 0 \quad ; \qquad \theta = -\frac{\pi}{6} \ , \ q < 0 \tag{3.65c}$$

$$S = -\frac{(2)^{\frac{1}{3}}}{3} q \tag{3.65d}$$

Since the deviatoric stress components obey relation (3.20), the relations (3.64) can be simplified in the following way:

$$\frac{\partial I}{\partial \sigma_{11}} = \frac{\partial I}{\partial \sigma_{22}} = \frac{\partial I}{\partial \sigma_{33}} = 1 \tag{3.66a}$$

$$\frac{\partial I}{\partial \sigma_{ij}} = 0 \qquad (i \neq j = 1,2,3) \tag{3.66b}$$

$$\frac{\partial J}{\partial \sigma_{11}} = -2 \frac{\partial J}{\partial \sigma_{22}} = -2 \frac{\partial J}{\partial \sigma_{33}} = \pm \frac{1}{3^{-\frac{1}{2}}} \tag{3.66c}$$

$$\frac{\partial J}{\partial \sigma_{ij}} = 0 \qquad i \neq j \ , \ (i,j = 1,2,3) \tag{3.66d}$$

$$\frac{\partial \theta}{\partial \sigma_{11}} = -2 \frac{\partial \theta}{\partial \sigma_{22}} = -2 \frac{\partial \theta}{\partial \sigma_{33}} = \frac{1}{q} \cdot \frac{\pm 1 - \sin 3\theta}{\cos 3\theta} \tag{3.66e}$$

$$\frac{\partial \theta}{\partial \sigma_{ij}} = 0 \qquad i \neq j \ , \ (i,j=1,2,3) \tag{3.66f}$$

$$\frac{\partial S}{\partial \sigma_{11}} = -2 \frac{\partial S}{\partial \sigma_{22}} = -2 \frac{\partial S}{\partial \sigma_{33}} = \frac{(2)^{\frac{1}{3}}}{3} \tag{3.66g}$$

$$\frac{\partial S}{\partial \sigma_{ij}} = 0 \qquad i \neq j \ , \ (i,j=1,2,3) \tag{3.66h}$$

where the sign "+" is retained in (3.66e) for q positive; for q negative, the sign "−" is chosen. The relation (3.66e) is defined by continuity and takes a zero value, when θ is equal to $\pm \frac{\pi}{6}$. It is undefined when q is zero, which corresponds to a stress state on the hydrostatic axis. The partial derivatives $\frac{\partial f}{\partial \sigma_{ij}}$ may be calculated from (3.66) and (3.63):

$$\frac{\partial f}{\partial \sigma_{11}} = \frac{\partial f}{\partial I} + \frac{\partial f}{\partial J} \cdot 3^{-\frac{1}{2}} + \frac{\partial f}{\partial S} \frac{(2)^{\frac{1}{3}}}{3} \tag{3.67a}$$

$$\frac{\partial f}{\partial \sigma_{22}} = \frac{\partial f}{\partial \sigma_{33}} = \frac{\partial f}{\partial I} - \frac{1}{2}\left[\pm \frac{\partial f}{\partial J} 3^{-\frac{1}{2}} + \frac{\partial f}{\partial S} \frac{(2)^{\frac{1}{3}}}{3} \right] \tag{3.67b}$$

$$\frac{\partial f}{\partial \sigma_{ij}} = 0 \qquad i \neq j \ (i,j=1,2,3) \tag{3.67c}$$

A similar set of relations may be obtained for the potential function g and its partial derivatives.

From the relations (3.67) and (3.9), the unit vectors respectively normal to the yield surface and the potential surface conform to the axisymmetric conditions as defined in (2.5). Therefore, from (3.41) the

plastic strain increment and consequently the total plastic strain (obtained by integrating the increments) corresponds to the axisymmetric state defined in relations (2.3). The isotropic elastic-plastic model can be formulated in p-q space during axisymmetric loading. Similarly to relation (3.56), the yield surface projection in p-q space is defined

$$f^*(p,q,\xi) = f(I,J,\pm\frac{\pi}{6},\xi) = f(3p,3^{-\frac{1}{2}}|q|,\pm\frac{\pi}{6},\xi) = 0 \qquad (3.68)$$

The unit vector n_p, n_q defined in relations (3.57) becomes

$$n_p = 3\frac{\partial f}{\partial I}\frac{1}{\xi} \qquad (3.69a)$$

$$n_q = \pm\left[\frac{\partial f}{\partial J}3^{-\frac{1}{2}} + \frac{\partial f}{\partial S}\frac{(2)\frac{1}{3}}{3}\right]\frac{1}{\xi} \qquad (3.69b)$$

where

$$\xi = \left[9\left[\frac{\partial f}{\partial I}\right]^2 + \pm\frac{\partial f}{\partial J}3^{-\frac{1}{2}} + \frac{\partial f}{\partial S}\frac{(2)\frac{1}{3}}{3}^2\right]^{\frac{1}{2}} \qquad (3.69c)$$

The sign "+" or "-" is selected as in relation (3.66e).

3.5 A CRITICAL REVIEW OF THE CONVENTIONAL PLASTICITY THEORY APPLICABLE TO SOILS

So far plasticity theory has been presented, dogmatically, by enunciating the concepts without mentioning any weakness. Now, when all the fundamental ideas have been disclosed, the validity of their appli-

cation to the material, soil, may be studied. Adopting the same sequence as in the presentation of plasticity theory, the experimental evidence for yield and plastic potential surfaces (existence and shape) is examined. The problems related to the hardening rules are also investigated. Then theoretical constraints on these surfaces, as enunciated by Drucker, are presented.

3.5.1 Existence of Yield Surface

By definition, a yield surface is a hypersurface in stress space which characterizes, with the yield criterion, the presence or absence of irreversible strain (Section 3.2.1). Introduced by generalization of the yield stress observed in uniaxial test, the existence of such a surface is difficult to demonstrate experimentally when the soil sample is subjected to a combined stress state. If a smooth yield surface exists, a hyperplane tangent to this surface at the stress state σ should be found as shown in Fig. 3.9. This "plane" separates the stress increments leading to plastic strain increments during small loading-unloading cycles about the initial stress state, from those giving only reversible strain. All stress increments staying in this transition plane correspond to neutral loading.

According to the Tatsuoka-Ishihara [3.12] tests, described in Appendix A, such a plane is difficult to exhibit. According to Figs. A.1, for the stress increment XG, only reversible strain occurs, but for XF some plastic strain is present. The yield surface would possess a locally corner-shaped aspect such as represented by Fig. 3.10. A

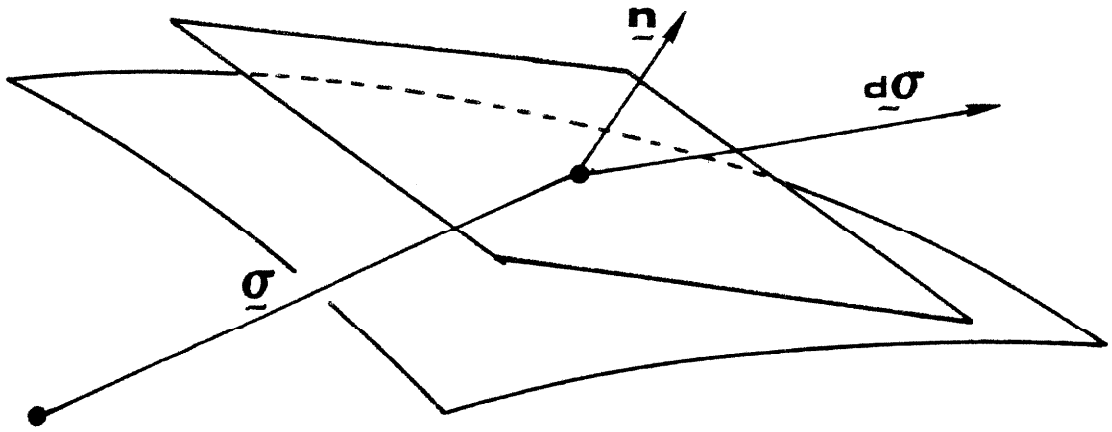

Fig. 3.9. Continuous smooth yield surface and its tangent plane in stress space.

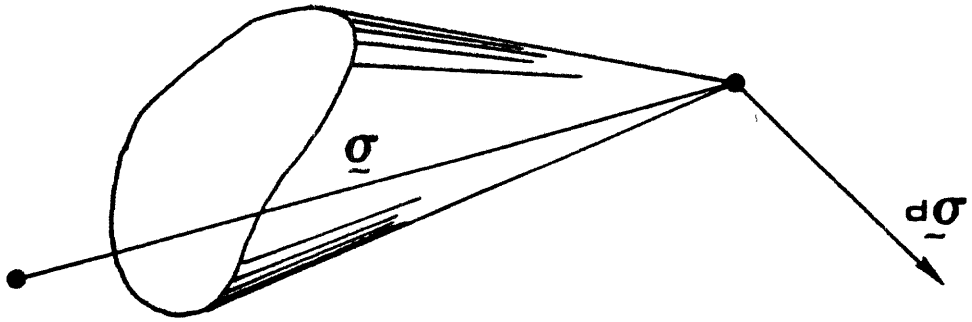

Fig. 3.10. Singular vertex shaped yield surface.

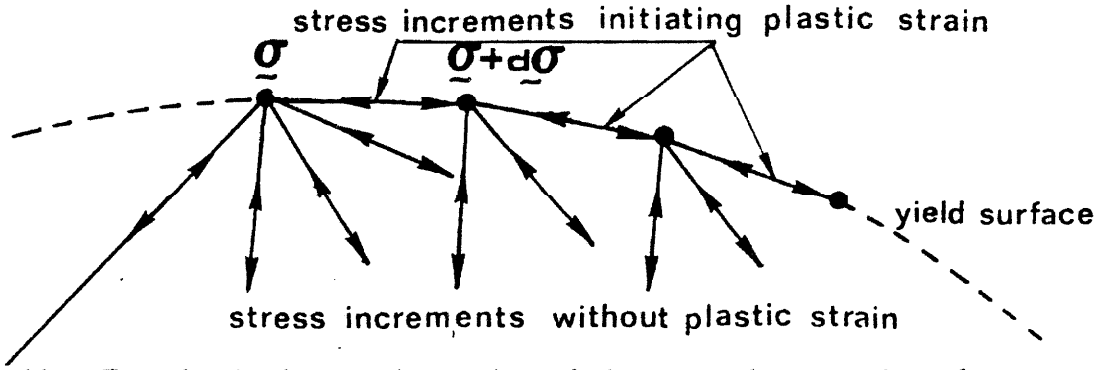

Fig. 3.11. Hypothetical experimental technique to characterize the yield surface by variation of stress increment direction: only stress increments initiating plastic strain generate the yield surface.

similar result was experimentally observed by Scott and Ko [3.11]. But a hypersurface with a vertex is difficult to represent mathematically, and has not been used extensively for soils.

3.5.2 Yield Surface Shape

Once a yield surface is assumed to exist, its shape must be characterized. This task is even more difficult experimentally and must be carried out with caution. One hypothetical experimental way to explore a yield surface is shown in Fig. 3.11. After reaching some stress state $\underline{\sigma}$, the yield surface is determined locally by applying some specific loading–unloading stress cycles from that stress state. From a stress increment creating only reversible strain, the stress increment direction is changed successively. When plastic strains start to appear during such cycles (neutral loading), the new stress state $\underline{\sigma}+d\underline{\sigma}$ lies on the same yield surface, unchanged since only a negligible or eventually very small plastic strain was created. If the same process is repeated about $\underline{\sigma}+d\underline{\sigma}$ a surface may be defined globally by iteration. In spite of its attractiveness, this technique has not been applied experimentally: it requires a testing apparatus in which the stress direction can be altered in every possible way. Avoiding this difficulty Tatsuoka and Ishihara [3.12], in the second experiment presented in Appendix A, have tried a different technique. From a stress point originally located on the yield surface, the stresses followed a stress path in the elastic domain (inside the yield surface). This stress emerges from the elastic domain, i.e., intersects the yield surface, when the strains exhibit

some "significant" changes (Figs. A.9b and A.9c). This intersection, which is the new yield stress, defines another point of the same yield surface. Since the yield surface moves after the intersection, only two points of the same surface are found at different stages of loading. These two points, when close together, characterize the surface locally; this local aspect, assumed to depend only on stress as in relation (A.1), is integrated to give the complete yield surface equation in relation (A.2). However, in order to perform this integration, the yield surface must have a local aspect independent of internal variables. This technique cannot be used to define the influence of the internal variables on the yield surface.

Generally in soil plasticity, the yield surface is smooth for convenience. The yield surface is commonly extrapolated either from the failure surface or from the plastic potential surface. The failure surface is usually fixed in stress space, and is not related to the past loading history; the yield surface is selected with the same analytical expression as the failure surface, but with different parameter values. This method, used by Lade]1.16] for example, relies on a local coincidence of both surfaces at the failure stress. When both surfaces coincide totally at failure, this technique generates a large elastic domain absolutely unrealistic for soil. Furthermore, the flow rule, which governs the plastic flow direction, must become non-associative to compensate for this simplification (e.g., Lade's model). Alternatively to extrapolation from the failure surface, the yield surface is found

from the plastic potential surface, by invoking an associative flow rule. This aspect is investigated in the following. All the questions relevant to the existence and shape of a yield surface may be repeated for a potential surface.

3.5.3 Existence of a Plastic Potential Surface

By definition, a plastic potential surface is a hypersurface in stress space, which gives the plastic flow direction. Any stress increment about a stress state, that points outwards from the yield surface, creates a plastic flow with a constant direction. In other words, the plastic flow direction is independent of the stress increment direction.

Such an independence is not observed in elasticity. The general relations of nonlinear isotropic elasticity may be specified, for axisymmetric loading, in the p-q space, as follows:

$$d\varepsilon_v = \frac{dp}{B} \tag{3.70a}$$

$$d\varepsilon_q = \frac{dq}{3G} \tag{3.70b}$$

where B and G, respectively the bulk and shear modulus, are appropriate functions of the stress state p,q. The ratio $d\varepsilon_q/d\varepsilon_v$ depends linearly on the ratio dq/dp according to the following relation:

$$\frac{d\varepsilon_q}{d\varepsilon_v} = \frac{2}{9}\,\frac{1+\nu}{1-2\nu}\,\frac{dq}{dp} \tag{3.71}$$

where ν, Poisson's ratio, may eventually be a suitable function of stresses. The strain and stress increment directions, respectively represented by the angles θ_σ and θ_ε, with tangent dq/dp and $d\varepsilon_q/d\varepsilon_v$, are plotted in Figure 3.12 for different constant values of Poisson's ratio. θ_ε varies with respect to θ_σ, which indicates that, in elasticity, the strain increment direction depends upon the stress increment direction. Experimental results on soil do not corroborate this dependence, and establish, to some extent, a constant direction for plastic flow. According to the first experiment of Tatsuoka and Ishihara, especially from Fig. A.1, plastic flow was found to have not only one but two different directions, e.g., the vectors OA, OB, OC, and OD have different orientations than the vectors OF and OE in Fig. A.1. This result suggests that the potential surface, like the yield surface, presents a vertex located at the stress state, with two different normals. Each normal depends on the stress increment direction. Such a result unsettles the fundamental concept of plastic potential, by removing the smoothness of this surface, and making it dependent on the stress increment.

3.5.4 Shape of Plastic Potential Surface

Once a smooth plastic potential is assumed, its shape must be defined. Only its local aspect about the stress state is relevant. For instance, in Fig. 3.6, the portion of the plastic potential surface located inside the yield surface is meaningless: plastic strain cannot exist there. The plastic potential surface is defined more easily by

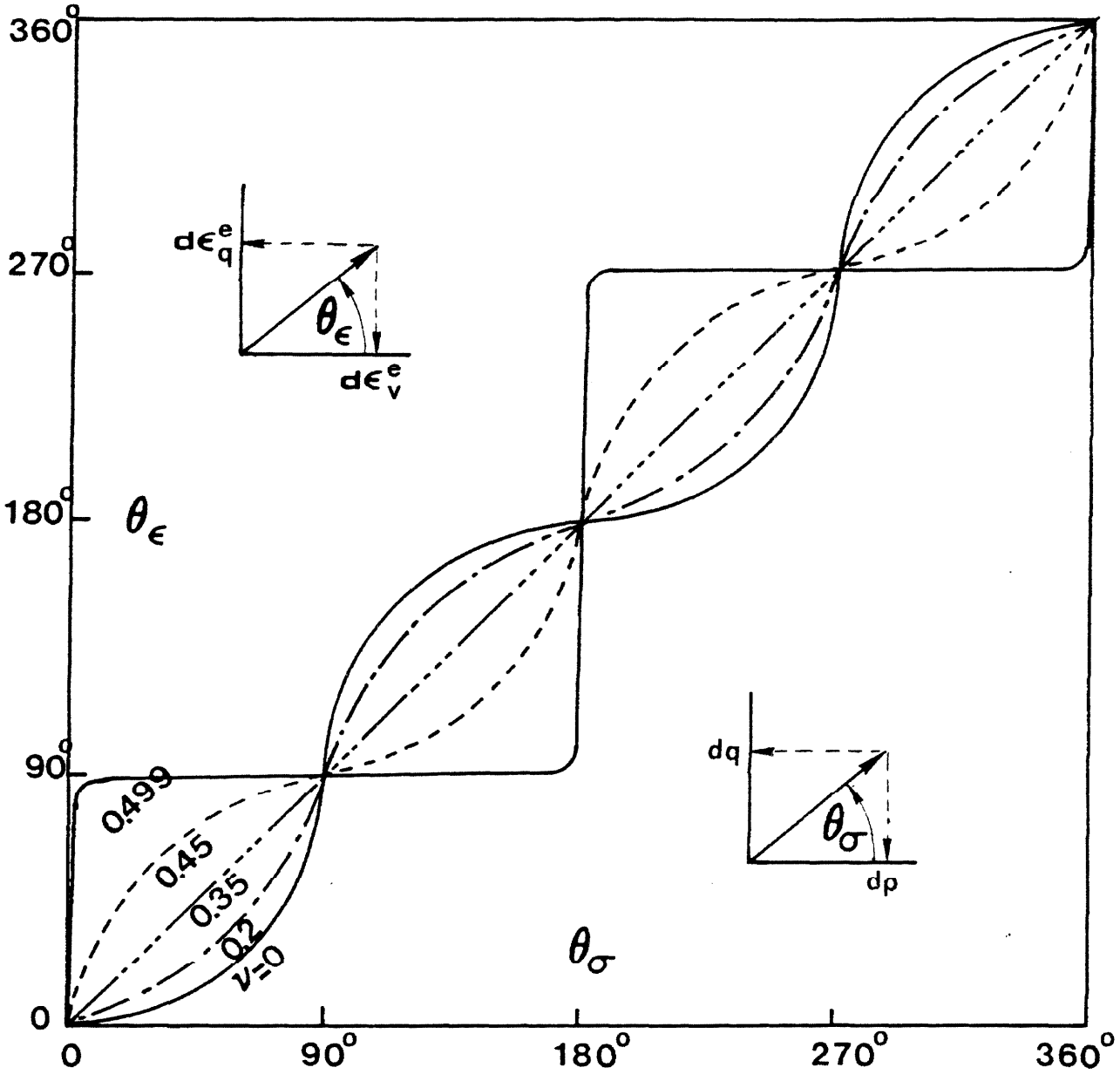

Fig. 3.12. Stress increment direction θ_σ versus strain increment direction θ_ε for linear isotropic elasticity with different values of Poisson's ratio.

experiment than the yield surface. If the plastic flow direction depends only on the stress state, the following technique may be applied to characterize its shape in the p-q space. First, from experimental results obtained from axisymmetric loading tests, the plastic strain increment is calculated at different stress states. These calculations are either performed by neglecting the elastic strain w.r.t. plastic strain or by subtracting the incremental elastic strain $d\underline{\varepsilon}^e$ (calculated with a selected elastic model) from the total strain increment $d\underline{\varepsilon}$. Then the plastic flow direction, characterized by its unit vector m_p, m_q, is related to the stress state p,q: m_p and m_q become known functions of p,q. Finally the plastic potential surface is found by integrating the following equation

$$m_p(p,q)dp + m_q(p,q)dq = 0 \qquad (3.72)$$

3.5.5 Hardening Rules

The motions of any surfaces, yield or plastic potential, as described by the hardening rules, are strongly related to the surface definitions. Once an analytical form has been selected for the surface, such as in equation (3.8a), only the parameters r_k control all changes. For instance, for Lade's models, only one parameter controls the yield surface size and therefore only an isotropic expansion about the hydrostatic axis is possible.

Different hardening rules have been used for soils; all are derived for the isotropic and kinematic hardenings presented for von Mises' model. The kinematic motion, certainly appropriate to soil behavior since it limits the elastic domain, requires more effort; a surface motion must be characterized. For von Mises' surface, this motion was assumed to be collinear to the plastic flow direction. Generally a combined isotropic-kinematic hardening allows a better description of the material response, since it gives more degrees of freedom.

3.5.6 Implications of Drucker's Postulate

While experiments may yield information on the shape of the yield surface, general principles, such as Drucker's postulate [3.3] enforce constraints which its shape must satisfy. This postulate, well known to any plastician, has been the object of a good deal of controversy. It is enunciated in Appendix B and has three major consequences regarding the yield surface.

a) "the plastic strain increment $d\underline{\varepsilon}^p$ points outwards from the yield surface"

b) "the plastic strain increments $d\underline{\varepsilon}^p$ must be normal to the yield surface at $\underline{\sigma}$"

c) the yield surface must be convex

All three consequences are easily proved by considering that the relation (B.5) must hold for any arbitrary initial stress state $\underline{\sigma}^o$ inside the yield surface. The first consequence does not allow strain-

softening and the second one prohibits a nonassociative flow rule. Then Lade's model, for example, violates Drucker's postulate.

The major impact of this postulate is to give restrictions on elastic-plastic models to provide uniqueness in boundary value problems. But these conditions are sufficient, not necessary, to obtain uniqueness.

Drucker's postulate may be invoked in a different way: some real materials exhibit nonunique solutions, when subjected to some prescribed force and/or displacement loading. This nonuniqueness may be expressed by bifurcation from one mode to a different mode of solution, according to slight perturbation on some parameters entering the boundary value problem. This is the case with dense sand which very often switches in the triaxial test from a uniform mode of deformation to a localized deformation along a shear plane. In order to describe such an ability to bifurcate, the model, which represents the material behavior, must not obey Drucker's postulate. A nonassociative flow rule may be sufficient to satisfy this requirement. Rudnicki and Rice [3.9] made use of this comment to represent localization of displacement with plasticity in pressure-sensitive materials.

CHAPTER IV

BOUNDING SURFACE PLASTICITY

Recently, in order to avoid the necessity of defining yield and potential surfaces and their respective motion, new theoretical frameworks, such as the "rate-type" constitutive equations, have been used to describe the rheological soil behavior. The rate-type relations, first qualified by Truesdell [4.6] as hypo-elastic, describe the material behavior in terms of a mathematical series expansion, without any hypersurfaces. The material behavior is not represented with geometrical analogies, but by more and more mathematics, which renders these new constitutive models less attractive to practicing engineers.

As an alternate to the option of completely new theories, conventional plasticity has been adapted to give a better description of material behavior. In 1967, Iwan [4.3] and Mróz [4.4] suggested replacing the single yield surface by several nested yield surfaces. This theory, called multiple yield surfaces plasticity, was applied to soil by Prevost [4.5].

In 1976, adopting a slightly different approach, Dafalias and Popov [4.1] introduced the idea of "bounding surface." This new concept brings new features to conventional plasticity without unduly complicating the mathematical formulation. To some extent, this last adaptation can be perceived as a generalization of conventional plasticity which

brings at the same time more freedom to represent material behavior. In the following, this new theory is linked with our previous presentation of plasticity; its new concepts are first defined from a uniaxial test, and then generalized to a six-dimensional stress space.

4.1 BOUNDING SURFACE IDEAS FROM UNIAXIAL TESTS

A typical material response to a loading-unloading cycle in a uniaxial test is schematized in Fig. 4.1. (Such a schematic behavior may represent metals, soils, or other materials.) Although eventually described by conventional plasticity, this illustrative behavior will be considered, after removal of the elastic strain, from a new and different point of view in Fig. 4.2.

At the beginning of loading, the response is elastic. After exceeding some stress σ^*, the stress-strain curve approaches asymptotically and merges with the bound represented by the straight line XX'. The slope of the response curve at any point is taken as a function of the distance AA', denoted δ, between the stress state and the bound XX'. This function decreases continuously and monotonically from infinity to the slope value of line XX'. The transition between the elastic and elastic-plastic range becomes continuous. The yield stress σ^* may be omitted if the function for the slope takes an arbitrarily large value when the distance δ is less than some quantity δ_{min}. The point A' on the bounding line XX' (Fig. 4.2) is called the "image point." During the plastic loading from A to B, it moves to a new position, B'. The infinitesimal changes of stress state and image point, respectively

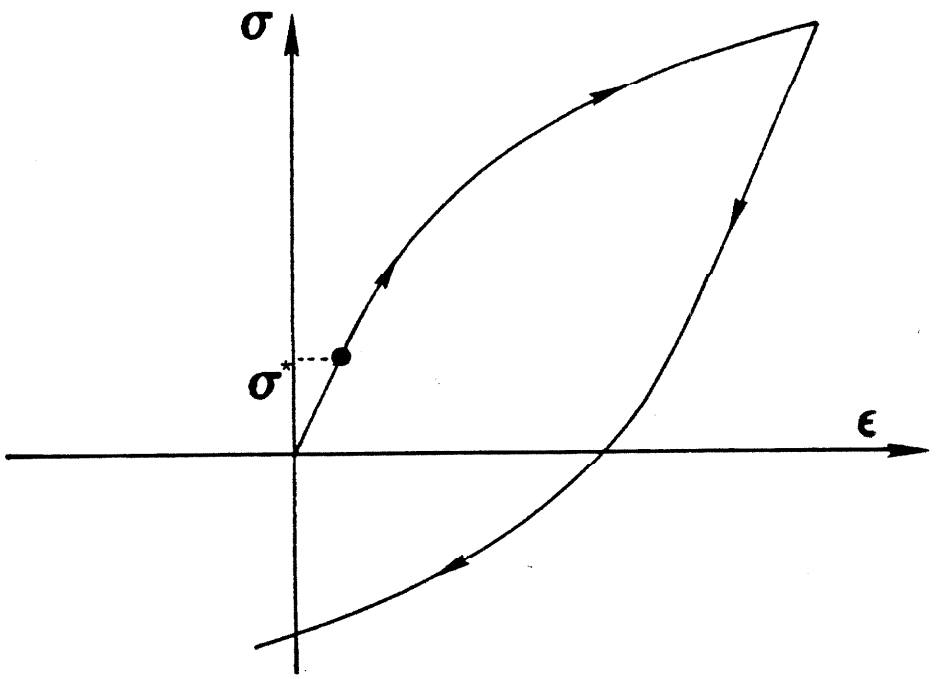

Fig. 4.1. Real typical material response during a loading-unloading cycle.

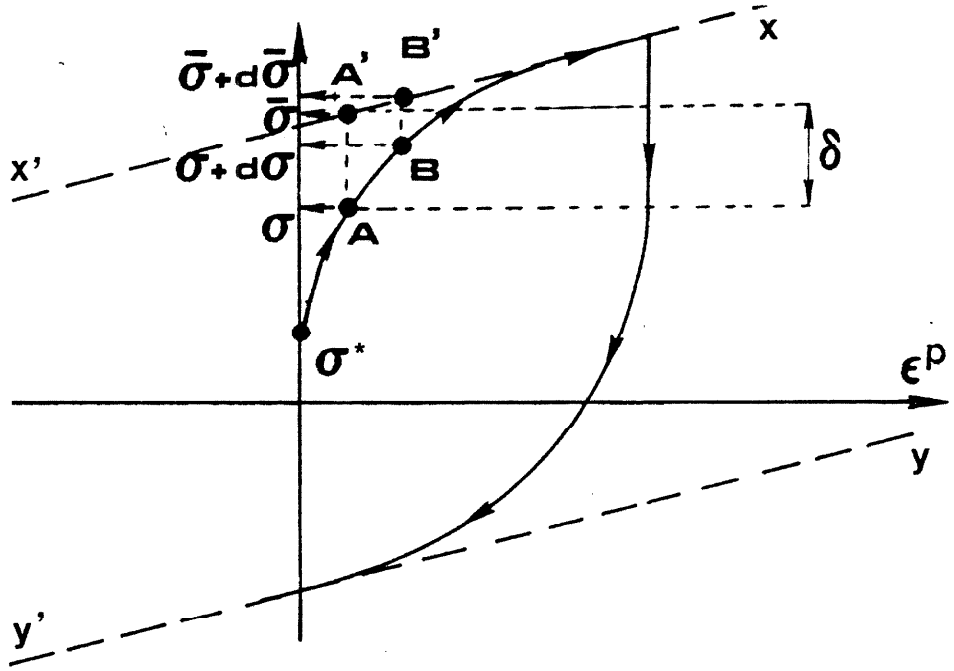

Fig. 4.2. Idealized material response for development of bounding surface plasticity.

denoted $d\sigma$ and $d\bar{\sigma}$, obey the following relation

$$\frac{1}{S} d\sigma = \frac{1}{S_B} d\bar{\sigma} \tag{4.1}$$

where S is the slope of stress-strain curve at A, and S_B the slope of bounding line XX' at A'.

During unloading (Fig. 4.2), the image point is selected now on the other bounding line YY'. All the ideas, defined during the previous loading, apply to describe the unloading response. Thus two new fundamental ideas have been added to conventional plasticity: the bounds and the response dependence upon the distance between the current stress state and these bounds. In conventional plasticity, the material behavior is only described by quantities related to the stress state and its past loading history (such as the yield surface). In bounding surface plasticity, the response also depends upon some exterior bounds corresponding to the maximum admissible stress states.

4.2 GENERALIZATION TO SIX-DIMENSIONAL STRESS SPACE

Applying the same geometrical considerations as in conventional plasticity, the yield stress σ^* becomes a yield surface; similarly, the bounds XX' and YY' transform into a hypersurface called the "bounding surface" (Fig. 4.3). The yield and bounding surfaces move simultaneously in stress space in a coupled way and possibly deform. They may come in contact, but do not intersect; this corresponds to the merging of a stress-strain curve with the bounds in the uniaxial case. All the

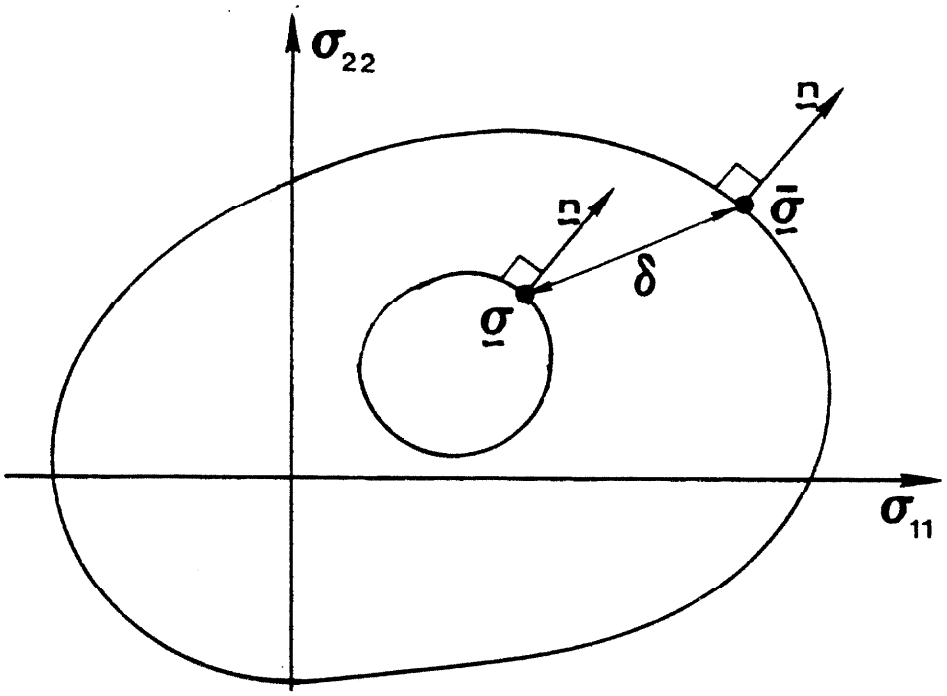

Fig. 4.3. Bounding surface and yield surface in stress space.

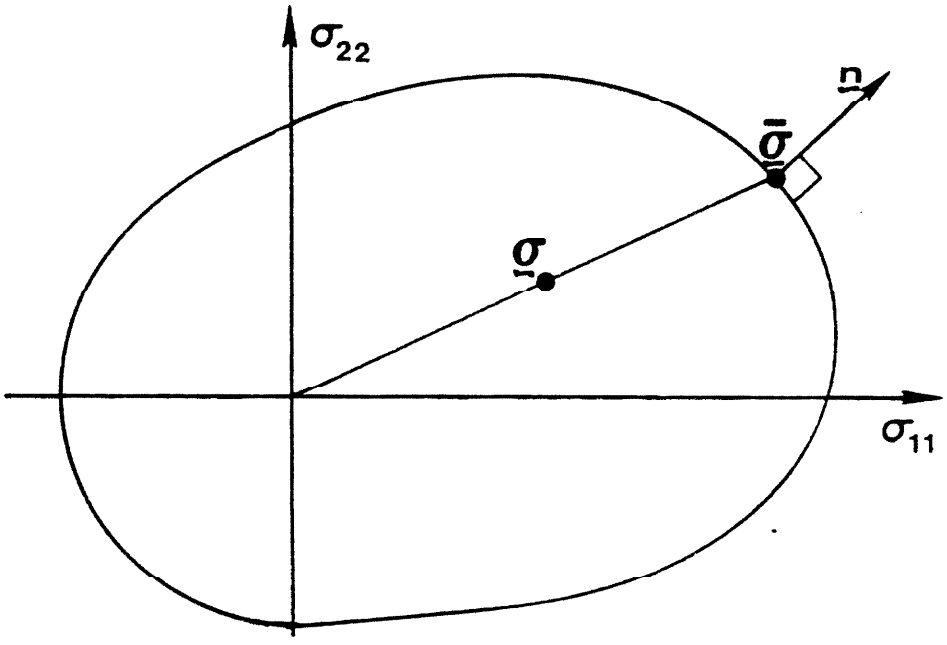

Fig. 4.4. Bounding surface and radial mapping rule in stress space.

internal variables, which control the material memory, are assumed to be dependent on the plastic strain $\underline{\varepsilon}^p$.

The bounding surface has for equation

$$f(\bar{\underline{\sigma}}, \underline{\varepsilon}^p) = 0 \tag{4.2}$$

where $\bar{\underline{\sigma}}$, with Cartesian component $\bar{\sigma}_{ij}$ $(i,j = 1,2,3)$, represents the image point. Among other possibilities, Dafalias and Herrmann [4.2] chooses this point $\bar{\underline{\sigma}}$ such that the yield and bounding surface have collinear normals respectively at $\underline{\sigma}$ and $\bar{\underline{\sigma}}$ (Fig. 4.3). The distance δ between image, $\bar{\underline{\sigma}}$, and stress state, $\underline{\sigma}$, is given by the Euclidean norm of $\sigma\bar{\underline{\sigma}}$ and is expressed in terms of coordinates such as:

$$\delta = [(\bar{\sigma}_{ij}-\sigma_{ij})(\bar{\sigma}_{ij}-\sigma_{ij})]^{1/2} \qquad \text{(sum on i,j=1,2,3)} \tag{4.3}$$

Once these generalizations have been performed, the plastic strain increment is defined, as in conventional plasticity, by specifying successively its existence, direction and amplitude. Plastic flow occurs if the stress increment and the stress state satisfy the yield criterion enunciated in Section 3.2.1. The plastic flow direction is characterized by the unit vector, denoted $\underline{n}$, normal at the image $\bar{\underline{\sigma}}$, and pointing outwards from the bounding surface. This vector is defined by relation (3.9) with substitution of $\bar{\sigma}_{ij}$ for σ_{ij}. Consequently, the

increment of plastic strain and stress increment obey relation (3.41) specialized for an associative flow rule.

However, the plastic flow amplitude, characterized by the plastic modulus H, is now related to the distance δ. This dependence is examined in two steps, depending on whether or not the image point and the stress state coincide.

When both stresses coincide, which corresponds to the merging of the stress-strain curve with the bound XX' of the uniaxial test (Fig. 4.2) and to a distance δ equal to zero, the plastic modulus is found by enforcing the stress state to remain on the bounding surface. This restriction, known as the consistency condition in conventional plasticity, is derived from equation (3.37), by specifying an associative flow rule ($\underline{n} = \underline{n}$) and substituting $\bar{\alpha}$ for $\underline{\alpha}$. It yields the following expression

$$H = H_B = -\left[\frac{\partial f}{\partial \bar{\sigma}_{rs}}(\bar{\underline{\sigma}},\underline{\varepsilon}^p) \cdot \frac{\partial f}{\partial \bar{\sigma}_{rs}}(\bar{\underline{\sigma}},\underline{\varepsilon}^p)\right]^{1/2} \frac{\partial f}{\partial \varepsilon^p_{k\ell}}(\bar{\underline{\sigma}},\underline{\varepsilon}^p)\, n_{k\ell} \qquad (4.4)$$

(sum on $r,s,k,\ell=1,2,3$)

The modulus H obtained in expression (4.4) is denoted by H_B, where the lower index "B" refers to the bounding surface. When the stress state and image points coincide, there is no difference between conventional and bounding surface plasticity. The bounding surface behaves

simultaneously as a yield and potential surface and the plastic modulus H, independent of δ, results from the consistency condition.

In the most general case, the image stress $\bar{\underline{\sigma}}$, the stress state $\underline{\sigma}$ and their respective changes denoted by $d\bar{\underline{\sigma}}$ and $d\underline{\sigma}$, are all different. However the increments $d\underline{\sigma}$ and $d\bar{\underline{\sigma}}$ become related by the consistency condition (3.35) applied to the image instead of the stress state. Using the relation (3.41) specialized for the associative flow rule, and the plastic modulus H_B defined by relation (4.4), the consistency condition (3.35) yields:

$$\frac{1}{H_B}\,\underline{n}\,d\bar{\underline{\sigma}} = \frac{1}{H}\,\underline{n}\,d\underline{\sigma} \tag{4.5}$$

This expression, where H_B given by (4.4) is generally different from H, generalizes the relation (4.1) obtained for the unidimensional state. H is a function of H_B and δ. Additionally, in order to achieve a continuous transition between a purely elastic and an elastic-plastic response, H is assumed to decrease continuously and monotonically from an arbitrarily large positive value when δ is large, to reach the value H_B when δ becomes zero.

4.3 ADVANTAGES OF BOUNDING SURFACE PLASTICITY OVER CONVENTIONAL PLASTICITY

The relation connecting the plastic moduli H, H_B and the distance δ introduces the most important advantage of bounding surface plasticity over conventional plasticity. In conventional plasticity, the plastic

modulus H is calculated as in relation (3.37), directly from the hardening rules, by enforcing the consistency condition. The amplitude of plastic flow is therefore essentially prescribed by a hypersurface motion. But such motions, obviously difficult to characterize, are generally derived from simple rules inspired from the kinematic and isotropic rules as observed in Section 3.2.3 for von Mises' model. Consequently, the plastic flow amplitude cannot be adjusted with much flexibility. This remark becomes particularly important during cyclic loading, when the hardening rules control essentially the predicted response. For instance, in Fig. 4.5, depending upon the selected hardening rule, von Mises' model exhibits very different responses resulting from strain-cycles between two extremes, denoted ε_{min} and ε_{max} respectively. For kinematic hardening the stress-strain curve stabilizes on a closed loop, while, for isotropic hardening, the response becomes purely elastic. In bounding surface plasticity, the changes occurring for the bounding and yield surfaces must also be specified. The plastic modulus H_B is calculated from such a surface motion as indicated in relation 4.4. But now the amplitude of plastic flow is less dependent upon hypersurface motions. The scalar relation between H, H_B and δ provides an additional degree of freedom to describe the material response, even during cyclic loading.

As the second major advantage of bounding surface plasticity, the yield surface may vanish; it may be shrunk to the stress state. In this eventuality, since a normal vector cannot be defined for a zero-sized

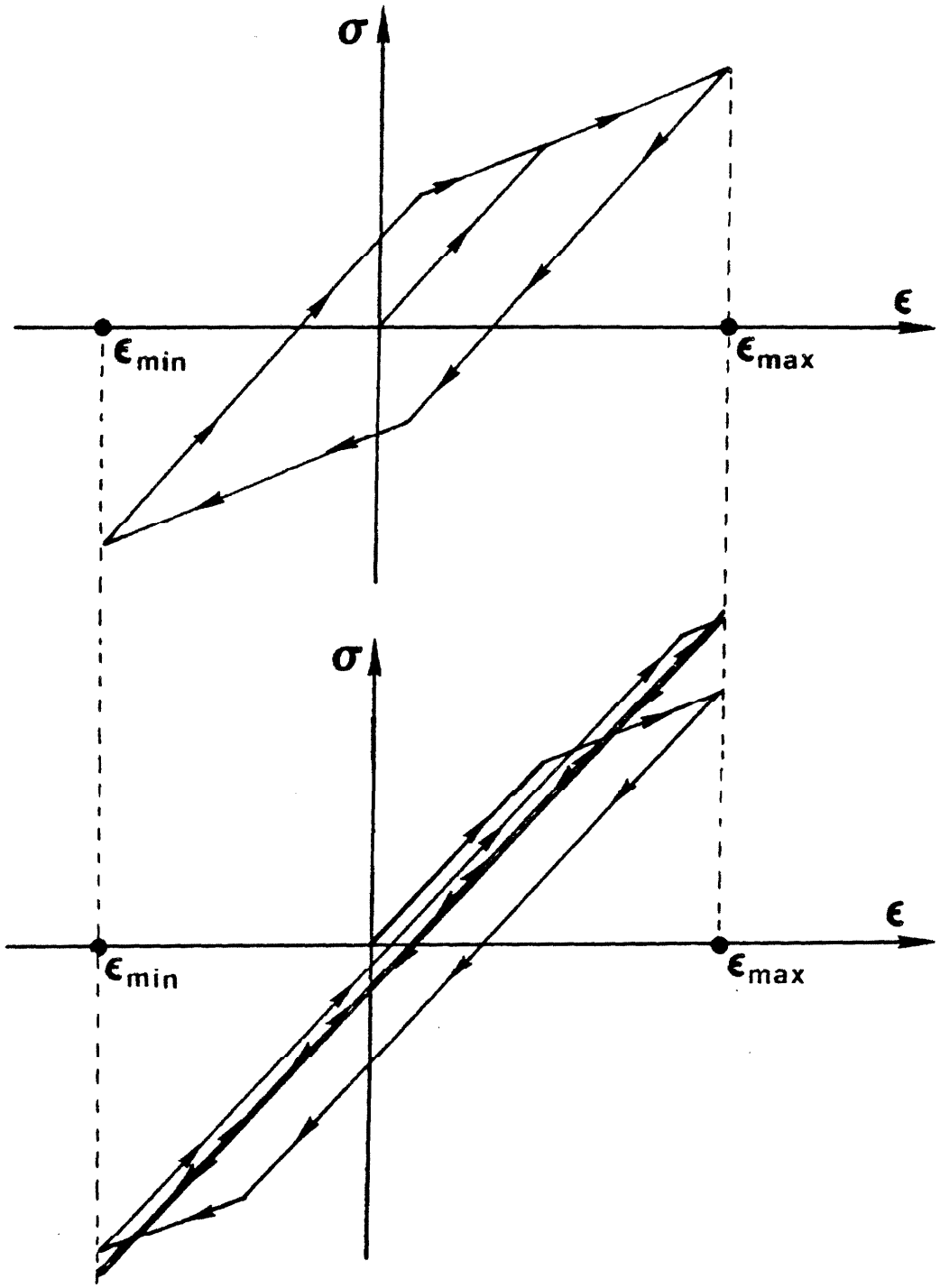

Fig. 4.5. Predicted response by von Mises' model with different hardening rules during strain cycles.

a) kinematic hardening
b) isotropic hardening

surface, a particular relationship, which is called the "mapping rule," must connect the stress state $\underline{\sigma}$ and the image $\bar{\underline{\sigma}}$. For example, Dafalias and Herrmann [4.2] defined the radial mapping so that

$$\bar{\underline{\sigma}} = x\underline{\sigma} \tag{4.6a}$$

or, expressed in terms of components,

$$\bar{\sigma}_{ij} = x\sigma_{ij} \qquad (i,j=1,2,3) \tag{4.6b}$$

where x is a scalar which satisfies the equation:

$$f(x\underline{\sigma}, \underline{\varepsilon}^p) = 0 \tag{4.7}$$

In equation (4.7), both $\underline{\sigma}$ and $\underline{\varepsilon}^p$ are known, while x is the unknown quantity. In other words, the image defined by (4.6) is the intersection of the bounding surface with the straight line passing through the origin of stress and the stress state (Fig. 4.4). In order always to obtain a unique image, the bounding surface must be convex and contain the origin of stress. Additionally, a rule, which specifies a particular point, must be defined when several images are possible. For radial mapping (Fig. 4.4) two points are generally possible: the closest one to the stress state is selected as the image.

Even without a yield surface, a finite elastic domain may be created. For instance, if the plastic modulus H takes on a large

positive value when δ is larger than some arbitrary value δ_{min}, then the response is almost purely elastic.

The radial mapping, as specified in relation (4.6), is only a particular example. Other choices may be considered such as a radial mapping with a pole different of the origin, or eventually a mapping related to the incremental stress direction.

4.4 FORMULATION OF BOUNDING SURFACE THEORY IN P-Q SPACE

The remarks applied to conventional plasticity theory regarding formulation in the p-q space (Sections 3.3, 3.4) still hold. If the bounding surface model is expressed in terms of stress invariants, it is said to be isotropic. In this eventuality, corresponding to axisymmetric stress states and stress increments, the predicted strain states and changes are axisymmetric; the p-q stress space and ε_v-ε_q strain space represent completely the material behavior. The model may be formulated in the simplified p-q space, as described by equations (3.59).

CHAPTER V

APPLICATION OF BOUNDING SURFACE PLASTICITY TO SOIL: A NEW SAND MODEL

5.1 INTRODUCTION

In 1979, Dafalias [5.5,5.6] was the first to apply bounding surface plasticity to soil and, particularly, to clays. In 1979, his model was simply derived from the early Roscoe-Burland model [5.20]: He transformed Roscoe-Burland elliptic yield surface into a bounding surface, and added an arbitrary relation between the plastic modulus H, H_B and the distance δ. As a result of these adaptations, overconsolidated clays, which had only elastic responses according to the Roscoe-Burland model, were now able to exhibit plastic deformation. In 1982, Dafalias and Herrmann [5.7] modified the bounding surface shape in order to improve the description of dilating and strain-softening responses. This new surface is composed of portions of two ellipses connected continuously with a hyperbola. In both model versions, the bounding surface is a yield and a plastic potential surface for normally consolidated clays. For a clay in an overconsolidated state, the bounding surface has a position related to its normally consolidated state. This influence of the overconsolidation ratio renders Dafalias models successful for clays. However, since granular materials depend more on the initial density than on the overconsolidation ratio,

Dafalias' model cannot be applied meaningfully to sands without substantial modifications.

In 1982, Aboim [5.1] proposed a simple bounding surface model for sand, composed of only six parameters. His bounding surface is elliptic, but with a variable aspect ratio, which allows it to match the measured sand response during the triaxial test at constant confining pressure. Although this recent model has not been studied herein as extensively as Dafalias' model, the relation between the plastic moduli H, H_B and the distance δ on it seems arbitrary, and strain-softening is not considered. It is therefore adapted to sands in a loose to medium dense state.

From the literature review, bounding surface plasticity is a new theory and has not yet been applied extensively to sands. Its successful application to metals and clays by Dafalias demonstrates its potential worth and its superiority over conventional plasticity to describe a material behavior, especially during cyclic loadings. A good representation of material cyclic response is particularly important for offshore technology or earthquake engineering. Heavy sea storms subject the foundations or piles of offshore platforms to large periodic wave forces. Although with shorter periods, earthquakes also generate cyclic loadings or structures. Eventually disastrous phenomena, known as soil liquefaction, may result from these cyclic loadings. However, bearing

in mind that complex cyclic loadings is the future goal, the model must first be developed for simple monotonic loadings.

A particular data set from tests on Sacramento River sand is used extensively to present the new model. These test results were published by Seed and Lee [5.12,5.23] and, were personally communicated to the author by Lade in their original and detailed laboratory data format. These experimental results, one of the few consistent set of tests that have been published on sands, are accepted by most researchers as reliable; they truly represent the rheological sand behavior. Although based principally on this data set, the new model may be applied to any sand, as it is founded on general observations of sand behavior.

The model presentation is adapted to the available laboratory experiments. Since all the tests were performed in the axisymmetric state of stress and strain as defined in Sections 2.2 and 2.3, the new model is formulated in the p-q stress space. First, the elastic contribution to the elastic-plastic material response is investigated; most elastic models used for sand are incorrect and need to be altered in order to conserve energy. Then the plastic contribution is examined with a new technique, which consists of following the incremental material behavior with an interactive computer code [5.2]. The computer has been used in soil modeling previously mostly to perform step-by-step integration, which leads ultimately to numerical predictions of soil behavior. But it has not been used commonly for the elaboration of a constitutive equation. Here it introduces a systematic exploration of

test results, and allows us to isolate some particular aspect of the material response. Although the experimental data were too sparse to be fully compatible with this new technique, a lot of useful information was extracted. For instance, the experimental direction of plastic flow was elucidated by this method and consequently a new bounding surface equation, different from Dafalias and Aboim's surfaces, is proposed. Following the bounding surface definition, its motion is specified by selecting an appropriate internal variable. Finally, from the plastic flow amplitude given also by the computer code, a relation between the moduli H, H_B and the distance δ is proposed. Arbitrarily selected by Dafalias and Aboim, this relation is investigated in more detail in this presentation.

Thus a new constitutive relation is established for sand. Once it has been fully derived in p-q space, it is extended to the six-dimensional stress state by invoking isotropy and a specific contribution of Lode's angle.

As an illustration, all the model constants are calculated for the dense Sacramento River sand. Finally the predicted sand behavior, obtained by numerical integration of the new constitutive equation, is compared not only to real experimental results, but also to another numerical predictions given by a different sand model.

5.2 ELASTIC CONTRIBUTION

According to relation (3.5), the strain increment is the sum of two simultaneous increments: one elastic and the other plastic. However, the plastic increment may vanish in some particular conditions and leaves the strain increment purely elastic. Such conditions are met exactly during unloading (the stress state moves inside the yield surface) or approximately at the beginning of loading (the plastic strain are negligible w.r.t. the elastic one). This last approximation must be considered with caution for the stress state lie on the yield surface. All the remarks on how to isolate the elastic response from the total response pertain for bounding surface plasticity: only stress reversals give accurate experimental data to characterize the reversible sand behavior.

5.2.1 Preliminary Remarks on Elastic Sand Models

For most of the elastic-plastic sand models, the elastic contribution is *isotropic* but *nonlinear*. *Isotropy* is a convenient hypothesis, since it lowers the number of elastic moduli to two; these two quantities are selected from Young's modulus E, Poisson's ratio ν, bulk modulus B or shear modulus G. Lame's modulus λ is rarely used in soil mechanics. All the preceding quantities are related as shown in Table 5.1. The nonlinearities are usually related to a pressure dependence. For instance, the bulk modulus is often selected as the following power function of the mean pressure p,

TABLE 5.1. RELATIONS AMONG ELASTIC QUANTITIES [5.25]

	G	E	ν	B
G,E			$\frac{E-2G}{2G}$	$\frac{GE}{3(3G-E)}$
G,ν		$2G(1+\nu)$		$\frac{2G(1+\nu)}{3(1-2\nu)}$
G,B		$\frac{9GB}{3B+G}$	$\frac{3B-2G}{2(3B+G)}$	
E,ν	$\frac{E}{2(1+\nu)}$			$\frac{E}{3(1-2\nu)}$
E,B	$\frac{3EB}{9B-E}$		$\frac{3B-E}{6E}$	
ν,B	$\frac{3B(1-2\nu)}{2(1+\nu)}$	$3B(1-2\nu)$		

$$B = B_o p^n \tag{5.1}$$

where B_o and n are material constants. Since Poisson's ratio is always difficult to measure accurately, it is commonly assumed to be equal to a constant ν_o; for most soils, ν_o is selected between 0.2 and 0.3. In this eventuality, from Table 5.1, Young's and shear moduli become also power functions as in expression (5.1), with the same exponent but different constants.

However, although commonly used in practice, the elastic models using relation (5.1) and a constant Poisson's ratio are not satisfactory: they dissipate or create some work during a closed stress cycle. A short proof of this assertion follows in the particular axisymmetric loading defined in sections (2.2) and (2.3). By definition, the incremental work dW corresponding to incremental strain $d\varepsilon_v^e, d\varepsilon_q^e$ about a stress state p,q is such as

$$dW = p d\varepsilon_v^e + q d\varepsilon_q^e \tag{5.2}$$

Substituting the elastic relations (3.70), dW is rewritten

$$dW = \frac{p}{B}\, dp + \frac{q}{3G}\, dq \tag{5.3}$$

In order for dW, which depends only upon the variables p and q, to be stress-path independent, dW must have a differential form; the following condition must be satisfied:

$$\frac{\partial}{\partial p}\left[\frac{q}{3G}\right] = \frac{\partial}{\partial q}\left[\frac{p}{B}\right] \tag{5.4}$$

If Poisson's ratio is constant, and the bulk modulus depends only upon p, relation (5.4) is not satisfied since each term can be written

$$\frac{\partial}{\partial p}\left[\frac{q}{3G}\right] = -\frac{2}{3}\frac{1+\nu_o}{1-2\nu_o}\frac{q}{B^2}\frac{\partial B}{\partial p} \neq 0 \tag{5.5a}$$

$$\frac{\partial}{\partial q}\left[\frac{p}{B}\right] = -\frac{p}{B^2}\frac{\partial B}{\partial q} = 0 \tag{5.5b}$$

As a consequence of (5.5), some work W is created or dissipated during closed stress cycles and the work W becomes dependent on the stress path. This result may be illustrated with two simple stress paths and a closed stress cycle as shown in Figure 5.1. These paths, located in the p-q space, connect an initial state (p_i,q_i) and a final state (p_f,q_f). Along the first path, defined by the successive state (p_i,q_i), (p_i,q_f) and (p_f,q_f), the work done is

$$W_1 = \frac{1}{3G(p_i)}\int_{q_i}^{q_f} q\,dq + \int_{p_i}^{p_f}\frac{p\,dp}{B(p)} \tag{5.6a}$$

Along the second path, which differs from the first one by the intermediate state (p_f,q_i), the work is

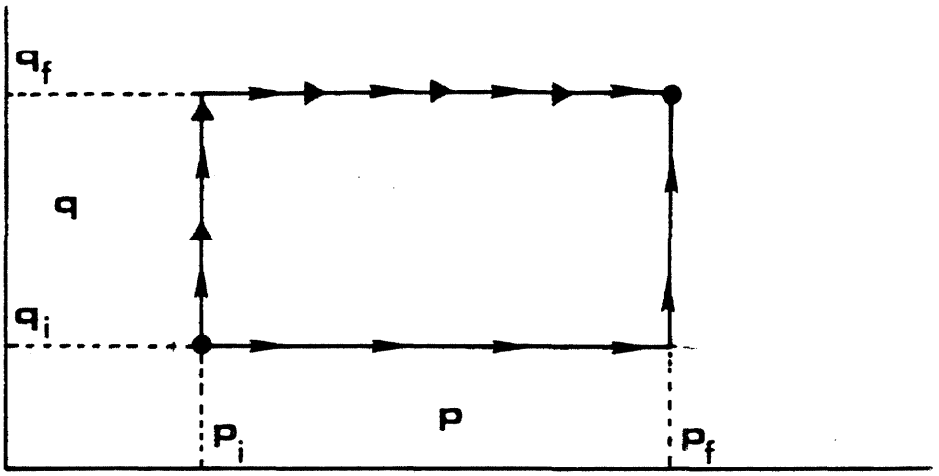

Fig. 5.1. Stress paths and stress cycle to calculate energy for a nonlinear isotropic elastic model.

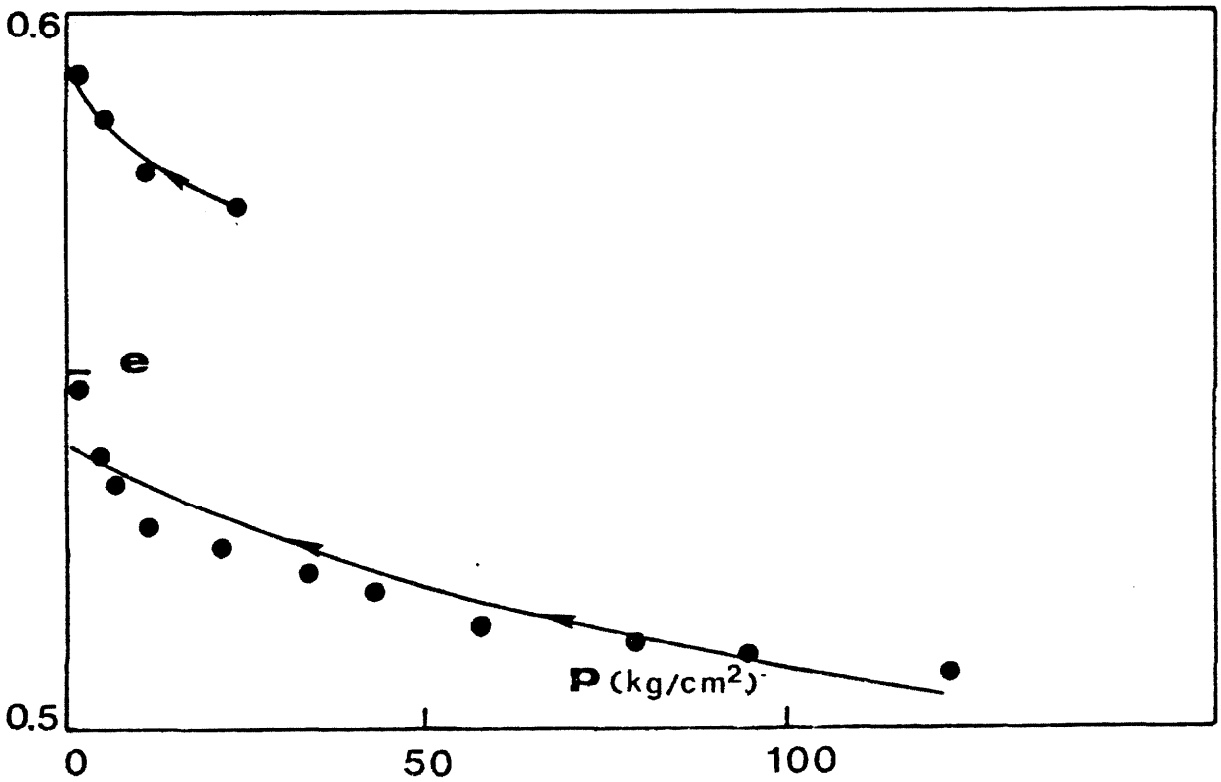

Fig. 5.2. Fitting of isotropic unloading test on the dense Sacramento River sand with the selected nonlinear elastic model.

$$W_2 = \frac{1}{3G(p_f)} \int_{q_i}^{q_f} q\,dq + \int_{p_i}^{p_f} \frac{p\,dp}{B(p)} \qquad (5.6b)$$

By virtue of expression (5.1) and Table 5.1, $G(p_i)$ is different from $G(p_f)$, if p_i differs from p_f. The work W depends on the stress paths relating initial and final state. Along the closed stress path, formed by following the first path and reversing the second path, the work is

$$W_c = W_1 - W_2 = \frac{1}{6}\left[q_f^2 - q_i^2\right]\left[\frac{1}{G(p_i)} - \frac{1}{G(p_f)}\right] \qquad (5.6c)$$

Since the work W_c is positive, energy is dissipated during this stress cycle.

This theoretical deficiency of the elastic model may be easily corrected by changing the relation (5.1). Instead of depending only upon p, the bulk modulus becomes a function of p and q with the restriction that it satisfies relation (5.1) for the particular isotropic loading (q = 0). Poisson's ratio is still assumed constant. The equation (5.5) is a partial differential equation: the unknown function B with variables p and q satisfies the boundary conditions given by relation (5.1) when q equals to zero and p is positive. The solution of this boundary value problem is:

$$B(p,q) = B_o\left[p^2 + \frac{2}{9}\frac{1+\nu_o}{1-2\nu_o}\,q^2\right]^{\frac{n}{2}} \qquad (5.7a)$$

where B_o and n are the same constants as defined in (5.1). This result, obtained for axisymmetric states, was generalized to the six-dimensional stress space by Loret [5.13]; in this case, the bulk modulus B is such that:

$$B(\sigma) = \frac{B_o}{3(1-2\nu_o)}\left[(1+\nu_o)\sigma_{ij}\sigma_{ij} - \nu_o(\sigma_{kk})^2\right]^{\frac{n}{2}} \qquad (5.7b)$$

(sum on i,j,k=1,2,3)

The corrections (5.7) apply only when Poisson's ratio is constant and when the bulk modulus is a power function of the mean pressure during the isotropic test. This corrective technique, which involves the solution of partial differential equation (5.4) with boundary conditions, may be generalized to any nonlinear isotropic elastic models, where two elastic moduli are arbitrary functions of the stress. For instance the shear modulus G is often assumed to be a function of the mean pressure p, while the bulk modulus B remains constant. Such an assumption violates clearly the relation (5.4) and may be corrected. However, nonlinear elastic models, which are defined from a strain energy function, always satisfy the expression (5.4). Investigated only by a few researchers, e.g., Chang, Ko, Westman and Scott [5.4], such models are

rarely used in constructing elastic-plastic soil models.

5.2.2 Choice of an Elastic Model

The corrected elastic model, as defined in the relations (5.7) is selected to represent the elastic contribution in the new elastic plastic model. The two material constants, B_o and n, are defined from isotropic cyclic tests. Poisson's ratio ν_o is arbitrarily chosen equal to 0.2. From relation (5.7a), this particular elastic model predicts that both the bulk and Young's moduli increase with the stresses p and q. Adopted for convenience and theoretically correct, this assertion has not been validated or refuted by any test found in the literature. However, if such a result was found not to comply with experimental data, Poisson's ratio may be selected as mean pressure dependent.

5.2.3 Calculation of Elastic Material Constants

The calculation of the material constants B_o and n are performed for the dense Sacramento River sand from two cycles of loading-unloading during an isotropic test. During isotropic tests, relations (5.7a) and (5.1) coincide. The incremental relation (3.70) is integrated from an arbitrary initial state $p_o, (\varepsilon_v^e)^o$ to the present state:

$$\varepsilon_v^e - (\varepsilon_v^e)^o = \frac{1}{B_o(1-n)} \left[p^{1-n} - p_o^{1-n}\right] \qquad (5.8)$$

In particular if the unloading is carried to zero pressure, (p_o is zero) relation (5.8) becomes:

$$\varepsilon_v^e - (\varepsilon_v^e)^o = \frac{1}{B_o(1-n)} p^{1-n} \qquad (5.9)$$

After taking the logarithm of (5.9), a linear regression technique is applied to the experimental data points in order to calculate B_o and n; it gives for the Sacramento River sand the values in Table 5.2. All the calculations were performed with a small programmable hand calculator [5.8]. A linear regression analysis was applied successively to each cycle, then to both cycles. Although the values differ slightly, relation (5.1) describes with good accuracy the bulk modulus dependence upon the mean pressure p, as shown in Figure 5.2. The parameters B_o and n, obtained by Lade [5.10], are also shown in Table 5.2.

5.2.4 General Remarks and Suggestions for Future Elastic Model

Within the context of bounding surface plasticity, the elastic contribution may be considered from a new point of view. When the stress state is far away from the bounding surface (δ large), the response is elastic; the strain increment corresponding to a given stress increment is small. On the other hand, when the stress state lies on the bounding surface, the strain increment, essentially plastic, is large. The continuous transition from the elastic to the elastic-plastic range, i.e., between small and large strain increments, is maintained since the plastic modulus H is a continuous function of the distance δ.

TABLE 5.2. ELASTIC CONSTANTS B_0 AND n FOR THE DENSE SACRAMENTO RIVER SAND

	B_o	n
First unloading only	829.5	0.28
Second unloading only	579.5	0.63
First and second unloadings (average)	729.0	0.47
Values given by Lade [5.10] $B_o = \frac{E_o}{3(1-2\nu)}$, $E_o = 1680$, $\nu = 0.2$	933.3	0.57

Contrary to general practice in elastic-plastic models, the elastic contribution may be coupled with the plastic response. The elastic parameters, such as the bulk and shear modulus, may depend not only upon the stress but upon the internal variables. When no plastic strains are created, i.e., when the internal variables are unchanged, the elastic model still predicts no energy dissipation or creation. When plastic flow occurs, the elastic moduli become dependent on the internal variables, and the elastic model may create or dissipate energy, which anyway becomes meaningless since energy is dissipated at the same time by plastic strain.

Such an elastic-plastic coupling, if used in the future, will allow a better description of densification. For instance in order to represent the densification of Sacramento River sand, the material constants B_0 and n may be selected as functions (in addition to stress) of internal variables, such as the plastic volumetric strain.

5.3 DIRECTION OF PLASTIC FLOW

Once the elastic contribution has been defined, the plastic strain increment needs to be characterized, successively by its direction, and its amplitude; its existence is specified afterwards. As mentioned in section 4.2, bounding surface plasticity theory predicts that the plastic flow direction is collinear with the normal to the bounding surface at the image point. As in conventional plasticity, the plastic flow direction is not related to the stress increment direction, and depends on the present stress state. This stress-dependence must respect, as

much as possible, well-known and observed aspects of the behavior of granular material, in particular, the three main concepts known as the critical state, the characteristic state and the stress-dilatancy relations. Each of these points, which are first reviewed and then verified for the dense Sacramento River sand, enforce constraints on the relation between plastic flow direction and stress state, and consequently on the possible shape of the bounding surface. Ultimately, a bounding surface is selected; its prediction of the plastic flow direction is compared with real values obtained for the Sacramento River sand. Since the bounding surface equation is established from general observations on granular material, it may be applied to any sand.

5.3.1 Critical State

As defined by Schofield and Wroth, [5.22] the critical state in soil mechanics is an asymptotic state, eventually reached during loading, characterized by no volume change, no stress change and infinite deviatoric strain: "It is as if the material has melted under stress."

For axisymmetric states of stress and strain, this definition is translated into the following mathematical terms:

$$d\varepsilon_v = 0 \quad , \quad d\varepsilon_q = \infty \tag{5.10a}$$

$$dp = dq = 0 \tag{5.10b}$$

According to Schofield and Wroth, the critical state has a location in the p-q-e space given by the following relations:

$$q = M_c p \quad , \quad \text{if } q > 0 \tag{5.11a}$$

$$q = M_e p \quad , \quad \text{if } q > 0 \tag{5.11b}$$

$$e = \Gamma - \lambda n(p) \tag{5.11c}$$

It is defined only by four material constants:

Γ value of critical void ratio at unit mean pressure.

λ slope of critical state line projection in $\ln(p)$-e plane.

M_c, M_e slopes of projection of critical state lines in p-q plane corresponding to positive and negative deviatoric stress.

For a clay, normally or slightly overconsolidated, the critical state line is unique, and its projection in the $\ln(p)$-e plane is parallel to the virgin consolidation line (response of a normally consolidated sample to an hydrostatic compression). It does not depend on the previous loading history of the material.

For most sands, the critical state is difficult to exhibit experimentally. As observed by Lade [5.11] and other experimentalists, the strains within a sand sample become often non-uniform, for instance, due to a strain-localization such as a shear band. The volume measurement, generally performed with interstitial water saturating the sample, underestimates the volumetric strain in the shear band, active part of the sample. The discontinuities, even more accentuated in the presence

of large deformation (e.g., 20% of axial strain in triaxial test), render the asymptotic critical state more difficult to determine experimentally in sands.

However, the critical state remains a valid assumption in the case of the Sacramento river sand. In Fig. 5.3, the experimental points of void ratio versus mean pressure at critical state obey a relation similar to (5.11c) for drained and undrained tests at different confining pressures. The critical state for sands depends on the initial sand density, and is not parallel to the isotropic consolidation response curve.

By applying a linear regression analysis to the data of Tables 5.3, corresponding to the equation (5.13), the following values were found (Fig. 5.4):

dense sand : $M_c = 1.38$, $\Gamma = 0.88$, $\lambda = 0.088$

and

loose sand : $M_c = 1.35$, $\Gamma = 1.0$, $\lambda = 0.084$

Within the context of an elastic-plastic theory, the critical state requires the plastic strain increment to be parallel to the q axis, which means that the unit vector defining the plastic flow direction has the following components:

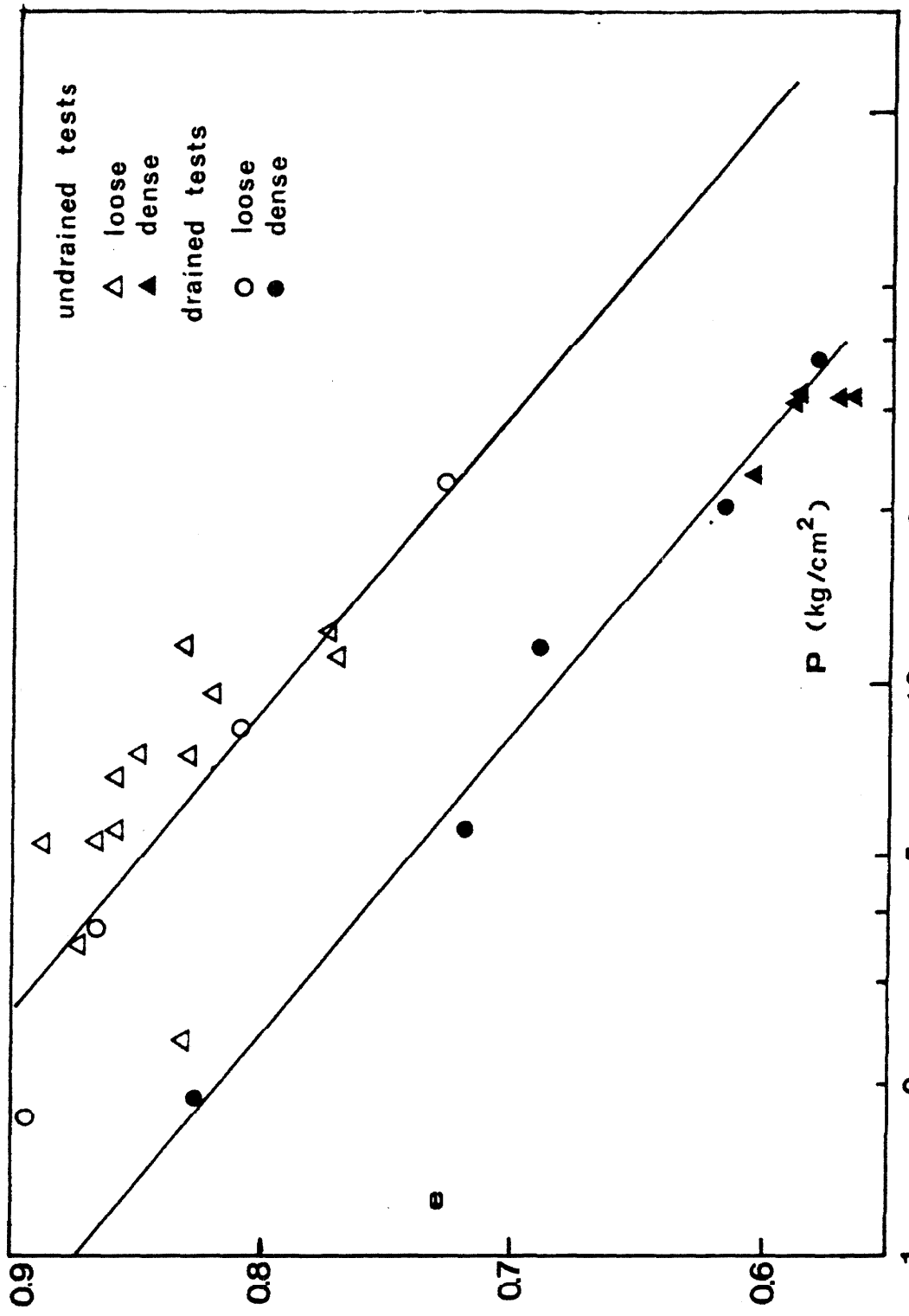

Fig. 5.3. Critical state for the loose and dense Sacramento River sand obtained from drained and undrained tests at different confining pressures.

TABLE 5.3a CRITICAL STATE DATA FROM DRAINED AND UNDRAINED TESTS ON DENSE SACRAMENTO RIVER SAND (AFTER SEED [5.12,5.23])

Initial Void Ratio e_0	Initial Confining Pressure (kg/cm^2)	Critical Void Ratio	p kg/cm^2	q kg/cm^2	M
0.638	1	0.826	1.88	2.64	1.40
0.629	3	0.719	5.51	7.53	1.37
0.61	6	0.691	11.43	16.3	1.43
0.592	10.5	0.617	19.53	27.09	1.39
0.576	20	0.576	35.47	46.4	1.31
0.628	1	0.628	3.82	5.92	tests
0.606	10.5	0.606	23.0	34.7	excluded
0.587	15.1	0.587	31.8	47.5	(cavitation)
0.587	20.2	0.587	30.63	43.6	1.42
0.571	29.9	0.571	30.7	43.2	1.41
0.564	40.1	0.564	31.8	41.2	1.30

TABLE 5.3b CRITICAL STATE DATA FROM DRAINED AND UNDRAINED TESTS ON LOOSE SACRAMENTO RIVER SAND (AFTER SEED [5.12,5.23])

Initial Void Ratio e_0	Initial Confining Pressure (kg/cm^2)	Critical Void Ratio	p kg/cm^2	q kg/cm^2	M
0.867	0.94	0.895	1.7	2.33	1.36
0.860	2.0	0.867	3.72	5.16	1.39
0.850	4.5	0.827	8.19	11.07	1.35
0.830	12.65	0.728	22.52	29.6	1.31
0.883	0.3	0.883	2.3	3.17	1.38
0.874	1.	0.874	3.51	4.87	1.39
0.891	1	0.891	5.21	7.03	1.35
0.859	3.	0.859	5.48	7.31	1.33
0.868	3.	0.868	5.25	6.86	1.31
0.860	5.	0.860	6.77	9.13	1.35
0.833	8.44	0.833	11.36	15.41	1.36
0.848	10.80	0.848	7.62	10.41	1.37
0.832	12.65	0.832	7.75	10.79	1.40
0.821	20.00	0.821	9.47	13.10	1.38
0.770	29.9	0.770	11.20	15.0	1.34
0.774	40.1	0.774	11.97	14.0	1.17

$$n_p = 0 \qquad (5.12a)$$

$$n_q = 1 \qquad (5.12b)$$

The critical state implies also that the amplitude of the plastic strain increment is infinite, i.e., the plastic modulus H becomes zero.

5.3.2 CHARACTERISTIC STATE

First observed experimentally by Shibata and Karube [5.24], the "characteristic state" was defined Luong [5.15] as the stress state where the rate of volumetric strain becomes equal to zero. Different from the critical state, which is always obtained for large strains, the characteristic state corresponds to small deformations. But like the critical state, the characteristic state is independent of the initial density. The characteristic state separates the contracting and dilating behaviors (Fig. 5.4). The contraction occurs in the subcharacteristic region, which is bounded in the p–q plane by the characteristic state lines, and the dilation takes place in the supercharacteristic region.

According to Luong's experiments on Fontainebleau sand, the characteristic state lines are similar to the critical state lines of relation (5.11):

$$q = M^*_c \cdot p \quad , \quad \text{if } q > 0 \qquad (5.13a)$$

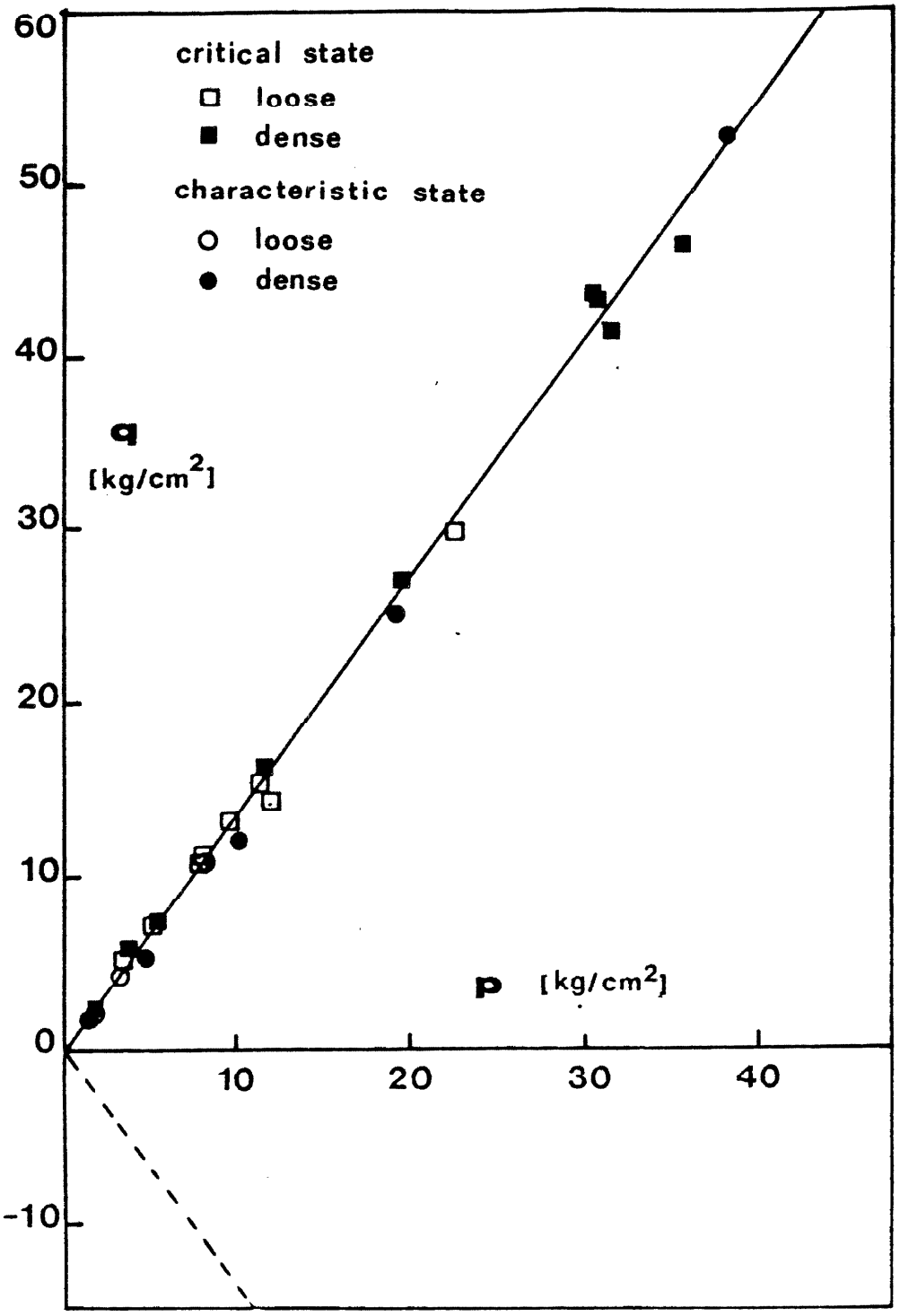

Fig. 5.4. Characteristic state line from drained tests at different confining pressures and critical state line from drained and undrained tests at different confining pressures; all tests are performed on the loose or dense Sacramento River sand.

$$q = M^*_e \cdot p \quad , \quad \text{if } q < 0 \qquad (5.13b)$$

where M^*_c, M^*_e are two material constants, generally slightly different from M_c and M_e. The dense Sacramento River sand obeys also relation (5.13a), as shown in Fig. 5.4.

However Luong's characteristic state is not satisfactory. Tensile triaxial tests at constant confining pressure performed by Robinet [5.19] have shown that some dense sands dilate continuously from the beginning of deviatoric loading. This absence of contraction implies that the subcharacteristic domain does not exist and consequently violates Luong's characteristic state. This deficiency may be avoided if the characteristic state is redefined as the stress state where the rate of plastic (instead of total) volumetric strain becomes equal to zero. This new state is still defined by the relations (5.13). But the continuous dilation observed by Robinet [5.19] in tensile test is now justified: the elastic volumetric strain may be negative (dilating) and larger in absolute value than the positive plastic strain (contracting), so that the total volumetric strain is negative (dilating). Within the context of plasticity, the characteristic state, like the critical state, requires the unit vector, collinear to the plastic flow, to satisfy relations (5.12), while the stress state satisfies (5.13). However, no condition is imposed on the plastic modulus H.

The "characteristic state" is an attractive feature to represent the cyclic behavior of sand, which may be illustrated by the complex

cyclic test performed by Luong [5.14] and shown in Fig. 5.5. During this drained test at constant confining pressure, eight successive series of twenty cycles of deviatoric stress q were applied to Fontainebleau sand. These cycles had a constant amplitude (0.1 MPa), are centered for different values of the ratio q/p, and were distributed on both sides of the characteristic state line (Fig. 5.5a). The resulting volumetric strains, which are shown versus q in Fig. 5.5b, change in agreement with the characteristic state. In the subcharacteristic domain, when the ratio q/p is between -0.75 and 1.26, densification is observed, whereas, in the supercharacteristic domain, dilation is recorded. The characteristic line remains fixed even during such a complex cyclic loading history.

5.3.3 Stress-Dilatancy Theories

All stress-dilatancy theories have one common goal: to explain how granular material dilates while it is subjected to shear stresses. Since they give qualitative and quantitative information on the direction of the strain increment, they, together with the characteristic and critical states, are useful for characterizing the plastic flow direction. The first of these theories was developed in 1962 by Rowe [5.21] and placed on a mathematical basis in 1965 by Horne [5.9]. Since then, other theories have appeared: Tatsuoka [5.27], Nova [5.17], Momen and Ghaboussi [5.16].

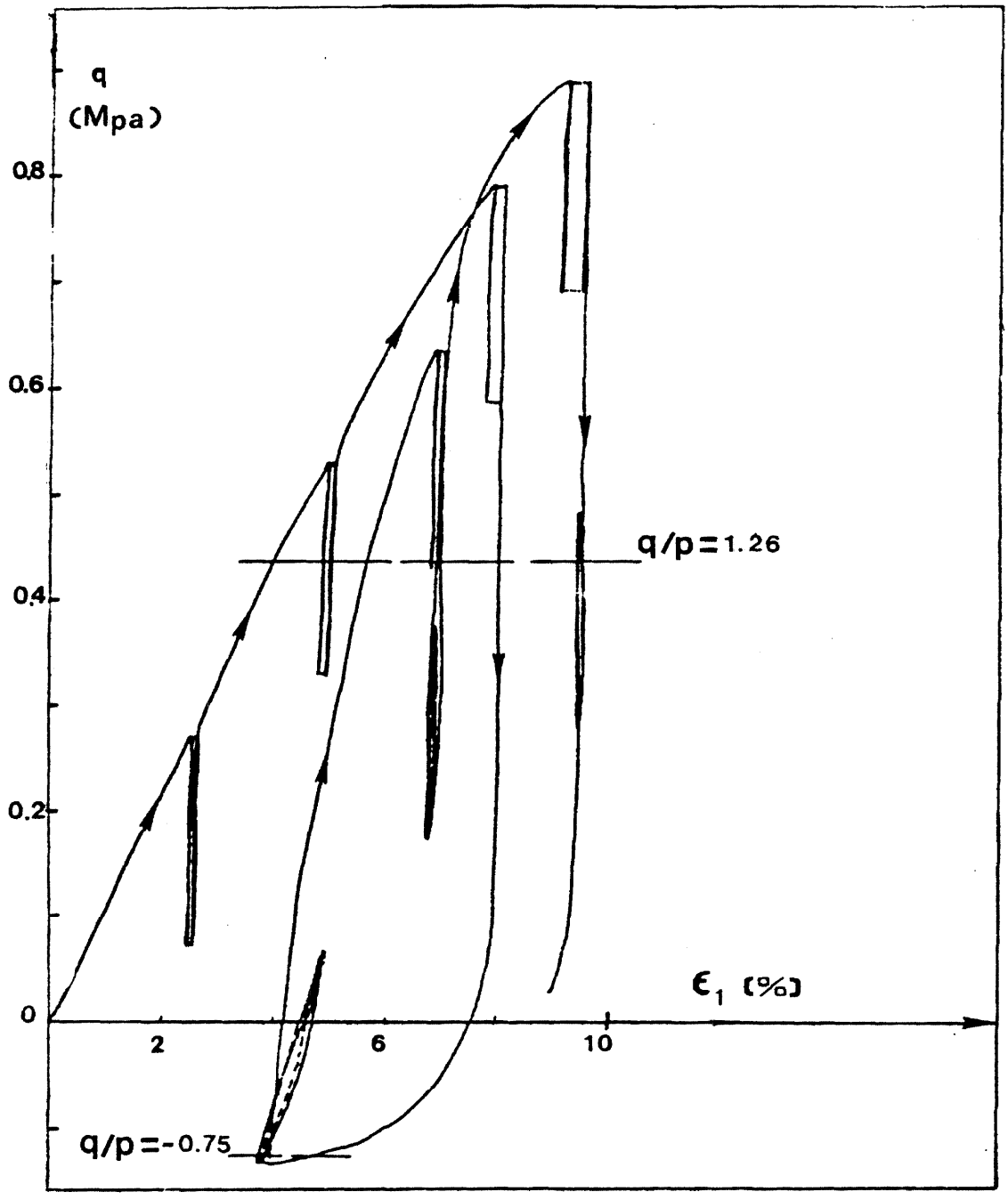

Fig. 5.5a. Drained cyclic loading at constant confining pressure on Fontainebleau sand (after Luong [5.15]).

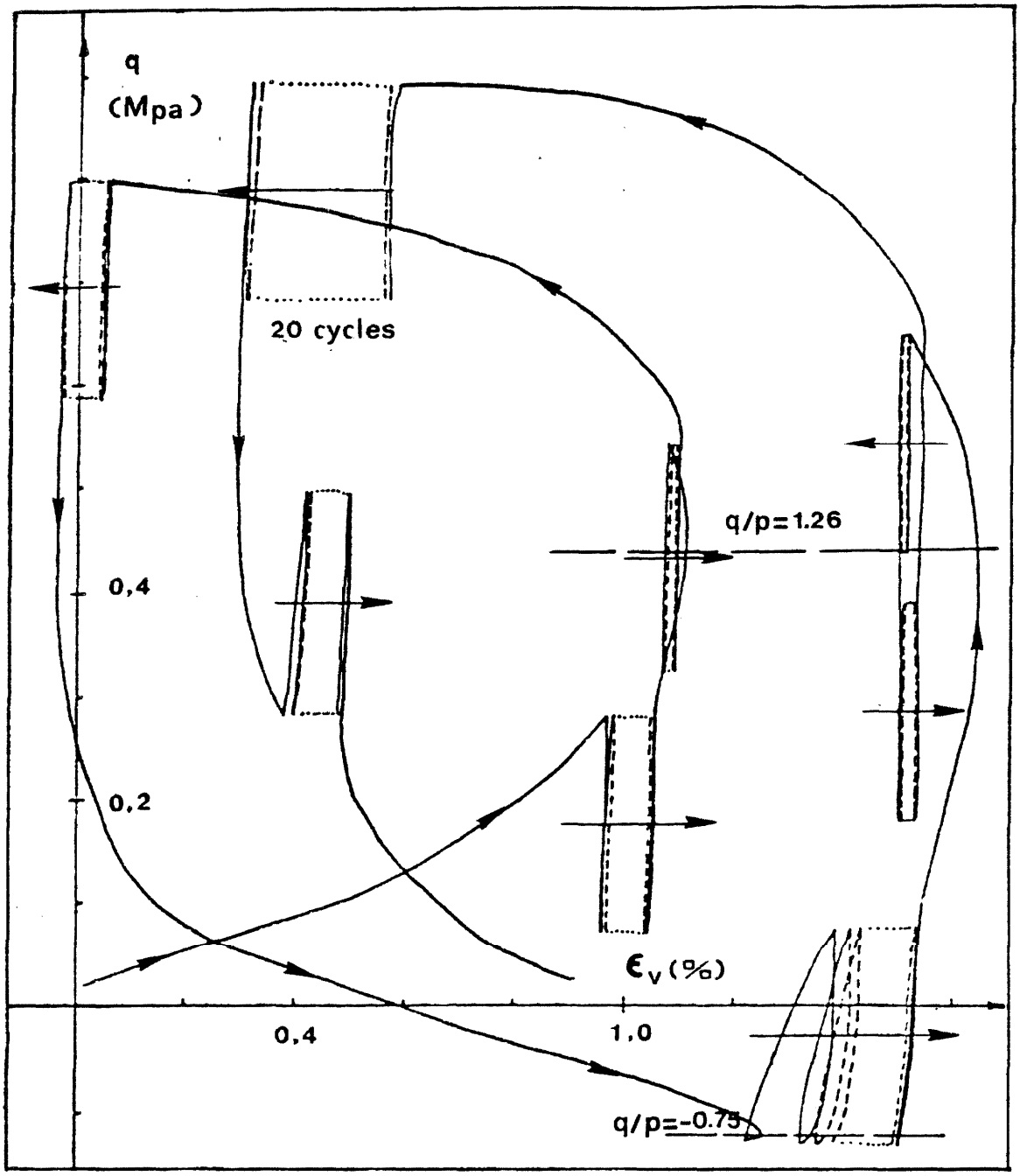

Fig. 5.5b. Drained cyclic loading at constant confining pressure on Fontainebleau sand (after Luong [5.15]).

As an illustration, only Rowe's and Nova's theories are presented.

5.3.3.a Rowe's Stress Dilatancy Theory (1962)

Rowe [5.21] considers, experimentally and theoretically, the behavior of assemblies of cohesionless, spherical particles of uniform size, arranged initially in regular arrays. These assemblies are subjected to an axisymmetric state of stress as defined in relation (2.5), with the axis of symmetry coinciding with the axis of symmetry of the initial packing. The associated strains satisfy the relation (2.3). Introducing the angle of solid friction between particles, denoted by ϕ_μ and assumed to be uniform and independent of pressure, Rowe obtained experimentally a relation between stress and strain increments in the following way:

$$\frac{\sigma_1}{\sigma_3} = -\left[1 - \frac{d\varepsilon_v}{d\varepsilon_1}\right] \tan^2\left[\frac{\pi}{4} + \tfrac{1}{2}\phi_\mu\right] \qquad (5.14)$$

where all strains and stresses are defined in sections 2.2 and 2.3.

The validity of Rowe's theory is tested in Fig. 5.6 by plotting σ_1/σ_3 versus $1 - d\varepsilon_v/d\varepsilon_1$ in the special case of the loose and dense Sacramento River sand subjected to drained tests at different confining pressure. In spite of a noticeable scattering, partially due to finite increments of strain, $d\varepsilon_1$ and $d\varepsilon_v$, the experimental points tend to lie on a straight line, as indicated in relation (5.14). From Fig. 5.6 and relation (5.14) the average angle of friction ϕ_μ is found equal to 32° for this soil.

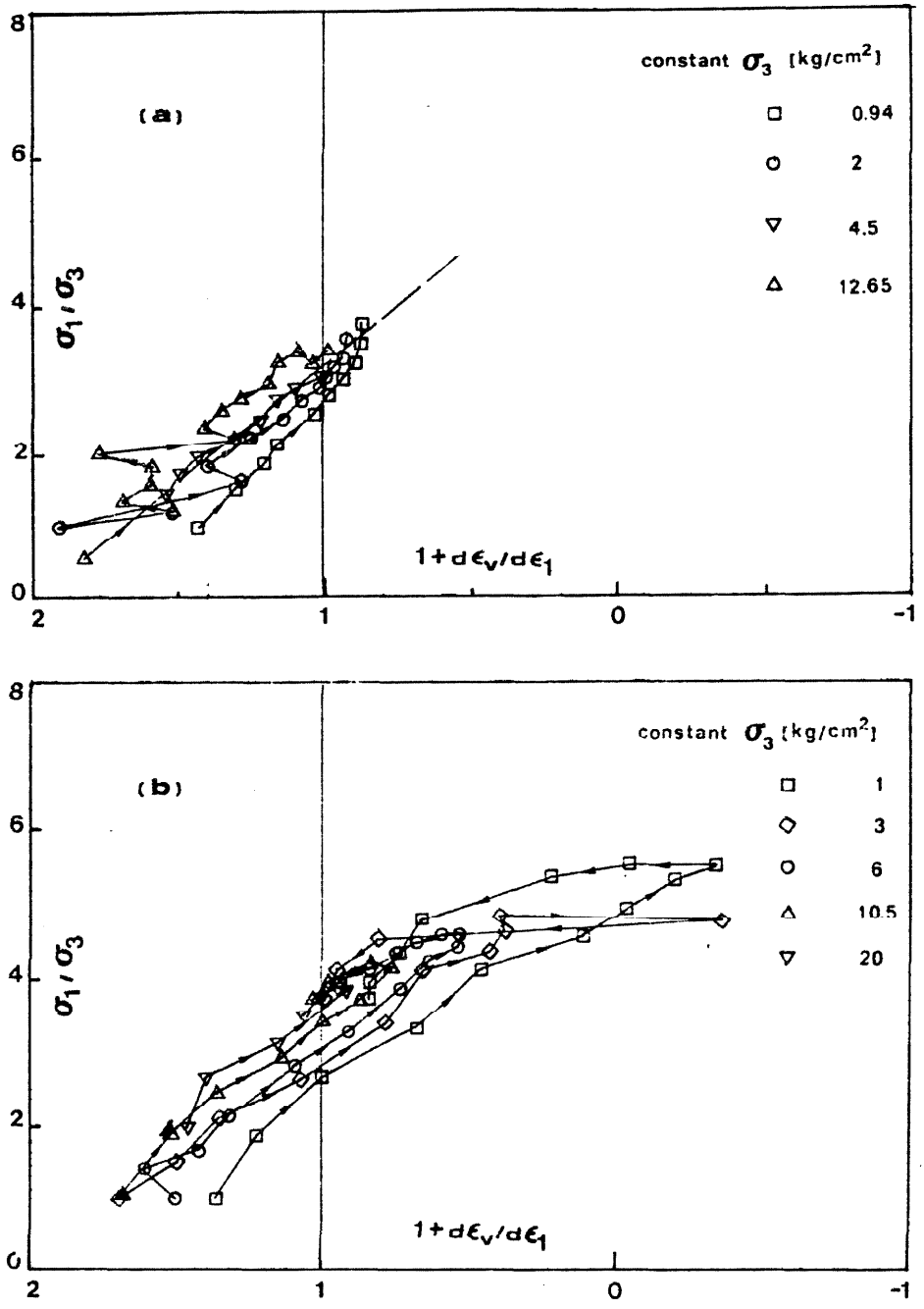

Fig. 5.6. Rowe's stress-dilatancy theory applied to drained tests with constant confining pressure performed on the Sacramento River sand.

a) loose sand
b) dense sand.

Within the context of plasticity theory, if the elastic strain increment is negligible w.r.t. the plastic one, the relation (5.14) indicates that the plastic flow direction, represented by $d\varepsilon_1/d\varepsilon_v$, depends upon the obliquity of the stress state, characterized by σ_1/σ_3. For the loose and dense Sacramento River sand, contraction occurs if the stress ratio σ_1/σ_3 is less than 3, followed by dilation if σ_1/σ_3 is greater than 3 (Fig. 5.6). This result agrees with Luong's characteristic state.

5.3.3.b Nova's Theory (1982)

Retaining the notion of characteristic state and the dependence of plastic flow direction on the stress obliquity, Nova (5.17) proposed a different stress-dilatancy theory based on the experimental work by Stroud [5.26], and defined as follows:

$$\frac{q}{p} = M - \mu \frac{d\varepsilon_v^p}{d\varepsilon_q^p} \qquad (5.15)$$

This relation is not satisfactory for the isotropic state (q=0) since it predicts a plastic deviatoric strain. In order to correct this deficiency, Nova assumes that, for low values of the ratio $\frac{q}{p}$, the stress-dilatancy is governed by another equation:

$$\frac{q}{p} = \frac{a}{\dfrac{d\varepsilon_v^p}{d\varepsilon_q^p}} \qquad (5.16)$$

where the constant a is found by assuming a smooth transition between relations (5.15) and (5.16),

$$a = M^2/4\mu \tag{5.17}$$

This transition is reached when the ratio $\frac{q}{p}$ is equal to $\frac{M}{2}$.

Nova's stress-dilatancy theory is checked by plotting in Fig. 5.7 the ratio $d\varepsilon_v^p/d\varepsilon_q^p$ versus $\eta = q/p$ for the dense Sacramento River sand. All results are obtained by a special computer code [5.2], which uses the following technique. After selecting the elastic model in section 5.2.2, the incremental elastic response $d\varepsilon_v^e, d\varepsilon_q^e$ is calculated for the finite stress increment dp, dq which connects two successive experimental stress states. Then the plastic strain increments $d\varepsilon_v^p$, $d\varepsilon_q^p$ are obtained by subtraction of the calculated elastic strain increment from the total strain increment $d\varepsilon_v$, $d\varepsilon_q$ which relates two successive recorded strain states ε_v, ε_q. Therefore the ratio $d\varepsilon_v/d\varepsilon_q$ is available as a function of the ratio $\eta = q/p$.

The important scattering in Fig. 5.7 is partially due to the sparse recordings of the strain and stress states p, q, and ε_v, ε_q, which produce too large strain or stress increments between two successive states. It is also partially caused by the elastic model selected in section 5.2.2. However, bearing in mind these sources of errors, Fig. 5.7 shows that $d\varepsilon_v^p/d\varepsilon_q^p$ depends upon the ratio η and this is noticeable for any type of tests, drained or undrained, at any confining pressure. In Fig. 5.7b, during the undrained tests (constant volume), the

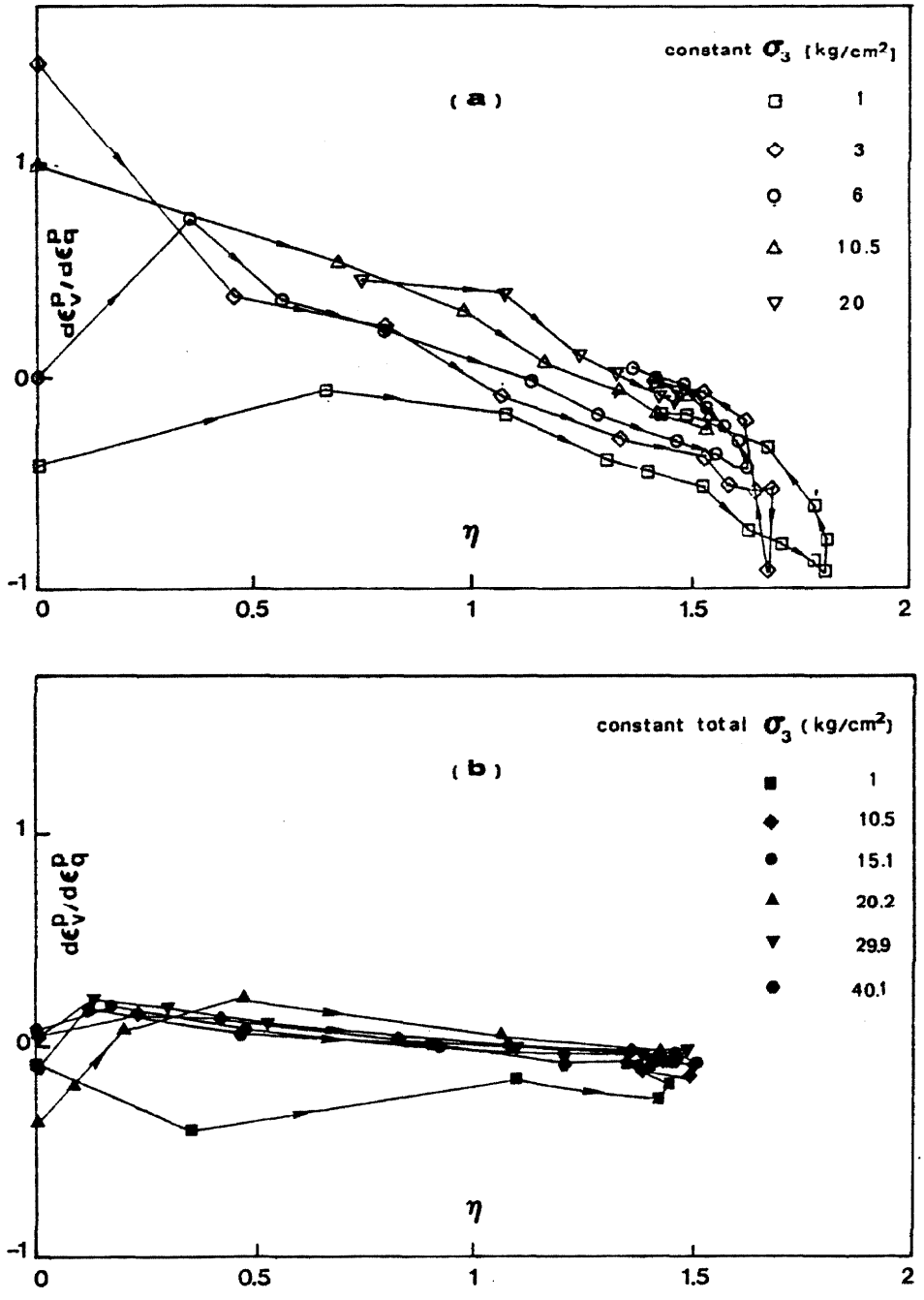

Fig. 5.7. Direction of plastic flow, represented by $d\varepsilon_v^p/d\varepsilon_q^p$, versus the ratio η during different tests on the dense Sacramento River sand.

a) drained tests at constant confining pressure
b) undrained tests at constant total confining pressure.

quantity $d\varepsilon_v^p/d\varepsilon_q^p$ is always positive and smaller than during drained tests (Fig. 5.7a). This discrepancy results from the elastic model; during an undrained test, in order to keep the volume constant, the plastic volumetric strain is equal but opposite to the elastic volumetric strain. From Fig. 5.7, for low values of η, $d\varepsilon_v^p/d\varepsilon_q^p$ is positive (the sand contracts). When η exceeds some fixed value close to 1.4, $d\varepsilon_v^p/d\varepsilon_q^p$ becomes negative (the sand dilates). After reaching a minimum negative value, $d\varepsilon_v^p/d\varepsilon_q^p$ increases back to, and stops finally at zero (critical state). From Fig. 5.7a, the branch, along which $d\varepsilon_v^p/d\varepsilon_q^p$ decreases is different from the branch where it increases back to zero. This non-reversible phenomenon is certainly due to loss of measurement accuracy for large deformation.

In summary, relations (5.15) and (5.16) describe qualitatively the direction of the plastic flow shown in Fig. 5.7; however, the scattering of the experimental results prevents us from calculating the values for μ and M of relation (5.15).

5.3.4 Definition of the New Bounding Surface

So far, from the review of the critical state, characteristic state and the stress-dilatancy theories, some constraints have been imposed on the plastic flow direction. These restrictions are summarized in Table 5.4 by using the unit vector, with components n_p and n_q, collinear to the plastic flow. Also from the experimental results on the Sacramento River sand (Fig. 5.4), no difference appears between the critical and the characteristic states. For convenience, and

TABLE 5.4 SUMMARY OF CONTRAINTS ON THE DIRECTION OF PLASTIC FLOW

Origin of Constraint	Nature of Constraint	Translation in Elastic-Plastic Terms
Characteristic State	At the characteristic state (relation 5.13) the plastic volumetric strain $d\varepsilon_v^p$ equals zero.	if $\frac{q}{p} = M^*_e$ or M^*_c, then $n_p = 0$ and $n_q = 1$ no condition on H
	In the subcharacteristic domain, $d\varepsilon_v^p$ is positive (contracting).	if $M^*_e < \frac{q}{p} < M^*_c$, then $n_p > 0$
	In the supercharacteristic domain, $d\varepsilon_v^p$ is negative (dilating).	if $\frac{q}{p} < M^*_e$ or $\frac{q}{p} > M^*_c$, then $n_p < 0$
Critical State	At the assymptotic critical state (relation 5.11), the plastic volumetric strain $d\varepsilon_v^p$ equals zero, and	if $\frac{q}{p} = M_c$ or M_c, then $n_p = 0$ and $n_q = 1$
	the plastic deviatoric strain $d\varepsilon_q^p$ is infinite	$H = 0$
Stress-dilatancy	The plastic flow direction depends on the stress obliquity, i.e., $\frac{q}{p}$	n_p and n_q are functions of $\frac{q}{p}$

invoking the difficulty of defining accurately both states, the critical and the characteristic states are assumed to coincide in the p-q space, i.e., relations (5.13) and (5.11) are identical.

In conclusion, from the experimental observations on the Sacramento River sand and from the literature review, the unit vector normal to the bounding surface obeys the following rule: when q is positive, the component n_p is positive, zero, or negative depending on whether the ratio $\frac{q}{p}$ is respectively smaller than M_c, equal to M_c, or larger than M_c; when q is negative, the same result holds for n_p by substituting M_e for M_c.

Since the ratio $\frac{n_p}{n_q}$ is only a function of the ratio $\frac{q}{p}$, the following equation is obtained

$$\frac{\bar{dq}}{\bar{dp}} = \frac{n_p}{n_q}\left[\frac{q}{p}\right] \qquad (5.18)$$

which results from equation (3.72). The bar added to dp and dq refers to the image point lying on the bounding surface. In order to solve the equation (5.18), a relation between the image and stress state must be specified. One such a rule is radial mapping, which is specified in relation (4.6), and becomes here

$$\bar{p} = xp \qquad (5.19a)$$

$$\bar{q} = xq \qquad (5.19b)$$

where x is scalar. When selecting such a mapping, the equation (5.18) becomes homogeneous, and may be solved to give the bounding surface equation. However, according to the experimental scattering observed in Fig. 5.7, the function $\frac{n_p}{n_q}\left[\frac{q}{p}\right]$ is difficult to define. The following alternative approach is therefore preferred.

Keeping the radial mapping, as enunciated in relation (5.19), a simple surface, with a suitable normal, is chosen. Composed of portions of ellipses, it is described by the following equations: if $|\bar{q}| \leq M\bar{p}$, (contracting domain),

$$\left[\frac{\bar{p}-A}{\rho-1}\right]^2 + \left[\frac{\bar{q}}{M}\right]^2 - A^2 = 0 \qquad (5.20a)$$

and if $|\bar{q}| > M\bar{p}$, (dilating domain),

$$\alpha(\alpha-2)(\bar{p}-A)^2 + \left[(\alpha-2)\frac{\bar{q}}{M} + A\right]^2 - (\alpha-1)^2A^2 = 0 \qquad (5.20b)$$

where M is equal to M_c or M_e, depending on whether $\bar{q}$ is positive or negative. Plotted in Fig. 5.8 this surface has a general equation

$$f(\bar{p},\bar{q},A,M,\alpha,\rho) = 0 \qquad (5.20c)$$

From the relations (5.19) and (5.20c) the stress state and the image points are related such that:

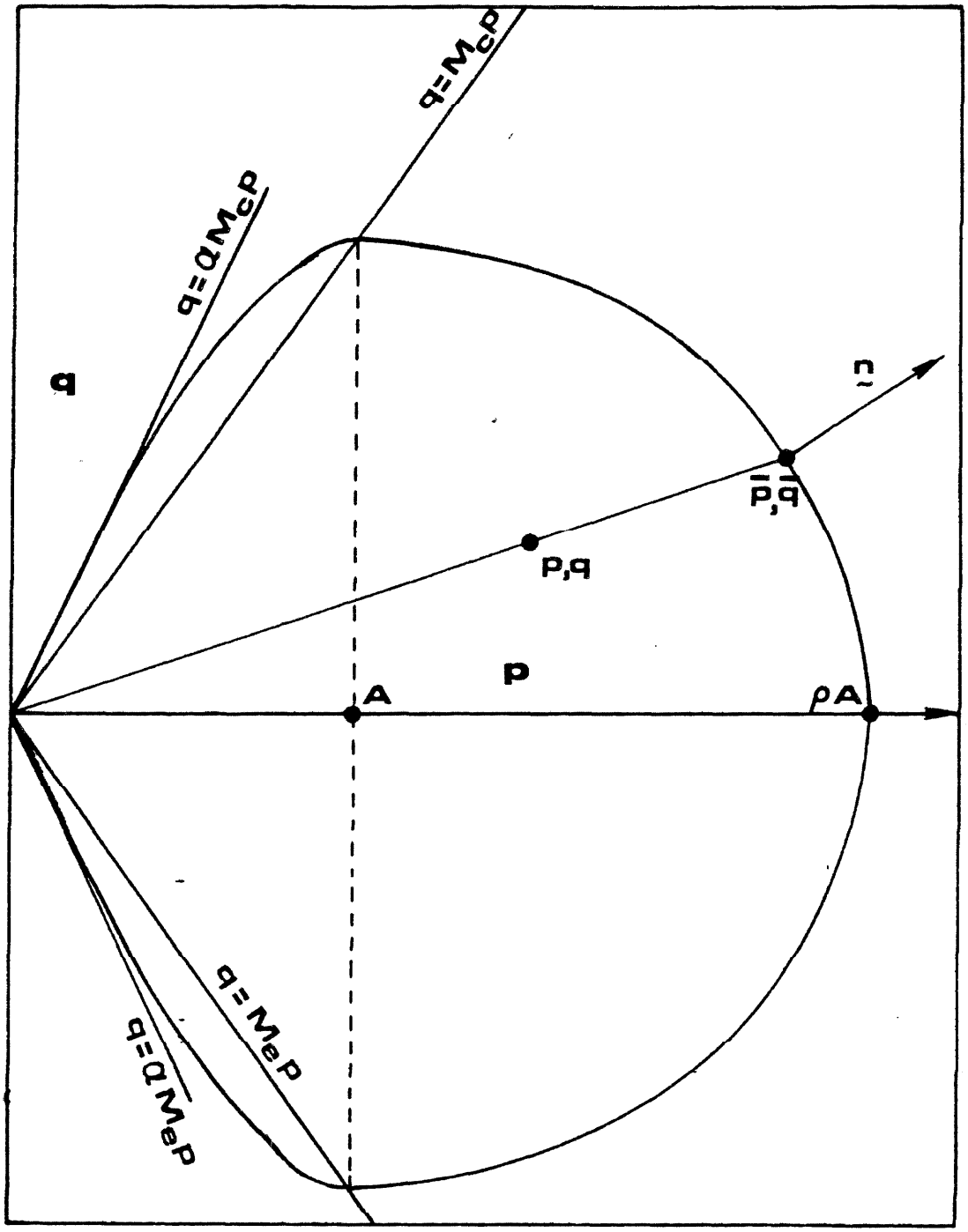

Fig. 5.8. The bounding surface in the p–q space.

$$\bar{p} = yA \tag{5.21a}$$

$$\bar{q} = y\frac{q}{p}A \tag{5.21b}$$

where y is found by solving the following equation:

$$f(yA,\ yA\frac{q}{p},A,M,\alpha,\rho) = 0 \tag{5.22}$$

The equation (5.22) yields the following results

if $|q| < Mp$,

$$y = \frac{1+(\rho-1)\ (1+zp(\rho-2))^{1/2}}{1+(\rho-1)^2z^2} \tag{5.23a}$$

and if $|q| > Mp$,

$$y = \frac{2(\alpha-z)}{\alpha+(\alpha-2)z^2} \tag{5.23b}$$

where

$$z = \frac{q}{Mp} = \frac{\bar{q}}{M\bar{p}} \tag{5.23c}$$

The distance δ, connecting the stress state and the image point, is given as follows

$$\delta = \left[(p-\bar{p})^2 + (q-\bar{q})^2\right]^{1/2} \tag{5.24a}$$

and, by using the relations (5.21), it becomes

$$\delta = (p-yA)\left[1 + \left(\frac{q}{p}\right)^2\right]^{1/2} \tag{5.24b}$$

The unit vector normal to the bounding surface at the image point is calculated from (3.57), (5.20) and (5.23), in the dilating domain to have components

$$n_p = \frac{\alpha M}{h}(y-1) \tag{5.25a}$$

$$n_q = \frac{1}{h}[(\alpha-2)yz+1] \tag{5.25b}$$

where

$$h = \left[\alpha^2M^2(y-1)^2 + ((\alpha-2)yz+1)^2\right]^{1/2} \tag{5.25c}$$

and in the contracting domain

$$n_p = \frac{1}{h}M(y-1) \tag{5.26a}$$

$$n_q = \frac{1}{h}(\rho-1)^2yz \tag{5.26b}$$

where

$$h = \left[M^2(y-1)^2 + (\rho-1)^4y^2z^2\right]^{1/2} \tag{5.26c}$$

The parameter M_e, M_c define the contracting and dilating domain. The direction of plastic flow is governed by two parameters: one in the contracting domain, ρ, and another in the dilating domain, α. The parameter A, which controls the size of the bounding surface, does not affect the plastic flow direction.

The quantities n_p/n_q, calculated from relations (5.25), (5.26), are plotted versus the ratio $\frac{q}{p}$ for different values of the constants ρ and α in Fig. 5.9. Although no perfect agreement between theoretical and experimental results is possible, due to the scattering of experimental points, the plastic flow direction predicted by the bounding surface agrees with the observed values.

5.4 BOUNDING SURFACE MOTION

Already partially specified by the equations (5.20), the motion of the bounding surface is completed by defining an evolution law for the parameters M,A,ρ, and α. All of these parameters must be regarded as depending upon some internal variables, which characterize the material memory.

5.4.1 Choice of Internal Variables

The internal variables must always be selected with discernment, since their contribution is fundamental to a description of the irreversible rheological behavior. For convenience, only one scalar internal variable is chosen. As any sand exhibits a behavior strongly dependent on its density, this variable must be related to the void ratio. Additionally it must only change when plastic flow occurs. Among other possibilities, the plastic void ratio e^p is retained. It is defined

$$e^p = e - e^e \qquad (5.27a)$$

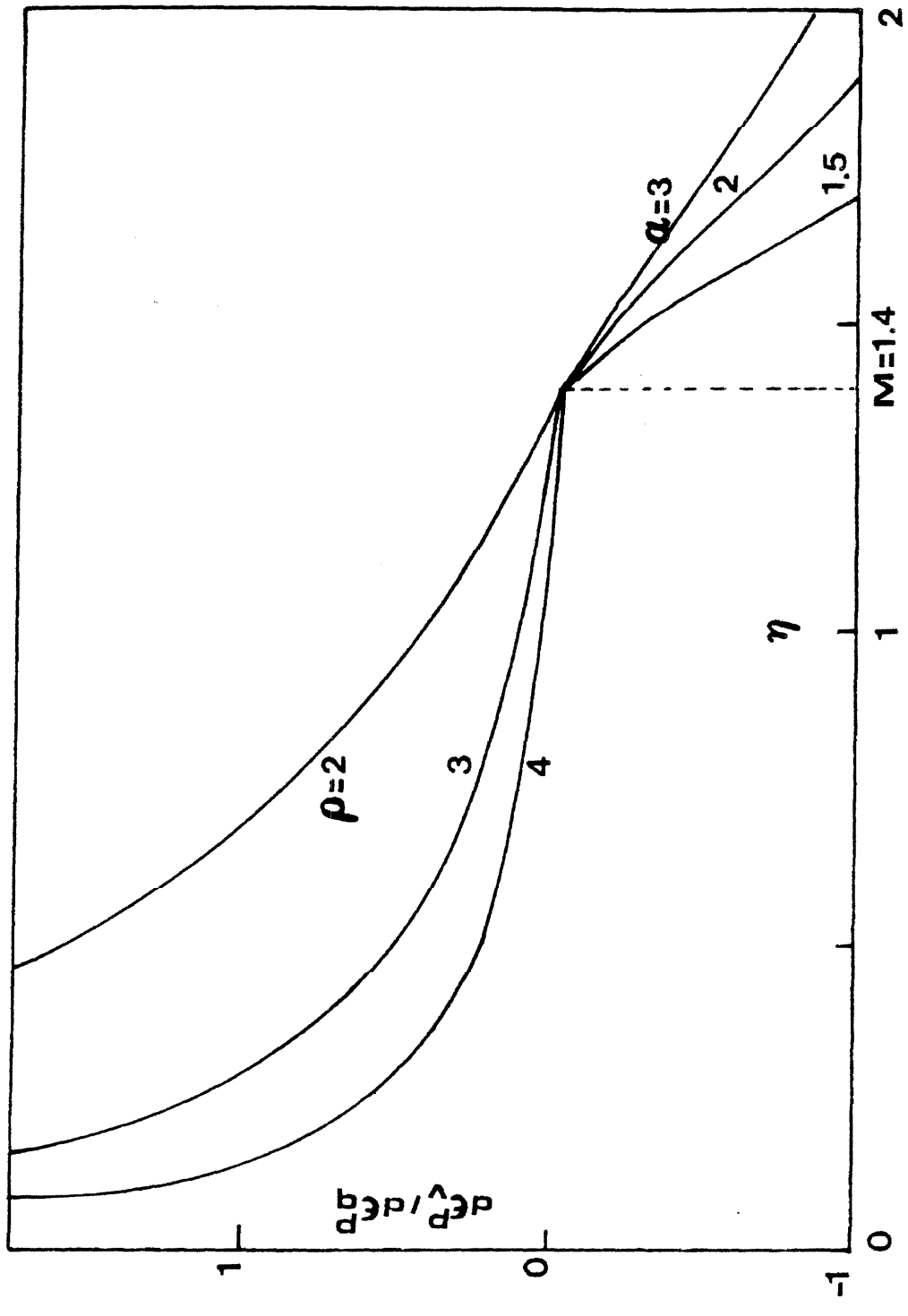

Fig. 5.9. Direction of plastic flow predicted by the new bounding surface for different values of the constants ρ and α (M_c=1.4).

where e is the total void ratio, and e^e the elastic void ratio, which depends only upon the selected elastic model and the present stress state in the following way

$$e^e = -(1+e_0)\int_0^p \frac{dp}{B(p,q)} \qquad (5.27b)$$

where e_0 is the initial void ratio.

The plastic void ratio e^p and the plastic volumetric strain ε_v^p are related as follows

$$\varepsilon_v^p = \frac{-e_0+e^p}{1+e_0} \qquad (5.28)$$

Other internal variables may be added to represent the material memory in more detail; for instance, a second variable is defined later to describe the cyclic behavior.

5.4.2 Motion of the Bounding Surface

In order to describe the bounding surface motion, the relations of the variable e^p with the other parameters M, ρ,α,A must be specified. From experimental observations on the direction of plastic flow, and for simplicity, M, ρ and α are assumed to be constant. The only variable left to depend on e^p is the parameter A; its relation with e^p is particular when the stress state reaches the critical state. At this stage, the stress state has reached its bound, and from relation (5.11) and Fig. 5.8, it lies on the summit of the bounding surface located at A, MA. Since the void ratio, and the stress do not change, by invoking

relation (5.27), the plastic void ratio remains also constant, and has a critical state of its own, which is described by a relation similar to the relation (5.11c):

$$e^p = \Gamma'_p - \lambda_p \ln A \qquad (5.29)$$

where Γ'_p and λ_p are two material constants, different from the constants Γ' and λ defined in (5.11c).

Using the nonlinear elastic model defined in section 5.1, from Tables 5.3, the quantities e^p are calculated at the critical state for the dense Sacramento River sand and plotted versus the mean pressure A in Fig. 5.10. By applying a linear regression analysis to the experimental points of Fig. 5.10, the following results were obtained: $\Gamma'_p = 0.88$ and $\lambda_p = 0.083$. Γ'_p and λ_p differ only slightly from Γ', λ defined for the critical state, since e^e may be neglected compared to e^p.

By extrapolation relation (5.29), which must hold in particular at the critical state, is assumed to be always satisfied. This relation describes fully the isotropic motion of the bounding surface.

5.5 AMPLITUDE OF PLASTIC FLOW

Once the bounding surface equation and a mapping rule are defined, the plastic flow direction is known. Its amplitude needs to be specified by the modulus H as a function of two variables: the distance δ and the modulus H_B. The plastic modulus H_B is defined analytically from the equation and motion of the bounding surface by applying the

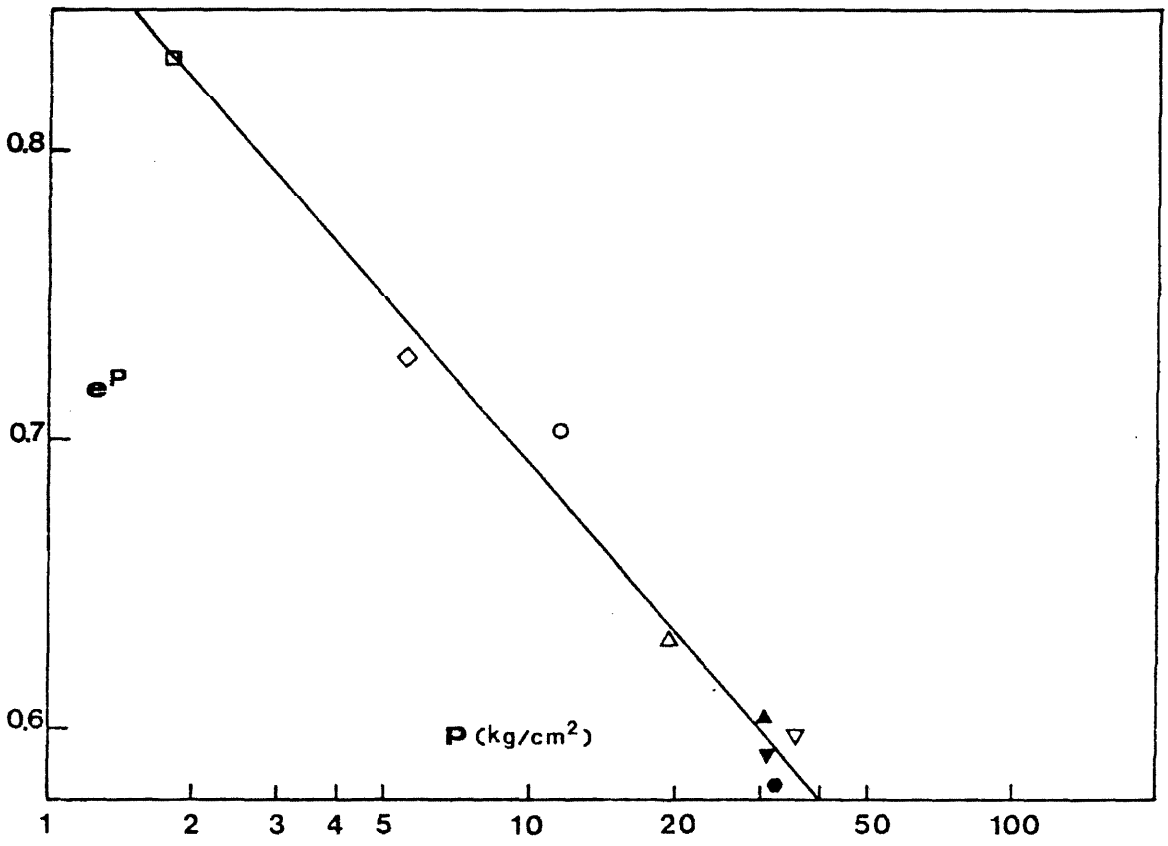

Fig. 5.10. Critical state for dense Sacramento River sand represented by plastic void ratio e^p versus mean pressure p.

consistency condition. The relation between H, H_B and δ is determined first by calculating their respective values during drained and undrained tests, then by fitting these values with appropriate dimensionless quantities.

5.5.1 Plastic Modulus H_B on Bounding Surface

The bounding surface depends only upon one internal variable, e^p, which is related to the plastic volumetric strain ε_v^p through (5.31). Since the relations (4.4) and (3.60) are satisfied, the plastic modulus H_B, evaluated at the image stress, is given by

$$H_B = - n_p \frac{\partial f}{\partial \varepsilon_v^p} \left[\frac{\partial f}{\partial p}^2 + \frac{\partial f}{\partial q} 2 \right]^{1/2} \qquad (5.30)$$

The partial derivative $\frac{\partial f}{\partial \varepsilon_v^p}$ is calculated easily from (5.28) and (5.29). Since A, the measure of the bounding surface size, is the only variable parameter in (5.20)

$$\frac{\partial f}{\partial \varepsilon_v^p} = \frac{\partial f}{\partial A} (1+e_0) \frac{A}{\lambda_p} \qquad (5.31)$$

According to the expressions (5.25), (5.30) and (5.31), the plastic modulus H_B is expressed

$$H_B = \frac{M^2(y-1)[y-1+(\rho-1)]^2}{M^2(y-1)^2 + (\rho-1)^4 y^2 z^2} (1+e_0) \frac{A}{\lambda_p} \quad , \quad \text{if } |q| \leq Mp \qquad (5.32a)$$

and

$$H_B = \frac{\alpha M^2 y(y-1)(\alpha-z)}{\alpha^2 M^2 (y-1)^2 + [(\alpha-2)yz+1]^2} (1+e_0) \frac{A}{\lambda_p} \quad \text{, if } |q| > Mp \qquad (5.32b)$$

where y and z are given by the relations (5.23).

The modulus H_B depends on the stress obliquity, represented by z (5.23c), and on A, the bounding surface size. A dimensionless plastic modulus, denoted by $\bar{H}_B$ and related only to z, is defined as follows:

$$\bar{H}_B = \frac{H_B \lambda_p}{(1+e_0)A} \qquad (5.33)$$

$\bar{H}_B$ is represented in Fig. 5.11 versus z for different values of the parameters ρ and α. $\bar{H}_B$ is maximum and equal to ρ for the isotropic stress state (z=0), goes through zero at the critical or characteristic state (z=1), reaches a negative minimum value, then finally increases to zero when z becomes equal to α.

5.5.2 Relation Between Plastic Moduli H and H_B and Distance δ

In order to examine their interrelation, the parameters H, H_B and δ are calculated from discrete experimental data points recorded during the drained and undrained tests on the Sacramento River sand. These calculations are performed by the computer code soil [5.2]. The plastic strain increments $d\varepsilon_v^p$, $d\varepsilon_q^p$ between two successive stress and strain states are defined as in section 5.2.3b. At a stress state represented by p,q, with its succeeding increment of stress dp, dq, the plastic modulus H may be calculated from relations (5.9)

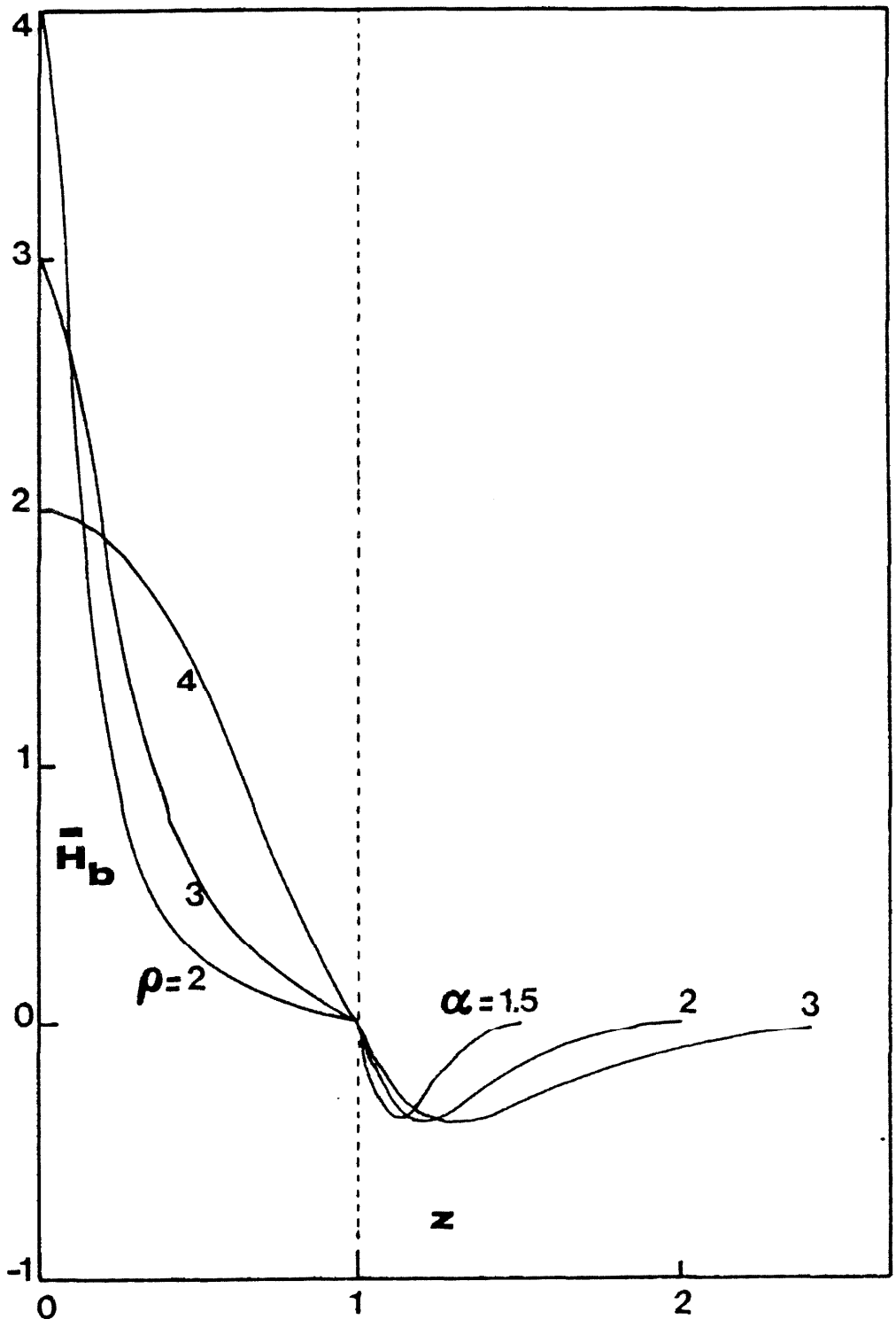

Fig. 5.11. Normalized plastic modulus $\bar{H}_B$ versus the ratio z for different values of ρ and α (M_c=1.4).

$$H = \frac{d\varepsilon_v^p dp + d\varepsilon_q^p dq}{\left[d\varepsilon_v^{p\,2} + d\varepsilon_q^{p\,2}\right]^{1/2}} \tag{5.34}$$

Since H_B and δ are known from the relations (5.30) and (5.24), all three quantities H, H_B and δ may be calculated simultaneously at any moment of an experiment. In order to exhibit a relation between H, H_B and δ, after several trials, the difference $H-H_B$ is plotted versus the distance δ in Fig. 5.12a and 5.12b, in the respective case of drained and undrained tests performed at different confining pressures. According to Fig. 5.12, the quantity $H-H_B$ is always positive when δ is positive, and tends monotonically towards zero when δ goes to zero. Consequently, like Dafalias and Herrmann [5.7], the following relation is suggested.

$$H = H_B + h(\delta) \tag{5.35}$$

where the function $h(\delta)$ must satisfy the following constraints:

$$h(\delta) > 0 \quad , \quad \text{when } \delta > 0 \tag{5.36a}$$

$$h(\delta) = 0 \quad , \quad \text{when } \delta = 0 \tag{5.36b}$$

$$h(\delta) \text{ large} \quad , \quad \text{when } \delta \text{ is large} \tag{5.36c}$$

$$h(\delta) \text{ is a continuous function of } \delta \tag{5.36d}$$

The first two constraints come from the previous observations of Fig. 5.12. The third restriction enforces the material response to be elastic far away from the bounding surface. Finally, the last

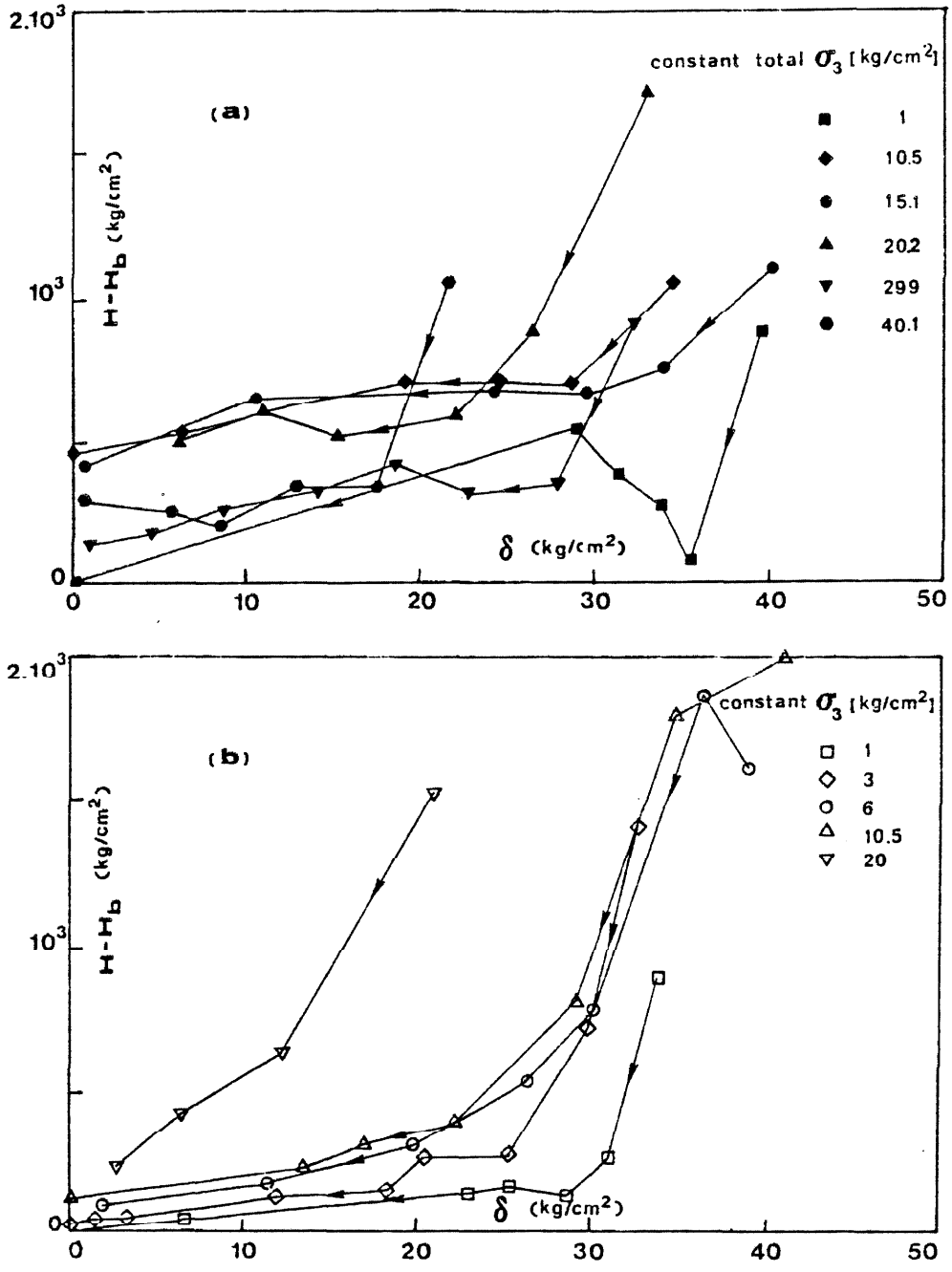

Fig. 5.12. Values of $H-H_B$ versus the distance δ calculated from experimental tests on the dense Sacramento River sand.

a) undrained tests at constant total confining pressure
b) drained tests at constant confining pressure.

constraint gives a continuous transition from purely elastic to elastic-plastic response. From relations (5.35), (5.36) and Fig. 5.11, the plastic modulus H is in agreement with the constraints mentioned in Table 5.4. When the stress state is located on the characteristic state (relation 5.13 or 5.11), the distance δ is different from zero: the plastic modulus H is different from zero whereas H_B equals zero. When the stress state reaches the critical state, the distance δ equals zero: both H and H_B are equal to zero. In addition, the relations (5.35) and (5.36) control the strain-softening effect. This last phenomenon, initiated when the plastic modulus H becomes negative, can only occur in the dilating domain, where H_B is negative. It cannot occur in the contracting domain.

The previous general relations between H, H_B and δ may be detailed by introducing the dimensionless quantities $\bar{H}$ and $\bar{\delta}$. $\bar{H}$, the normalized plastic modulus, is defined as $\bar{H}_B$ in relation (5.36). $\bar{H}$, which is calculated simultaneously with H, H_B and δ is represented versus the ratio $\eta = \frac{q}{p}$ in Fig. 5.13a and 5.13b for drained and undrained tests at different confining pressures. From Fig. 5.13, $\bar{H}$ depends on η.

The normalized distance, denoted $\bar{\delta}$, is defined as:

$$\bar{\delta} = \frac{\delta}{\delta_{max}} \qquad (5.37a)$$

where δ_{max}, maximum distance between any stress state and image point, is the distance between the origin of stress and the image.

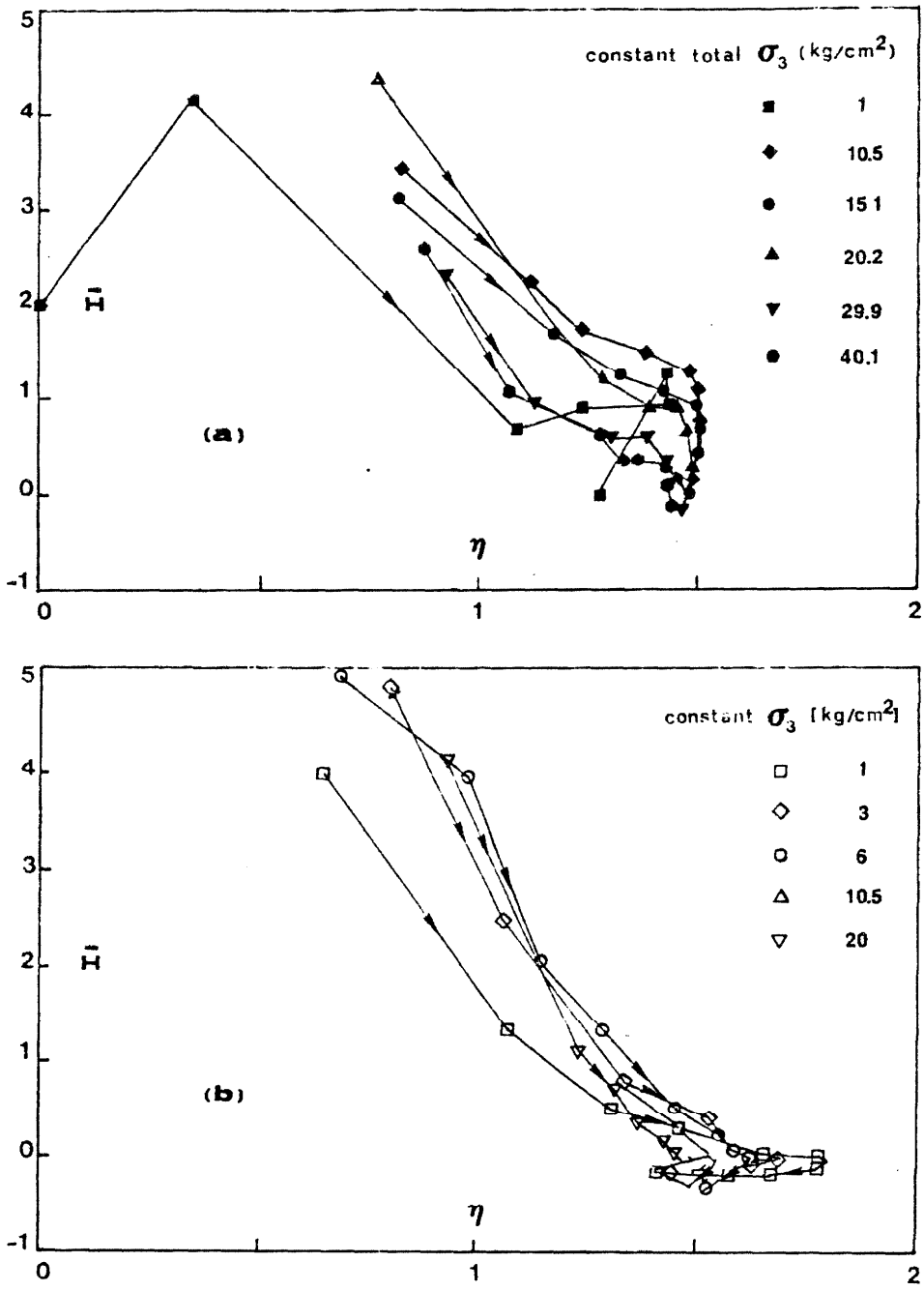

Fig. 5.13. Normalized plastic modulus $\bar{H}$ versus the ratio η calculated from experimental tests on the dense Sacramento River sand.

a) undrained tests at constant total confining pressure
b) drained tests at constant confining pressure.

According to (5.24b), the normalized distance can be expressed as

$$\bar{\delta} = 1 - \frac{p}{yA} \tag{5.37b}$$

where y is given by (5.23) and A is the bounding surface size. The stress states corresponding to the same $\bar{\delta}$ belong to a surface, which is homothetic to and smaller than the bounding surface.

For simplicity, the variables $\bar{\delta}$ and η are assumed to have separate effects on the function $h(\delta)$. Then, after the normalization specified in (5.33), the relation (5.35) becomes

$$\bar{H} = \bar{H}_B + a(\eta) \cdot b(\bar{\delta}) \tag{5.38}$$

where the functions $a(\eta)$ and $b(\bar{\delta})$ describe the separate influence of η and $\bar{\delta}$ on the modulus $\bar{H}$.

According to Fig. 5.13, the function $a(\eta)$ must decrease when η increases. After several trials, the following form was retained:

$$a(\eta) = \frac{a_0}{2}\left[\cos\left(\pi\left(\frac{\eta}{\eta_p}\right)^{a_1}\right) + 1\right] \tag{5.39}$$

where a_0, a_1, and η_p are three material constants. This arbitrary relation has been selected mainly for one reason: it describes a wide range of variations from a maximum value to a zero value, when the parameters a_0, a_1 and η_p vary. Such a general variation may be appreciated from Fig. 5.14, where $a(\eta)/a_0$ has been plotted versus η/η_p for different values of a_1. The parameter a_1 offers different types of continuous

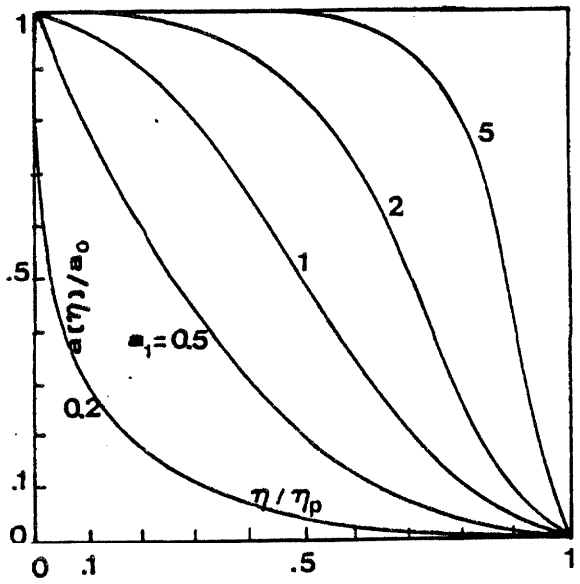

Fig. 5.14. Function a(η) represented by a $(\eta)/a_o$ versus the quantity η/η_p for different values of a_1.

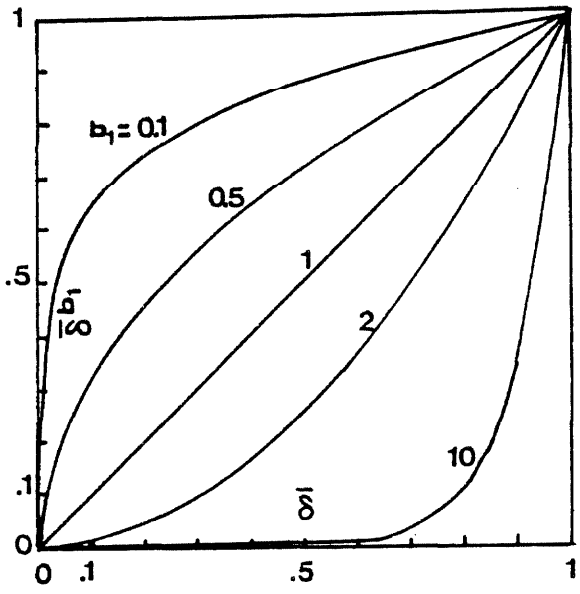

Fig. 5.15. Function $\bar{\delta}^{b_1}$ versus $\bar{\delta}$ for different values of b_1.

decrease for $a(\eta)$, and is selected in an arbitrary way. The constant a_0 maximum value for $a(\eta)$, is chosen from isotropic test since $a(0)$ is equal to a_0. The constant η_p, for which $a(\eta_p)$ equals zero, is related to the peak failure stress. η_p is larger than or equal to the critical state slope, M, depending on whether or not strain-softening is present. For the dense Sacramento River sand, which exhibits strain-softening during drained tests, the constant η_p has been selected, by trial and error, so that the predicted peak values are close to the experimental values: $\eta_p = 2$. The constant a_0, independent from a_1 and η_p has been chosen so that predicted and experimental isotropic tests are close enough: $a_0 = 6$. Finally a_1 is arbitrarily selected: $a_1 = 2$.

The function $b(\bar{\delta})$, which characterizes the dependence of $\bar{H}$ upon $\bar{\delta}$ in relation (5.38), is assumed to have the following composite form:

$$b(\bar{\delta}) = \bar{\delta}^{b_1} + \exp[b_2(\bar{\delta}-\bar{\delta}_{min})]H_e(\bar{\delta}-\bar{\delta}_{min}) \qquad (5.40)$$

where b_1 and b_2 are two material constants, $H_e(x)$ is the Heaviside function and $\bar{\delta}_{min}$ is a new internal variable. Only helpful for cyclic loading, $\bar{\delta}_{min}$ represents the smallest normalized distance $\bar{\delta}$ which has been reached during the past loading history. As relation (5.89), relation (5.40) has been selected to be as general as possible, especially regarding the first term $\bar{\delta}^{b_1}$. During any monotonic loading, $\bar{\delta}$ is equal to $\bar{\delta}_{min}$: The Heaviside function vanishes. In this eventually, the function $b(\bar{\delta})$ becomes equal to $\bar{\delta}^{b_1}$ and has been plotted in Fig. 5.15 for

different values of b_1 varying from 0.1 to 10. From Fig. 5.15, the parameter b_1 gives different aspects to the function $\bar{\delta}^{b_1}$. For the dense Sacramento River sand, the constant b_1 was found, by trial and error, in order to fit the drained tests: $b_1 = 1$.

The additional term of relation (5.40), depending upon $\bar{\delta}_{min}$ and b_2, controls arbitrarily the amount of plastic strain created during cyclic loadings. When $\bar{\delta}$ becomes larger than $\bar{\delta}_{min}$, the function $b(\bar{\delta})$ takes larger values controlled by the parameter b_2, which implies a larger plastic modulus and consequently less plastic strain. For the dense Sacramento River sand, b_2 was estimated in order to approximate the plastic strain generated during cyclic isotropic loading: $b_2 = 8$. The constant b_2, has an effect on the predicted response only for cyclic loadings, not for monotonic loadings.

Trial and error computations are required to specify the constants a_0, a_1, η_p, b_1, and b_2. The relations (5.39) and (5.40) are the weakest points of the theory and need to be improved in the future.

5.6 MODEL CONSTANTS

All the material constants necessary to specify a material response are summarized in Table 5.5. The values given in Table 5.5 are obtained for the dense Sacramento River sand. The material constants are divided into four different groups, which characterize separately particular aspects of the material response.

TABLE 5.5 MATERIAL CONSTANTS AND NUMERICAL VALUES FOR DENSE SACRAMENTO RIVER SAND

Notation	Meaning	See Section	Value	Unit
	Elastic Constants			
B_0	Bulk modulus constant	5.2	729	kg/cm^2
n	Bulk modulus constant	5.2	0.47	Dimensionless
ν_0	Constant Poisson's ratio	5.2	0.2	
	Direction of Plastic Flow, Bounding Surface			
ρ	Aspect ratio of ellipse in contracting domain	5.3.4	3	
α	Slope of ellipse in dilating domain	5.3.4	2	
	Critical state, motion of bounding surface			
Γ_p	Critical plastic void ratio for unit pressure (kg/cm^2)	5.4.2	0.883	
λ_p	Slope of critical state line in e^p–$\ln p$ plane	5.4.2	0.0832	
M_c	Slope of critical state for positive deviatoric stress	5.3.1	1.4	
M_e	Slope of critical state for negative deviatoric stress	5.3.1	1.4	
	Relation Between H, H_B and δ			
a_0	Dependence of $\bar{H}$ on η	5.5.2	6	
a_1	Dependence of $\bar{H}$ on η	5.5.2	2	
η_p	Dependence of $\bar{H}$ on η	5.5.2	2	
b_1	Depencence of $\bar{H}$ on $\bar{\delta}$	5.5.2	1	
b_2	Depencence of $\bar{H}$ on $\bar{\delta}$	5.5.2	8	

The first group, composed of B_0, n, ν_0, represents the elastic contribution to the total elastic-plastic response. B_0 and n are calculated by fitting the unloading response during an isotropic test (section 5.2.3). ν_0 is arbitrarily chosen equal to an admissible value, about 0.2 or 0.3.

The second group, constituted by ρ and α, characterizes the plastic flow direction in the contracting and the dilating domains respectively. They define the bounding surface shape by giving the aspect ratio of the ellipse in the contracting domain and the slope of the ellipse in the dilating domain at the origin of stress. ρ and α are estimated by comparing the predicted flow direction of Fig. 5.9 with the experimental flow direction as shown in Fig. 5.7.

The third group, made up of Γ'_p, λ_p, M_c and M_e, represents the critical state, coincident with the characteristic state. M_c and M_e define not only the relative size of the contracting and dilating domains, but also the critical state lines for positive and negative deviatoric stress. M_c and M_e are calculated as in section 5.3.1. Γ'_p and λ_p specify the location of the critical state, and the motion of the bounding surface; they are estimated as in section 5.4.1.

The fourth and last set of model constants, a_0, a_1, η_p, b_1 and b_2 defines the relation between the plastic moduli H, H_B and the distance δ. The constants a_0, a_1, η_p represent the dependence of H upon the ratio q/p and are estimated by trial and error as in section 5.5.2. The

constants b_1 and b_2 define the influence of the distance δ upon the plastic moduli H. They are also evaluated by trial and error as in section 5.5.2.

All the calculations of the model constants have been performed in Chapter V for the particular case of the dense Sacramento River sand. They may be repeated for any other sand.

5.7 THEORY VERSUS EXPERIMENT

The new constitutive relations were implemented in the interactive computer code soil [5.2] in order to simulate numerically isotropic, drained and undrained shear tests for different confining pressures given in Table 5.6. To each loading there corresponds a constraint on stress or strain. For the isotropic test, the deviatoric stress q equals zero. For the drained tests, the confining pressure is fixed, whereas for the undrained tests the volumetric strain remains equal to zero. Each constraint transforms the incremental constitutive relations, as shown by relation (3.59), into a system of non-linear ordinary differential equations, which was integrated step by step by the interpolation method introduced by Burlish and Stoer [5.3].

For an isotropic test, the incrementing variable is the mean pressure p, while, for drained and undrained shear tests, the axial strain ε_1 is preferred in order to describe a possible strain-softening. The increment values, respectively equal to 0.5 for the mean pressure and

TABLE 5.6 SUMMARY OF DRAINED AND UNDRAINED TESTS ON THE DENSE SACRAMENTO RIVER SAND

Tests	σ_3 (kg/cm^2)
Drained tests at constant effective confining pressure σ_3	1. 3. 6. 10.5 20.
Undrained tests at constant total confining pressure σ_3	1. 10.5 15.1 20.2 29.9 40.1

0.001 for the axial strain, may be decreased to a lower value in order to enforce the numerical convergence.

All the numerical simulations are compared in Fig. 5.16, 5.17 and 5.18 with the experimental results obtained on the dense Sacramento River sand. An isotropic test with two loading-unloading cycles is simulated in Fig. 5.16. In contrast to conventional plastic models, the new model predicts plastic strain during each reloading. The parameter b_2 controls this nonreversible cyclic behavior and may be decreased in order to obtain larger plastic volumetric strain. Undrained tests at different confining pressures are simulated in Fig. 5.17. Although the predicted and real behavior agree qualitatively well, the simulated pore pressure are too large (Fig. 5.17c). This pore pressure excess implies that the effective stress paths in Fig. 5.17a are not vertical enough before crossing the characteristic line. This discrepancy may be caused by the parameter ρ, which defines the plastic flow direction below the critical state line. A larger value of ρ gives a stress path more vertical. This discrepancy is also due to experimental errors. During undrained tests, the rubber membrane, which isolates the soil sample from its surrounding, penetrates between the sand grains. This penetration is due to difference of pressure between the confining pressure and the internal pore-water pressure. A correction of the experimental results which compensates the membrane penetration effect would improve the agreement between theory and experiment. For the drained tests (Fig. 5.18), the theory shows a good agreement with the experiment,

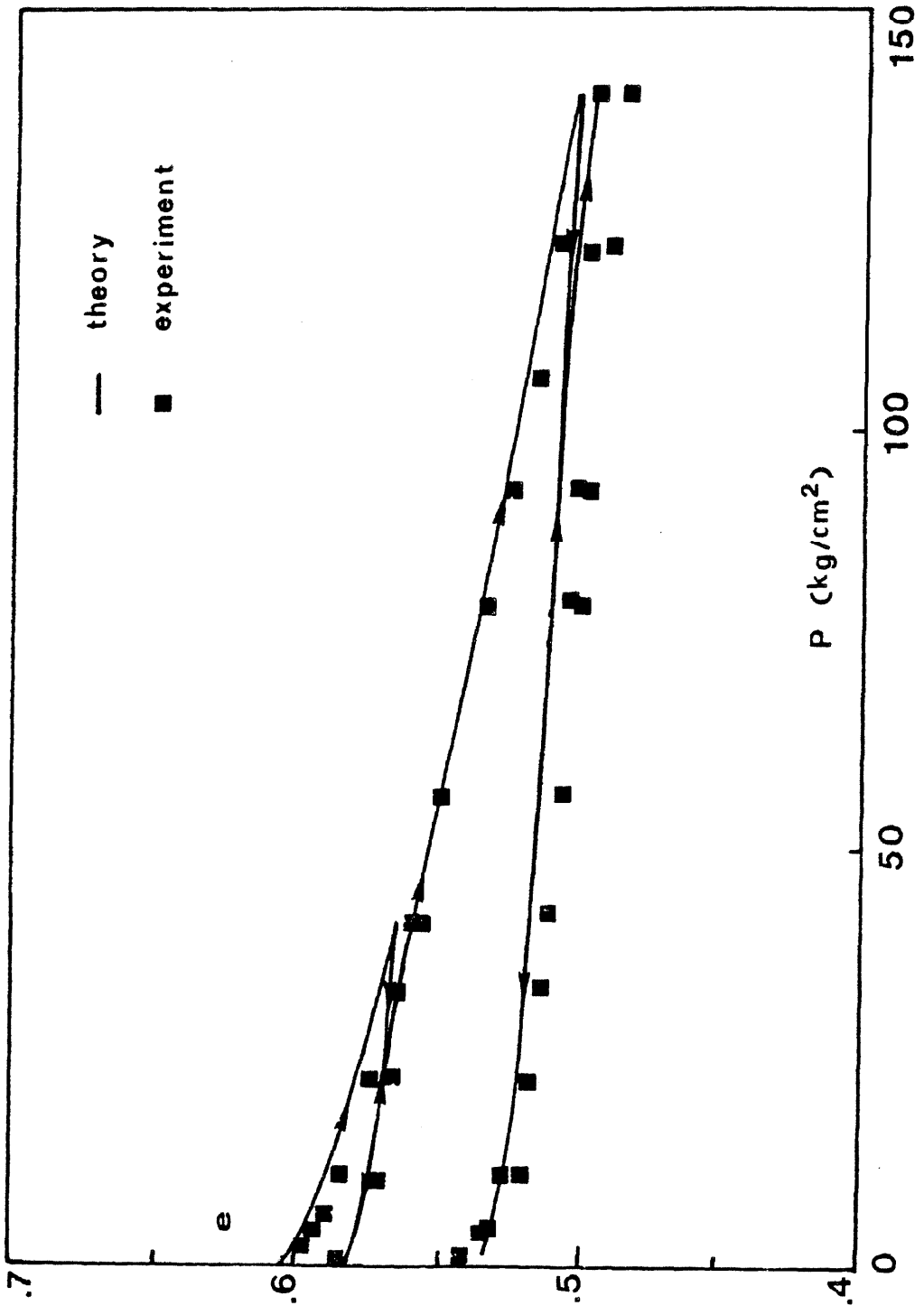

Fig. 5.16. Predicted and experimental isotropic tests on the dense Sacramento River sand.

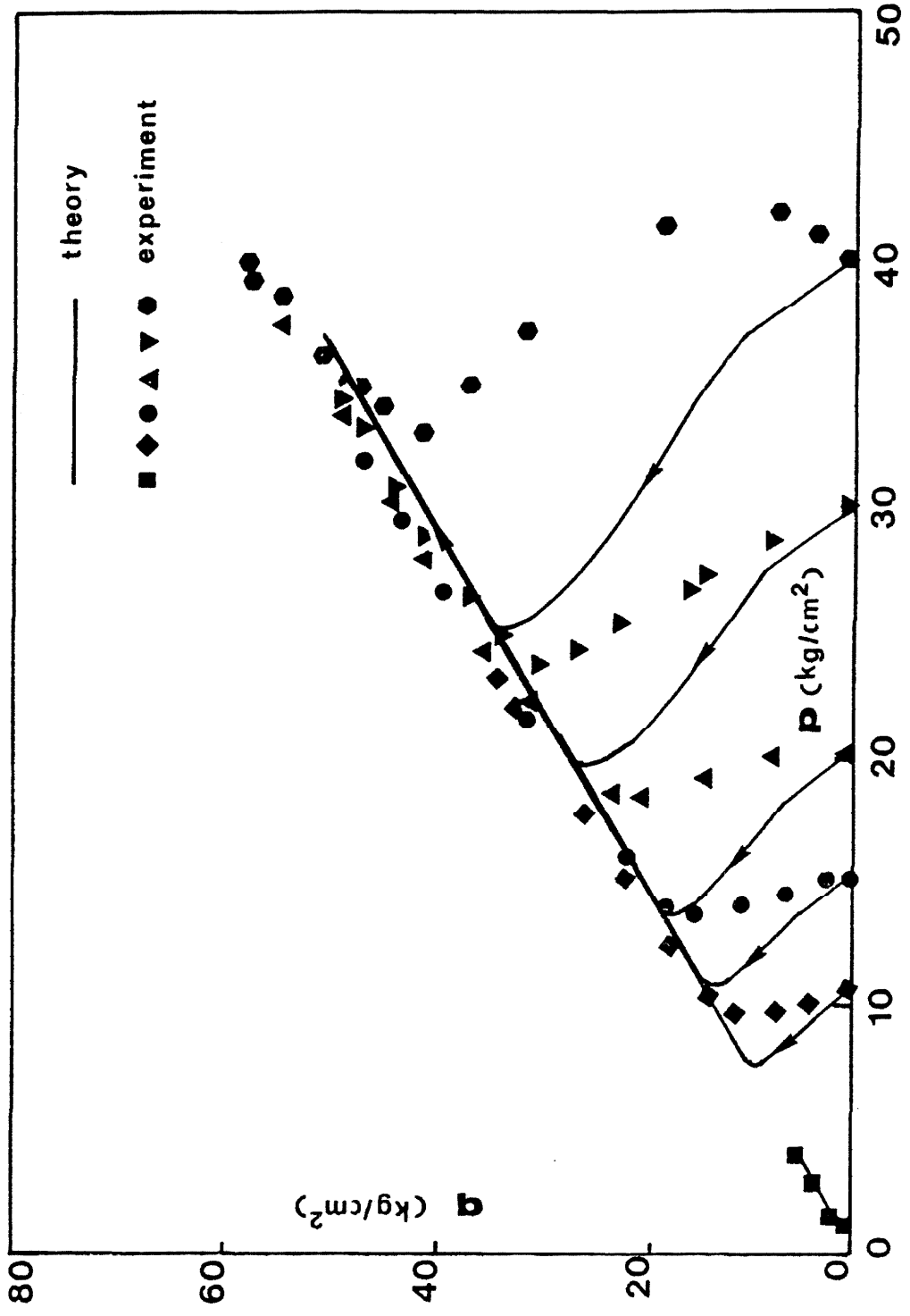

Fig. 5.17a. Predicted and experimental undrained tests at different confining pressures (dense Sacramento River sand).

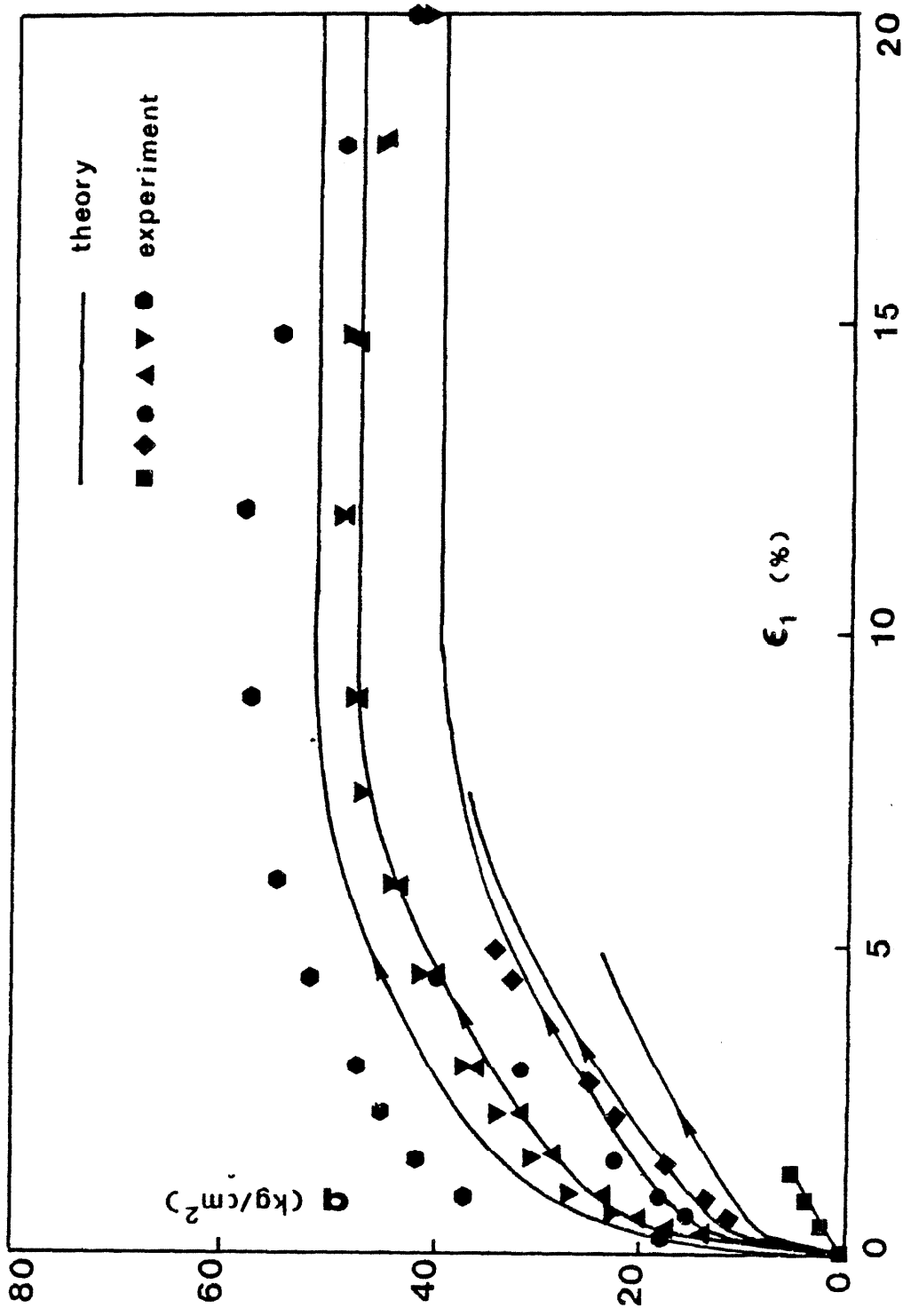

Fig. 5.17b. Predicted and experimental undrained tests at different confining pressures (dense Sacramento River sand).

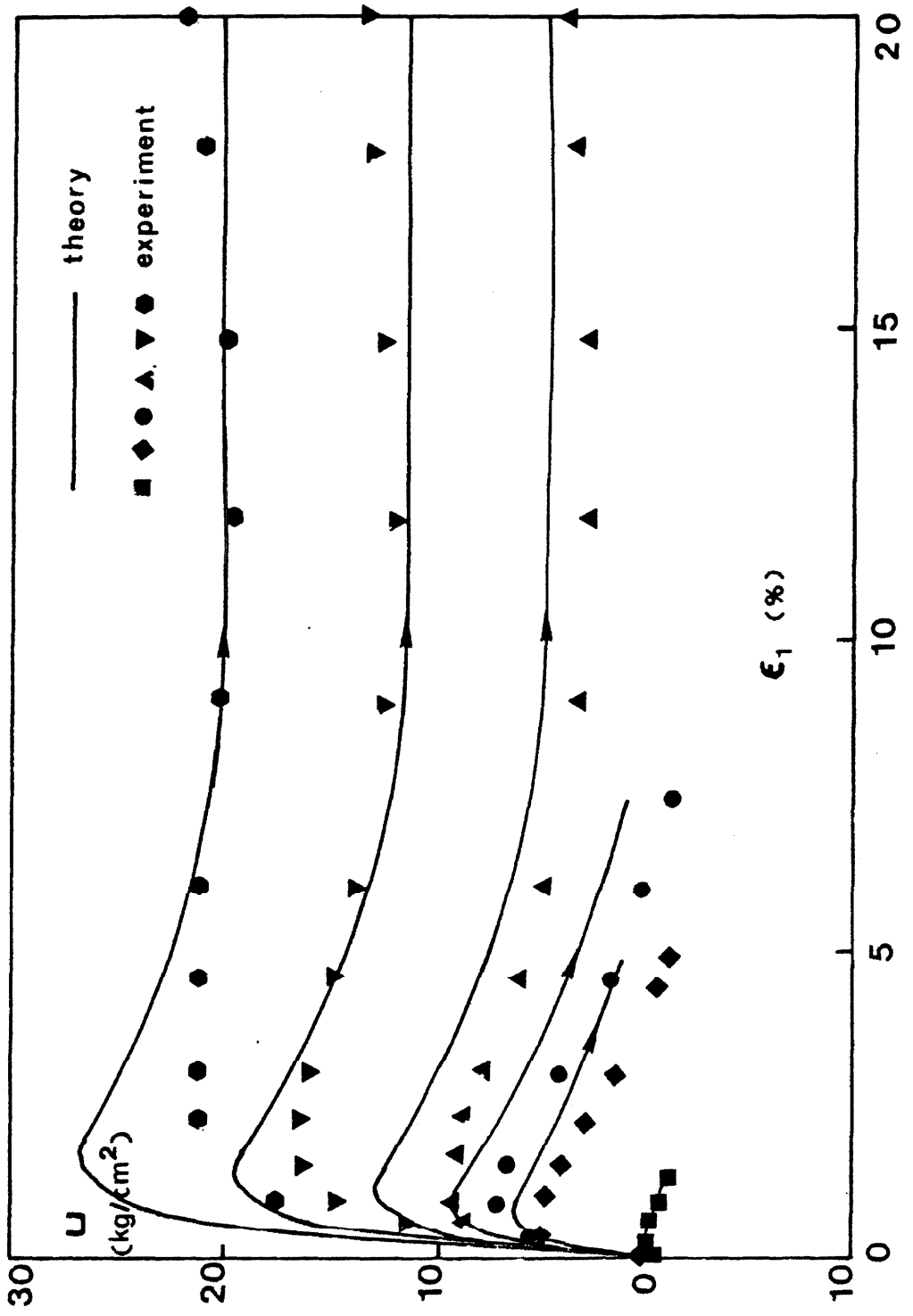

Fig. 5.17c. Predicted and experimental undrained tests at different confining pressures (dense Sacramento River sand).

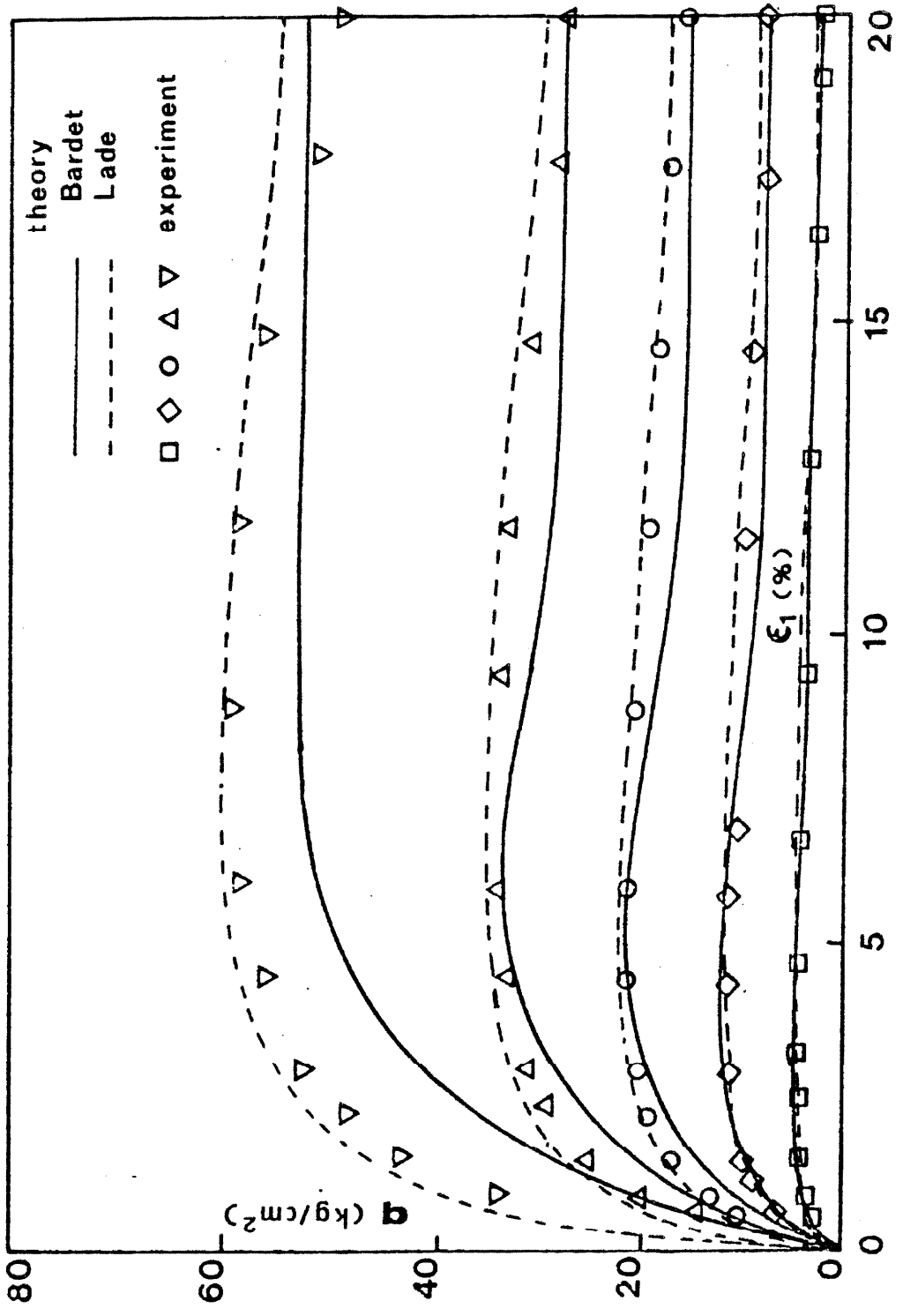

Fig. 5.18a. Predicted and experimental drained tests at different confining pressures (dense Sacramento River sand).

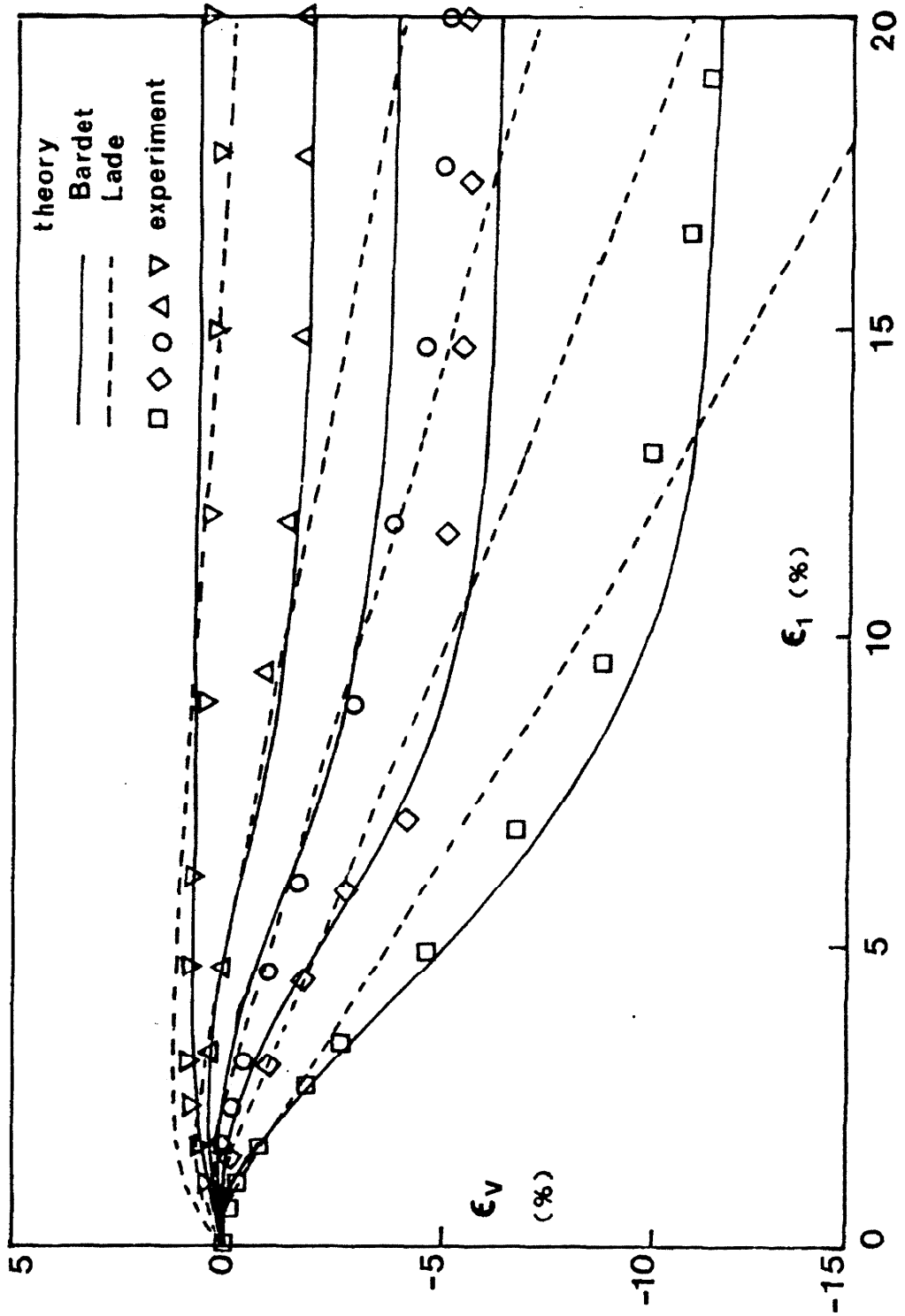

Fig. 5.18b. Predicted and experimental drained tests at different confining pressures (dense Sacramento River sand).

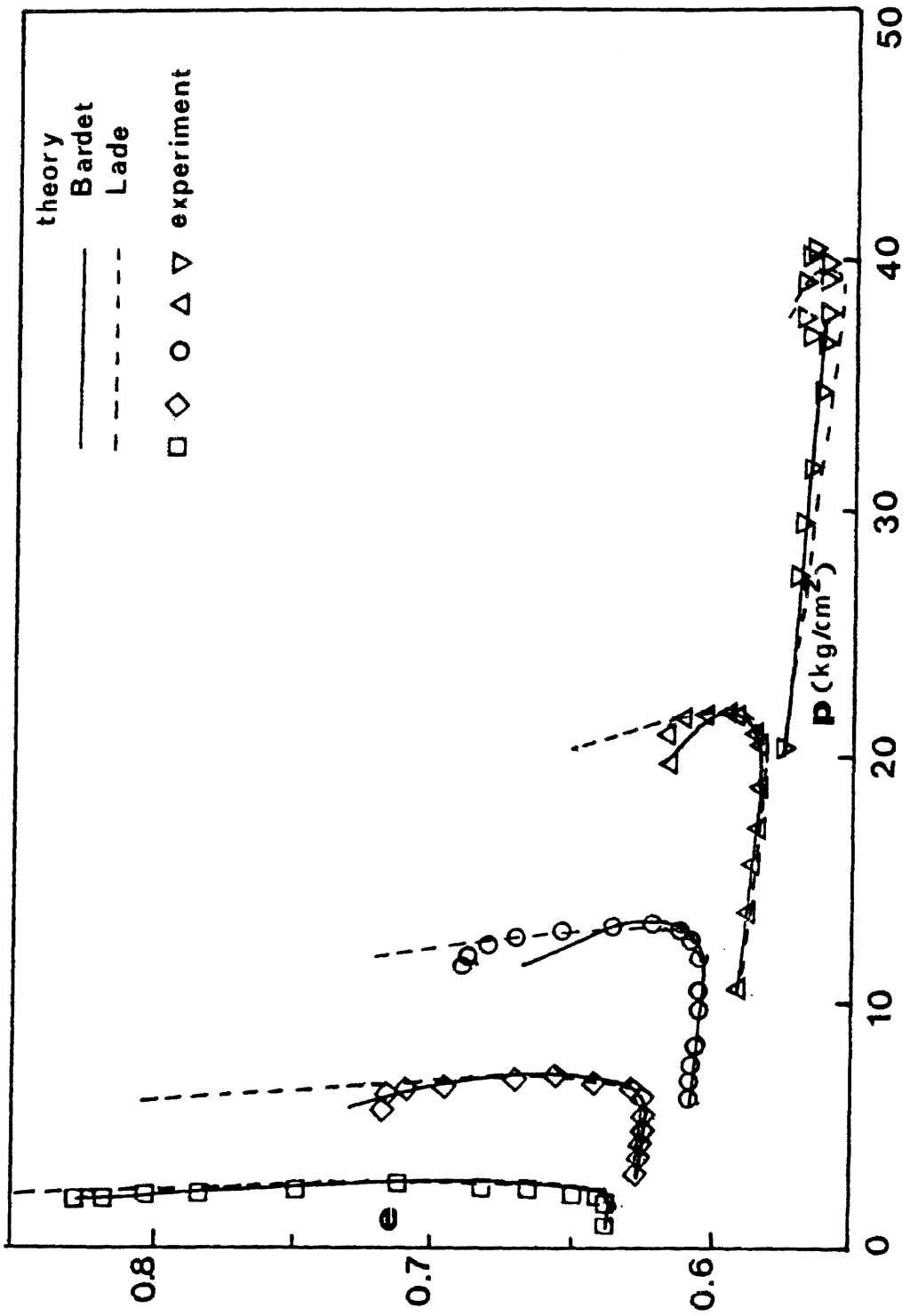

Fig. 5.18c. Predicted and experimental drained tests at different confining pressures (dense Sacramento River sand).

especially to describe the void ratio (Fig. 5.18c) from its initial to final critical value. As observed experimentally, the stress drop following the peak stress become less important when the confining pressure is increased; finally the stresses and volumetric strain reach an asymptotic value for large axial strain. However the simulated response is softer than the observed one, which is certainly caused by low values of the plastic modulus H.

In Fig. 5.18, the new constitutive model is compared to Lade's second model [5.10], which constitutes a good example of the application of conventional plasticity to describe the sand behavior. The main change w.r.t. Lade's first model presented in section 3.2.1 is a new composite yield surface, which is composed of a cone slightly different of the original yield surface and of an elliptic cap centered on the hydrostatic axis. The numerical predictions, shown in Fig. 5.18c, was performed with the fourteen model constants given by Lade [1.17]. Lade's model predicts a better response for small axial strain, but forecasts a continuous stress drop after the maximum stress (Fig. 5.18a) and a continuous dilatancy (Fig. 5.18b). For large axial strain, the stress drop becomes so large that the deviatoric stress becomes negative, and the soil volume keeps increasing to reach a nonphysical value.

Although the corresponding laboratory tests on the Sacramento River sand were unavailable, two cyclic loadings were predicted in Fig. 5.19 and 5.20. In Fig. 5.19, ten undrained cycles were performed with the

deviatoric stress q varying between 0 and 10 kg/m^2; the calculated pore pressure increases until it reaches a maximum (Fig. 5.19c), which implies that the stress path (Fig. 5.19a) stabilizes in the p-q space. The dense Sacramento River sand does not liquefy according to the numerical simulation. For a larger initial void ratio, the parameter b_2 may take a smaller value so that the effective stress path can reach the failure line (liquefaction). In Fig. 5.20 two sets of five drained cycles at constant confining pressure were also predicted. The deviatoric stress q was cycled first from 5 to 10 kg/m^2 in the subcharacteristic domain, then from 15 to 20 kg/m^2 in the supercharacteristic domain. For the first cycles series, the material contracts, whereas for the second one, it dilates. This result is similar to Luong's experimental results presented in Fig. 5.5 and could not be simulated by a conventional plastic model like Lade's model since no plastic volumetric strain could be created by cycles inside the yield surface. Both predictions of drained and undrained cyclic responses, although they could not be corroborated by experimental data, are encouraging: they represent qualitatively and quantitatively representative of a dense sand behavior.

5.8 GENERALIZATION FROM AXISYMMETRIC TO SIX-DIMENSIONAL STRESS STATE

The new constitutive equation has been constructed only for axisymmetric stress states, corresponding to the only available test results on the Sacramento River sand. In order to be operational in a finite element data code, where any combined stress state becomes possi-

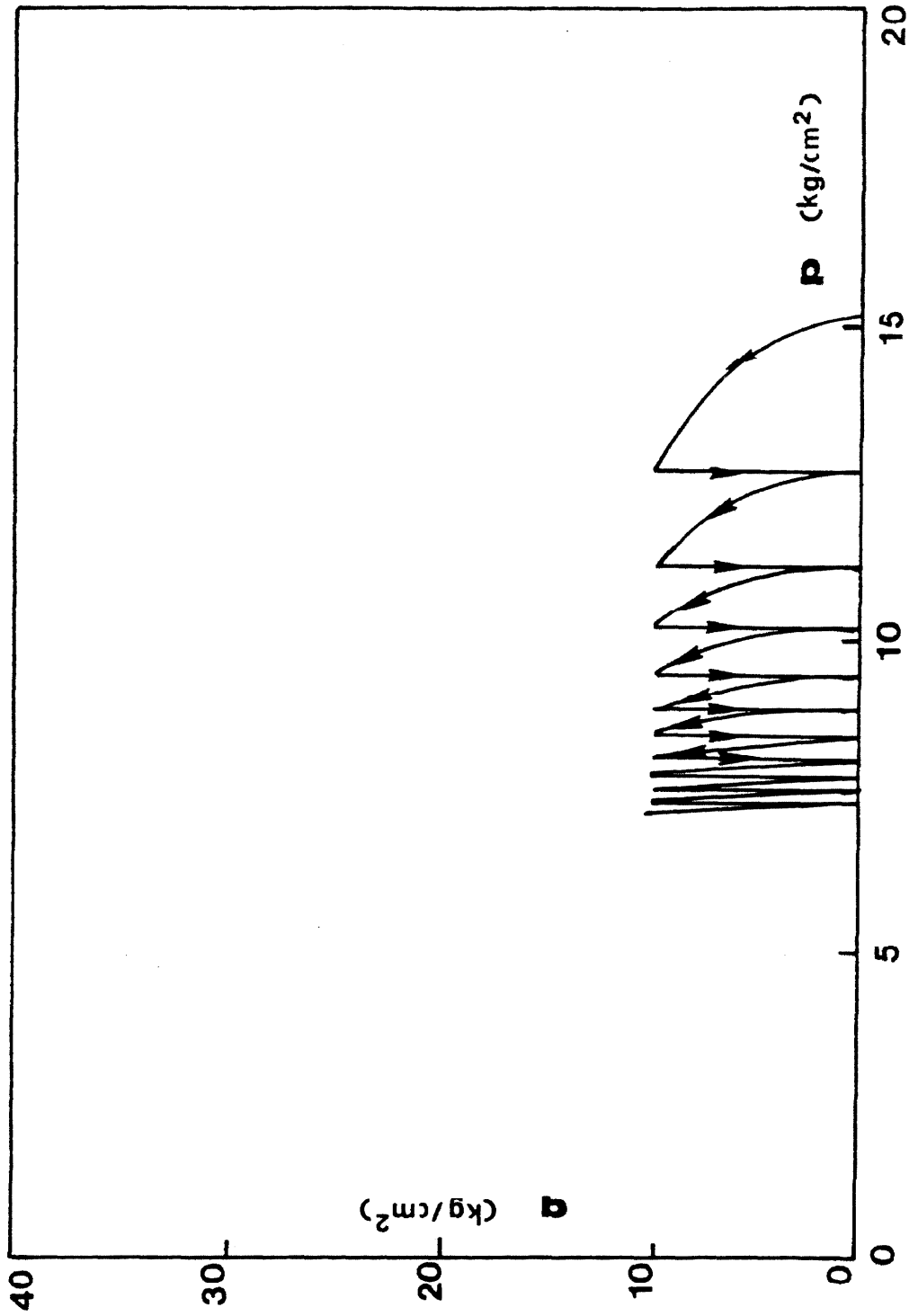

Fig. 5.19a. Simulated undrained cyclic test on the dense Sacramento River sand.

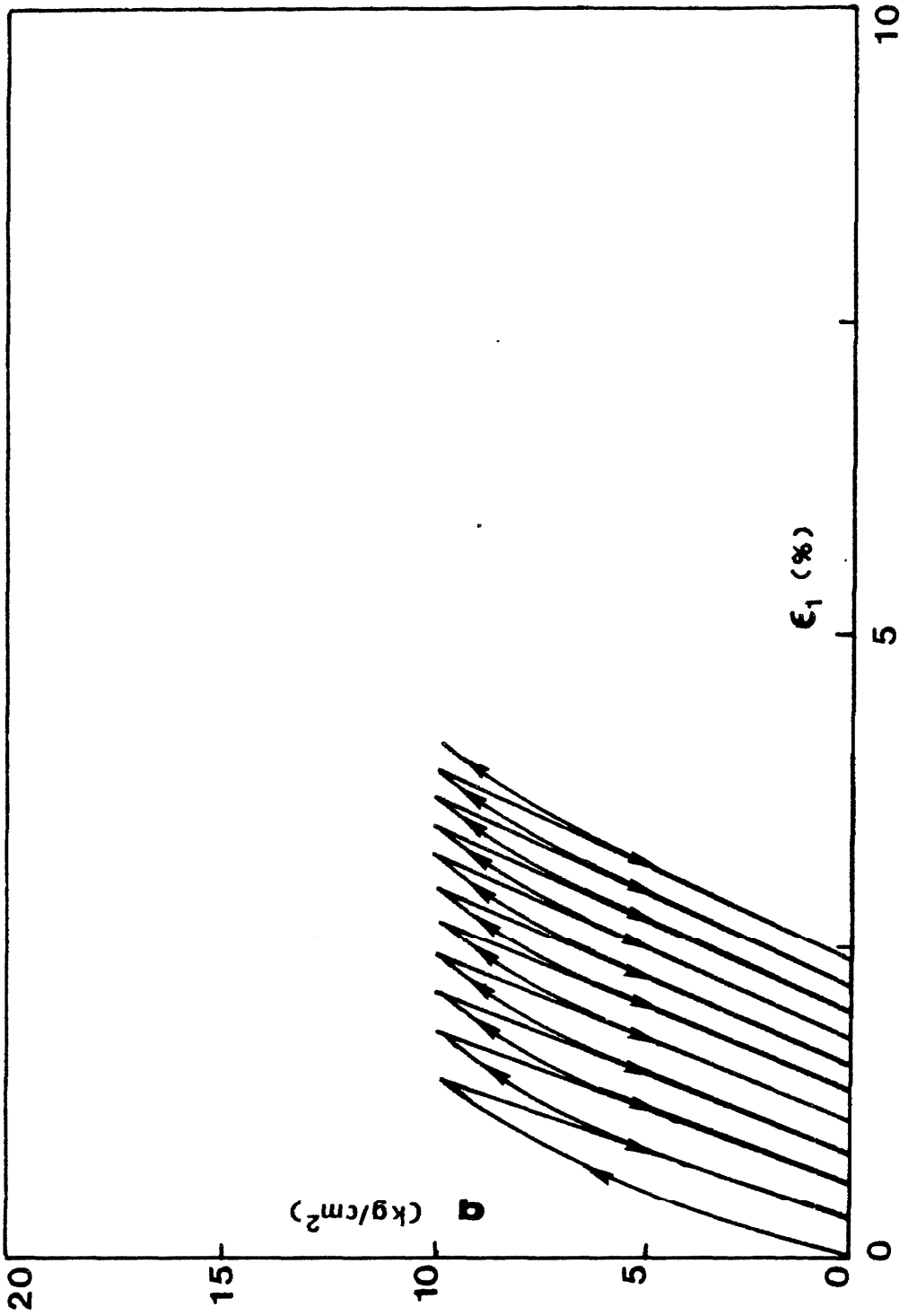

Fig. 5.19b. Simulated undrained cyclic test on the dense Sacramento River sand.

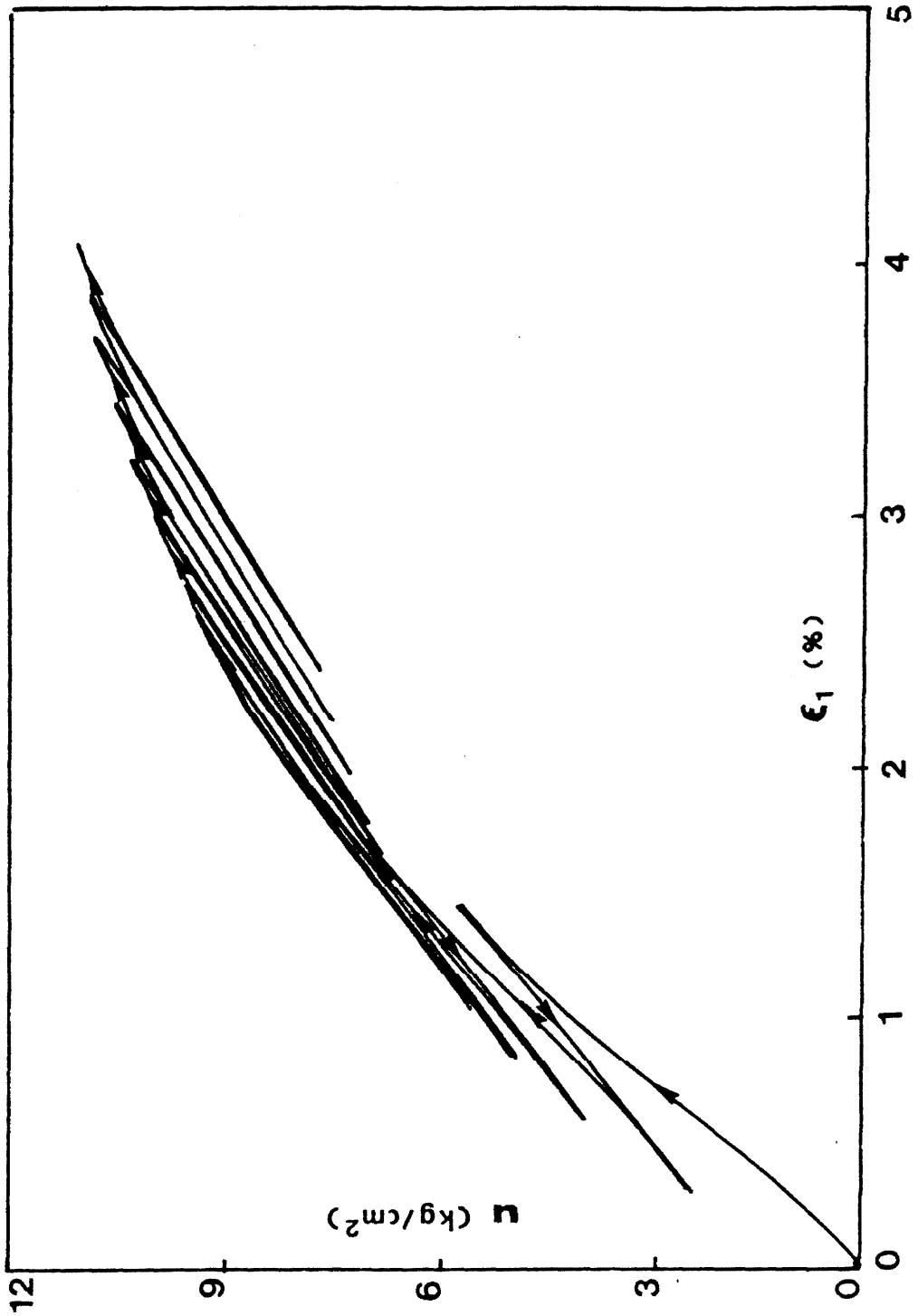

Fig. 5.19c. Simulated undrained cyclic test on the dense Sacramento River sand.

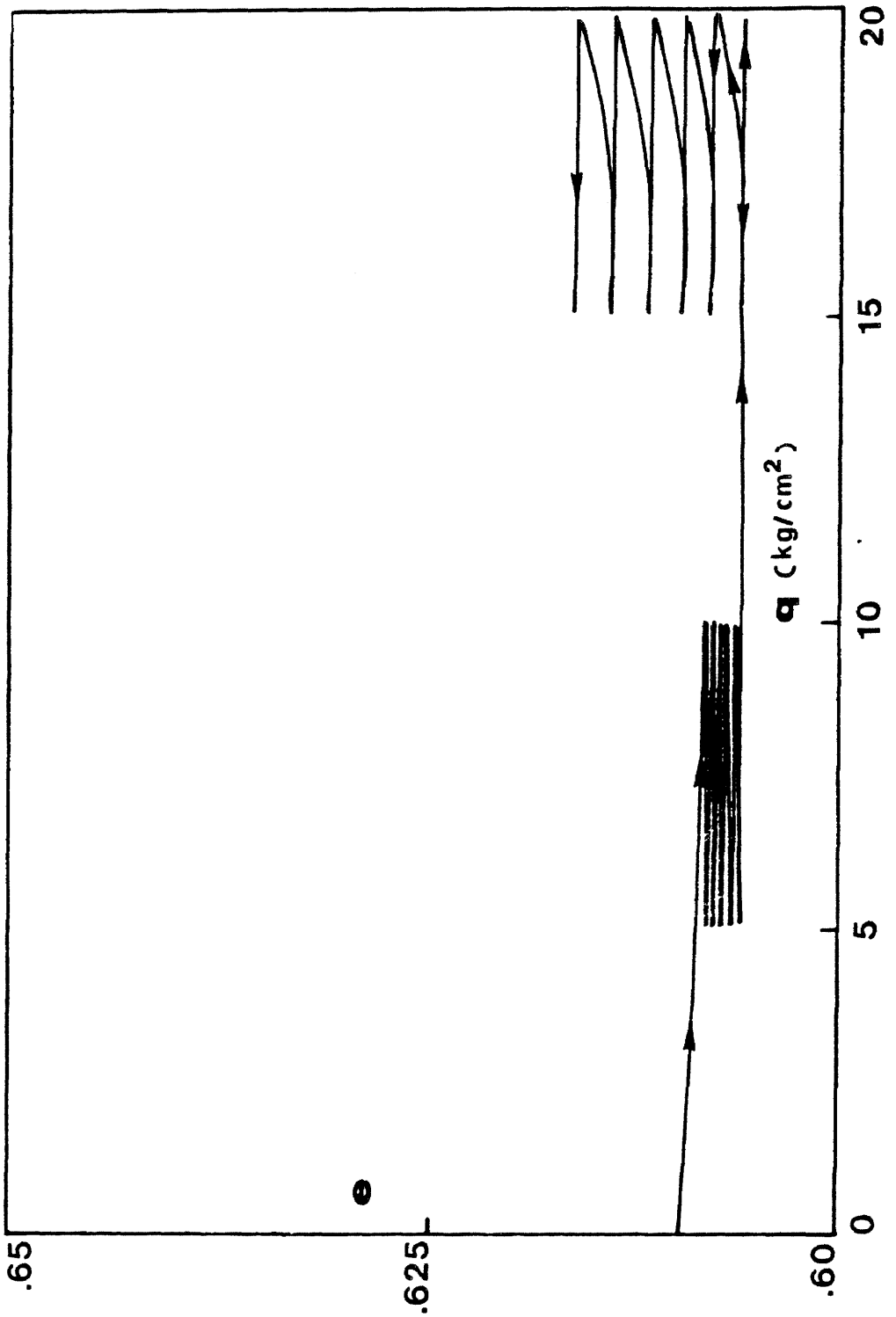

Fig. 5.20. Simulated drained cyclic test on the dense Sacramento River sand.

ble, the new model must be generalized to six-dimensional stress space. This generalization process, commonly used in any material modeling, can be illustrated with the transformation of a surface, which may be a yield, potential or bounding surface, from the p-q space into a hypersurface in the six-dimensional space. This example is used next to generalize the new model.

5.8.1 From Surface in p-q Space to Hypersurface in Six-Dimensional Stress Space

Given a surface in p-q space, denoted by $f^*(p,q,\xi) = 0$, a hypersurface must be found such that its projection onto the p-q space coincides with the surface f^*. Excluding in particular the nonisotropic surfaces, such as von Mises' surfaces not centered on the hydrostatic axis, two specific classes of surfaces in the p-y space are only extended into hypersurfaces in six-dimensional stress space. This particular generalization is performed by creating an isotropic surface, represented by $f(I,J,\theta,\xi) = 0$, the projection of which is the surface f^* in the p-q space.

The first category comprises the surfaces symmetric about the p axis, which implies that, for any p and q:

$$f^*(p,-q,\xi) = f^*(p,q,\xi) = 0 \qquad (5.41)$$

Considering the relation (3.60c), these surfaces are easily generalized in the stress invariant space into surfaces independent of Lode's angle and satisfy the following relation

$$f(I,J,\xi) = f^*(\frac{I}{3},3^{1/2}J,\xi) = 0 \qquad (5.42)$$

In a principal stress space, such a surface intersects a deviatoric plane along a circle centered on the hydrostatic axis. For example, the Roscoe-Burland model [5.20], one of the earliest plastic soil models, has an elliptic yield surface (Fig. 5.21a) in the p-q space:

$$f^*(p,q,p_{nc}) = \frac{q^2}{M^2} + p(p-p_{nc}) = 0 \qquad (5.43)$$

This surface is generalized according to relation (5.42) such as

$$f(I,J,p_{nc}) = 3\left[\frac{J}{M}\right]^2 + \frac{I}{3}\left[\frac{I}{3} - p_{nc}\right] = 0 \qquad (5.44)$$

and is represented in Fig. 5.21b.

A more general category is composed of surfaces which obey the following relation:

$$f^*(p,-q,\xi) = f^*(p,\frac{q}{\beta},\xi) \quad \text{for} \quad q > 0 \qquad (5.45)$$

where β is a positive scalar.

The symmetric surfaces, defined by the expression (5.41), belong to this category and are obtained for β equal to unity. All the surfaces satisfying (5.45) are extended into isotropic hypersurfaces which obey the following relation

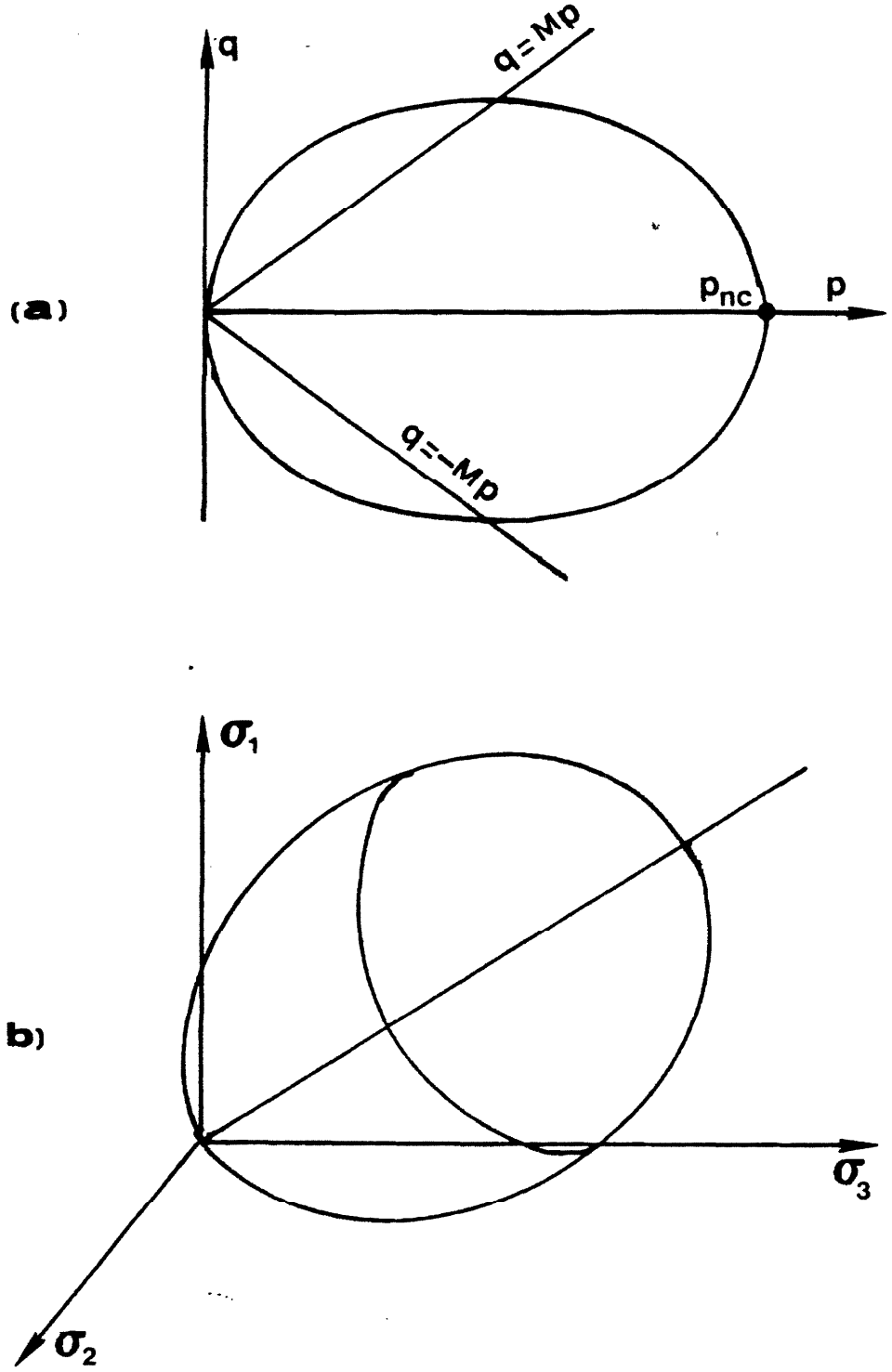

Fig. 5.21. Roscoe-Burland yield surface

a) in p-q space
b) in principal stress space without influence of Lode's angle.

$$f(I,J,\theta,\xi) = f^{*}\left[\frac{I}{3}, 3^{3/2}\frac{J}{g(\theta,\beta)}, \xi\right] \tag{5.46}$$

where $g(\theta,\beta)$ is a continuous interpolating function of Lode's angle and β which obeys the following constraints:

$$g(\frac{\pi}{6}, \beta) = +1 \tag{5.47a}$$

$$g(-\frac{\pi}{6}, \beta) = \beta \tag{5.47b}$$

An example of such a function is given by Dafalias and Herrmann [5.7].

$$g(\theta,\beta) = \frac{2\beta}{1+\beta - (1-\beta)\sin 3\theta} \tag{5.48}$$

$g(\theta,\beta)$ is represented in Fig. 5.22 for different values of β. This function of Lode's angle scales the radial distance of a point on the surface to the hydrostatic axis. If β is close to 0.8, Fig. 5.22 presents some similarities with Fig. 3.5a, which represent the intersection of Lade's yield surface with a deviatoric plane.

For example, the Roscoe-Burland model may be adapted by requiring the following change in relation (5.46)

$$\begin{aligned} M &= M_c \quad \text{if} \quad q \geq 0 \qquad M = M_c \\ &= M_e \quad \text{if} \quad q < 0 \qquad = M_e \end{aligned} \tag{5.49}$$

After such a modification the surface satisfies (5.48) where β is equal to $\frac{M_e}{M_c}$.

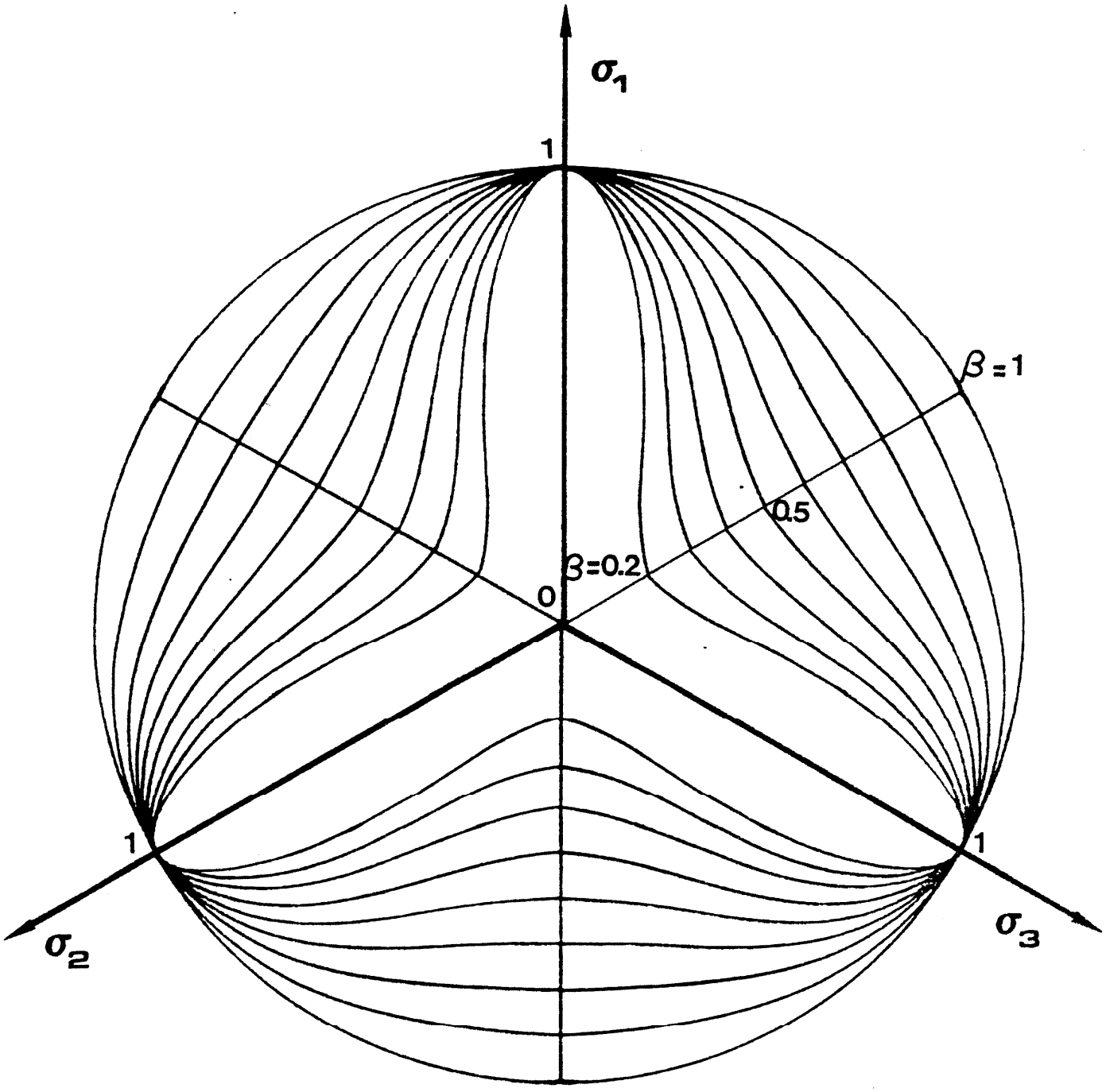

Fig. 5.22. Influence of Lode's angle in a deviatoric plane on yield, potential or bounding surfaces for different values of β.

The generalized surface becomes:

$$f(I,J,\theta,\underline{\xi}) = 3\left[\frac{J}{g(\theta,\beta)M_c}\right]^2 + \frac{I}{3}\left[\frac{I}{3} - p_{nc}\right] = 0 \qquad (5.50)$$

If M_c and M_e are equal, the relations (5.50) and (5.44) coincide.

Two particular and simple generalizations of surfaces into hypersurfaces have been presented. This mathematical abstraction, although convenient, needs to be corroborated by experimental investigations. The influence of the Lode's angle and the isotropy assumption should be examined by specifying the influence of the intermediate principal stress σ_2 and the effect of rotation of principal stresses.

5.8.2 Generalization of New Model

The new model defined in the p-q space must be extended to six-dimensional stress space. Since no experimental result was available on which to base this generalization, the simplest solution was adopted. The model is assumed to be isotropic, which implies from Section (3.4) that its six-dimensional formulation may be derived from stress-invariant space.

The radial mapping (5.22) becomes

$$\mathbf{I} = x\, I \qquad (5.51a)$$

$$\mathbf{J} = x\, J \qquad (5.51b)$$

$$\bar{\theta} = \theta \tag{5.51c}$$

where $\bar{I},\bar{J},\bar{\theta},I,J,\theta$ represent respectively the invariants of the image stress and stress state, and x is given by solving the following equation

$$f(x\,I, x\,J, \theta, \xi) = 0 \tag{5.52}$$

The bounding surface, denoted $f(\bar{I},\bar{J},\theta) = 0$ and originally described by the relation (5.20), becomes according to (5.46)

$$\left[\frac{\bar{I}-3A}{p-1}\right]^2 + \left[\frac{\bar{I}}{N}\right]^2 - (3A)^2 = 0 \quad , \quad J \leq N\,I \tag{5.53a}$$

$$\alpha(\alpha-2)(\bar{I}-3A)^2 + \left[(\alpha-2)\,\frac{\bar{I}}{N} + 3A\right]^2 - (\alpha-1)^2(3A)^2 \quad , \quad J > NI \tag{5.53b}$$

where

$$N = \frac{M_c}{3\,3^{1/2}}\,g(\theta,\beta) \tag{5.53c}$$

and

$$\beta = \frac{M_c}{M_e} \tag{5.53d}$$

and $g(\theta,\beta)$ is given by (5.51).

The relation (5.39) transforms into:

$$a\left(\frac{J}{I}\right) = \frac{a_0}{2}\left[\cos \pi \frac{J}{IN_p}^{a_1} + 1\right] \tag{5.54a}$$

where

$$N_p = \eta_p \frac{g(\theta,\beta)}{3\ 3^{1/2}} \tag{5.54b}$$

All other useful relations in the stress invariant space are easily derived by using the expressions (3.60). The final expressions (3.41) relating the plastic strain increment and the stress increment may be calculated from the partial derivatives $\frac{\partial f}{\partial \sigma_{ij}}$ obtained by using (3.58) and differentiating (5.53). Therefore, the new model is formulated in six-dimensional stress space.

CHAPTER VI

CONCLUSIONS

In the past twenty years, the representation of rheological soil behavior through constitutive equations has been gaining so much interest among researchers and practicing engineers that it has created a new branch in soil mechanics. With the powerful combination of continuum mechanics and numerical techniques (finite elements), complex and practical geotechnical problems may be solved as boundary value problems.

Regarding the soil, always made of a multitude of discrete mineral particles, as a continuous medium, permits us to describe the motion of its grains and the forces acting on them in a simple form. However this drastic assumption conceals some fundamental physical characteristics of the material, which should be discovered by further microscope studies.

Among all the constitutive theories treating soil as a continuum, plasticity remains the most commonly used in geotechnical works. Although this theory was used successfully for metals, its fundamental ideas do not fit exactly the more complex soil behavior. In general, basic concepts, such as yield and potential surfaces, are arbitrarily mathematical and hardly verified experimentally. When exhibited by difficult and lengthy experiments, these surfaces are found to possess irregularities, such as corner or vertices. Even basic plasticity

requirements, such as Drucker's postulate, do not apply to soils, which frequently show a strain-softening behavior.

Very recently, Dafalias and Popov brought about some changes in plasticity theory and recast most of its conventional concepts without changing its mathematical formulation. This new theoretical framework, "bounding surface" plasticity, has been applied to construct a new model for sand. Step by step, each element of this new constitutive relation has been assembled. The elastic contribution was described by a truly nonlinear elastic model. The plastic flow direction was characterized by a bounding surface composed of two ellipses. Its amplitude was determined by a relation connecting the plastic moduli H and H_B with the distance δ. This new model, with eleven material constants, describes well the behavior of the dense Sacramento River sand. Since the model is founded on rheological behaviors commonly observed for granular materials, it is believed it may adapt to any sand by appropriate selection of the material constants. First, the constitutive equation was formulated in the simple p-q space (axisymmetric loading) in order to use the only tests available on the Sacramento River sand, then it was extended to more general states of stress by invoking the isotropy assumption and a specific contribution of Lode's angle. In its six-dimensional formulation, the new model is ready to be implemented in a finite element code to represent the rheological behavior of sand.

The new model has a certain advantage over any conventional plastic model: it can describe with more flexibility the complex cyclic behavior observed for sands. The plastic strain amplitude is now controlled by a scalar relation between H, H_B and δ and is not governed by complex relations describing changes in hypersurfaces. In the present analysis, the new model has only been validated for monotonic loadings. It had to represent simple monotonic behavior before complex cyclic responses. However the new model is believed to adapt to most experimental data set obtained on sands during cyclic loadings, either by adjusting the value of the parameter b_2, or by slightly modifying the relation between plastic moduli H, H_B, and distance δ.

Although totally completed, and ready to be used, the new model may still be improved in different ways.

The elastic contribution, and especially the dependence of the bulk modulus upon the deviatoric stress, was defined by a theoretical correction in order to conserve energy. It could be verified experimentally. Additionally, a coupling between the elastic response and the plastic internal variables may improve the representation of sand densification during cyclic loading.

Like in conventional plasticity theory, the strain increment direction predicted by the new model was assumed to be independent of the stress increment direction. This assumption is contrary to experimental results found by Tatsuoka and Ishihara [A.1], but could not be modified

according to insufficient experimental evidence. When further experimental data become available, the plastic flow directions predicted by the new model may become dependent of the stress increment direction. The mapping rule (relation between the stress state and the image stress) may depend on the stress increment. With such a mapping rule, the plastic strain direction may be related to stress increment direction, while a smooth form (no vertex) is preserved for the bounding surface.

The amplitude of the plastic flow, defined by the scalar relation connecting H, H_B and δ, could also be improved. The constants entering this relation are fitting parameters without physical meaning. They are difficult to determine, since they are evaluated by trial and error. Future improvement may come from the introduction of the peak failure location, where the plastic modulus H becomes zero for any distance δ, and H_B.

The influence of Lode's angle and isotropy have presently been assumed for convenience. Lode's angle contribution yields for some values of model constants, M_e, M_c, a concave bounding surface; this effect should be studied in three-dimensional tests with different principal intermediate stresses. The isotropy hypothesis, which brings a good deal of simplicity for passing from axisymmetric state to six-dimensional state, could also be reexamined when sufficient data are available on the effect of principal stress rotation.

The existing model, in its present state, may be implemented in a finite element code, with the numerical integration scheme, as selected by Dafalias and Herrmann [5.7]. This technique involves a predictor multiple-corrector method, which calculates the equivalent tangential stiffness and the finite stress increment corresponding to a finite strain increment. This model implementation constitutes the next immediate project, and gives meaning to this new constitutive equation. It will help practicing engineers to represent sand behavior with more accuracy when dealing with complex geotechnical problems.

CHAPTER VII

REFERENCES

Chapter I

1.1 Aboim, C.A. and W.H. Roth, "Bounding-Surface Plasticity Theory Applied to Cyclic Loading of Sand," International Symposium on Numerical Models in Geomechanics, Zurich, Switzerland, September 13-17, 1982.

1.2 Ansal, A.M., Z.P. Bazant and R.J. Krizek, "Viscoplasticity of Normally Consolidated Clays," Journal of the Geotechnical Engineering Division, GT4, April 1979, pp. 519-537.

1.3 Arthur, J.R.F., K.S. Chua and T. Dunstan, "Dense Sand Weakened by Continuous Principal Stress Direction Rotation," Geotechnique, 29, 1979, pp. 91-98.

1.4 Bazant, Z.P., A.M. Anzal and R.J. Krizek, "Viscoplasticity of Transversely Isotropic Clays," Journal of the Engineering Mechanics Division, EM4, August 1979, pp. 549-565.

1.5 Bazant, Z.P. and R.J. Krizek, "Endochronic Constitutive Law for Liquefaction of Sand," Journal of the Engineering Mechanics Division, April 1976, pp. 225-238.

1.6 Cuellar, V., Z.P. Bazant, R.J. Krizek and M.L. Silver, "Densification and Hysteresis of Sand Under Cyclic Shear," Journal of the Geotechnical Engineering Division, GT5, May 1977, pp. 399-416.

1.7 Dafalias, Y.F. and L.R. Herrmann, "A Bounding Surface Soil Plasticity Model, International Symposium on Soils Under Cyclic and Transient Loading, Swansea, U.K., 1980, pp. 253-282.

1.8 Darve, F. and S. Labanieh, "Incremental Constitutive Law for Sands and Clays: Simulations of Monotonic and Cyclic Tests," International Journal for Numerical and Analytical Methods in Geomechanics, Vol. 6, 1982, pp. 243-275.

1.9 Davis, R.O. and G. Mullenger, "A Rate-Type Constitutive Model for Soil with a Critical State," International Journal for Numerical and Analytical Methods in Geomechanics, Vol. 2, 1978, pp. 285-282.

1.10 DiMaggio, F.L. and I.S. Sandler, "Material Model for Granular Soils," Journal of the Engineering Mechanics Division, ASCE, June 1971, pp. 935-950.

1.11 Drucker, O.C., R.E. Gibson and D.J. Henkel, "Soil Mechanics and Work-Hardening Theories of Plasticity," Proc. Am. Soc. Civil Eng., 81, No. 798, 1955.

1.12 Gudehus, G. and D. Kolymbas, "A Constitutive Law of the Rate-Type for Soils, Proceedings Third International Conf. Num. Meth. Geomechanics, Aachen, Ed. W. Wittke, Balkema, Rotterdam, 1979.

1.13 Hill, R., The Mathematical Theory of Plasticity, Oxford University Press, 1950.

1.14 Kjellman, W., "Report on an Apparatus for Consumate Investigation of the Mechanical Properties of Soils," Proc. 1st Intl. Conf. Soil Mech. Found. Eng., 2, 1936, p. 16.

1.15 Ko, H.Y. and R.F. Scott, "A New Soil Testing Apparatus," Geotechnique, Vol. 17, May 1977, pp. 40-57.

1.16 Lade, P.V., "Elastoplastic Stress-Strain Theory for Cohesionless Soil," Journal of the Geotechnical Engineering Division, October 1975, pp. 1037-1053.

1.17 Lade, P.V., "Elasto-Plastic Stress-Strain Theory for Cohesionless Soil with Curved Yield Surfaces," International Journal of Solids Structures, Vol. 13, 1977, pp. 1019-1035.

1.18 Mróz, Z. and S. Pietruszczak, "On Hardening Anisotropy of K_0-Consolidated Clays," International Journal for Numerical and Analytical Methods in Geomechanics, Vol. 7, 1983, pp. 19-38.

1.19 Parry, R.H.G., "Strength and Deformation of Clay," Ph.D. Thesis, University of London, 1956.

1.20 Pender, M.J., "A Model for the Behavior of Overconsolidated Soil," Geotechnique, 28, No. 1, 1978, pp. 1-25.

1.21 Prevost, J.H., "Plasticity Theory for Soil Stress-Strain Behavior," Journal of the Engineering Mechanics Division, EM5, October 1978, pp. 1177-1194.

1.22 Prevost, J.H., "Anisotropic Undrained Stress-Strain Behavior of Clays," Journal of the Geotechnical Engineering Division, GT 8, August 1978, pp. 1075-1080.

1.23 Roscoe, K.H. and J.B. Burland, "On the Generalized Stress-Strain Behavior of 'Wet' Clay," Engineering Plasticity, J. Heymann and F.A. Leckies, Eds., Cambridge University Press, Cambridge, England, 1968, pp. 535-608.

1.24 Roscoe, K.H., A.N. Schofield and C.P. Wroth, "On the Yielding of Soils," Geotechnique, 9, 1958, pp. 22-53.

1.25 Sandler, I.S., F.L. DiMaggio and G.Y. Baladi, "Generalized Cap Model for Geological Materials," Journal of the Geotechnical Division, ASCE, July 1976, pp. 683-697.

1.26 Schofield, A.N. and C.P. Wroth, Critical State Soil Mechanics, McGraw-Hill, London 1968.

1.27 Symes, M.J., D.W. Hight and A. Geno, "Investigating Anisotropy and the Effects of Principal Stress Rotation and of the Intermediate Principal Stress Using a Hollow Cylinder Apparatus," IUTAM Conference on Deformation and Failure of Granular Materials, Delft, August-September 1982, pp. 441-449.

1.28 Valanis, K.C. and H.E. Read, A New Endochronic Plasticity for Soils Mechanics - Transient and Cyclic Loads, Edited by G.N. Pande and O.C. Zienkiewicz, John Wiley and Sons, Ltd., 1982, pp. 375-417.

1.29 Wu, H.C. and T.P. Wang, "Densification and Dilation of Drained Sand Due to Static Reversed Loading," Report G189, 1-003, Division of Materials Engineering, The University of Iowa, 1981.

1.30 Wu, H.C. and T.P. Wang, "Endochronic Theory for the Mechanical Behavior of Cohesionless Soil Under Static Loading," Report G189-80-001, Division of Materials Engineering, The University of Iowa, 1980.

Chapter II

2.1 Biot, M.A., Mechanics of Incremental Deformation, New York, Wiley, 1965.

2.2 Christoffersen, J., M.M. Mehrabadi, and S. Nemat-Nasser, "A Micromechanical Description of Granular Material Behavior," J. Appl. Mech., 48, pp. 333-344, 1981.

2.3 Cundall, D.A. and O.D.L. Strack, "A Discrete Numerical Model for Granular Assemblies," Geotechnique 29, No. 1, pp. 47-65, 1979.

2.4 Cundall, P.A. and O.D.L. Strack, "The Development of Constitutive Laws for Soils Using the Distinct Element Method," Numerical Methods in Geomechanics, Aachen, Ed. W. Wittke, 1979, pp. 289-298.

2.5 Cundall, P.A., A. Drescher, and O.D.L. Strack, "Numerical Experiment on Granular Assemblies; Measurements and Observations," IUTAM Conference on Deformation and Failure of Granular Materials, Delft, August-September 1982, pp. 355-370.

2.6 Dantu, P., "Contribution a l'etude Mecanique et Geometrique des Mulieux Pulverulents," Proc. Fourth Intl. Conf. Soil Mech. Found Eng., London, 1957, pp. 144-148.

2.7 De Josselin de Jong, G. and A. Verruijt, "Etude Photo-elastique d'un Empilement de Disques," Cahiers du Groupe Francais des Etudes Rheologique, 2, 1969, pp. 73-86.

2.8 Deresiewicz, H., "Mechanics of Granular Matter," Advances in Applied Mechanics, Vol. 15, Academic Press, New York, 1958, pp. 233-306.

2.9 Horne, M.R., "The Behavior of an Assembly of Rotund, Rigid Cohesionless Particles," Proceedings of Royal Society, Parts I and II, A286, pp. 62-97; Part III, A310, 1965, pp. 21-34.

2.10 Lambe, T.W. and R.V. Whitman, Soil Mechanics, Part II, John Wiley & Sons, Inc., 1969.

2.11 Luong, M.P., "Mechanical Aspects and Thermal Effects of Cohesionless Soils Under Cyclic and Transient Loading," IUTAM Conference on Deformation and Failure of Granular Materials, Delft, August-September 1982, pp. 239-246.

2.12 Malvern, L.E., Introduction to the Mechanics of a Continuous Medium, Prentice-Hall, Inc., 1969.

2.13 Nemat-Nasser, S., "Fabric and Its Influence on Mechanical Behavior of Granular Materials," IUTAM Conference on Deformation and Failure of Granular Materials, Delft, August-September 1982, pp. 37-42.

2.14 Oda, M. and J. Konishi, "Microscopic Deformation of Granular Material in Simple Shear," Soils Found., 14, 1974, pp. 25-38.

2.15 Rowe, P.W., "The Stress Dilatancy Relation for Static Equilibrium of an Assembly of Particles in Contact, Proc. Royal Society, A269, pp. 500-527, 1962.

2.16 Scott, R.F. and M.J.K. Craig, "Computer Modeling of Clay Structure and Mechanics," Proceedings ASCE, Vol. 106, GT1, January 1980, pp. 17-33.

2.17 Truesdell, C. and R. Toupin, "Classical Field Theories," Handbuch der Physik, (Ed.) S. Flugge, Vol. III/1, 1960.

2.18 Van der Kogel, H., "Wave Propagation in Saturated Porous Media," Ph.D. Thesis, California Institute of Technology, Pasadena, May 1977.

Chapter III

3.1 Arthur, J.R.F., K.S. Chua, and T. Dunstan, "Dense Sand Weakened by Continuous Principal Stress Direction Rotation", Geotechnique, 29, 1979, pp. 91-98.

3.2 Dafalias, Y.F. and E.P. Popov, "Plastic Internal Variables Formultion of Cyclic Plasticity," Journal of Applied Mechanics, vol. 98, no. 4, Dec. 1976, pp. 645-651.

3.3 Drucker, D.C., "A Definition of Stable Inelastic Material," J. Applied Mech., 26, 1959, pp. 106-112.

3.4 Hill, R., The Mathematical Theory of Plasticity, Oxford:Clarendon Press, 1950.

3.5 Lade, P.V. and J.M. Duncan, "Elastoplastic Stress-strain Theory for Cohesionless Soil," Journal of the Geotechnical Engineering Division, GT10, Oct. 1975, pp. 1037-1053.

3.6 Lubliner, J., "On the Structure of the Rate Equations of Materials with Internal Variables, Acta Mech\., Vol. 17, 1973, p. 109.

3.7 Naghdi, P.M., and J.A. Trapp, "The Significance of Formulating Plasticity Theory with Reference to Loading Surfaces in Strain Space," International Journal of Engineering Science, vol. 13, no. 9/10, Sept./Oct., 1975, pp. 785-787.

3.8 Poorooshab, H.B., "Deformation of Sand in Triaxial Compression," Fourth Asian Conference on Soil Mechanics and Foundation Engineering, Bangkok, Vol. 1, 1971, pp. 63-66.

3.9 Rudnicki, J.W. and J.R. Rice, "Conditions for the Localization of Deformation in Pressure-sensitive Materials", J. Mech. Phys. Solids, Vol. 23, 1975, pp. 371-394.

3.10 Symes, M.J., D.W. Hight, and A. Geno, "Investigating Anisotropy and the Effects of Principal Stress Rotation and of the Intermediate Principal Stress Using a Hollow Cylinder Apparatus," IUTAM Conference on Deformation and Failure of Granular Materials, Delft, August-Sept. 1982, pp. 441-449.

3.11 Ko, H. Y. and R. F. Scott, "Deformation of Sand in Shear," Journal of the Soil Mechanics and Foundations Division, ASCE, Vol. 93, No. SM5, Proc. paper 5470, Sept. 1967, pp. 283-310.

3.12 Tatsuoka, F. and K. Ishihara, "Yielding of Sand in Triaxial Compression," Soils and Foundations, vol. 14, no. 2, June 1974, pp. 63-76.

3.13 Yoder, P., A Strain-Space Plasticity, Theory and Numerical Implementation, Ph.D. Thesis, California Institute of Technology, Pasadena, 1981.

Chapter IV

4.1 Dafalias, Y.F., and E. Popov, "Plastic Internal Variables Formalism of Cyclic Plasticity," Journal of Applied Mechanics, vol. 98, no. 4, December 1976, pp. 645-651.

4.2 Dafalias, Y.F., and L.R. Herrmann, "Bounding Surface Formulation of Soil Plasticity," Soil Mechanics - Transient and Cyclic Loads, Edited by G.N. Pands and O.C. Zienkiewicz, John Wiley and Sons Ltd., 1982, pp. 253-282.

4.3 Iwan, W.D., "On a Class of Models for the Yielding Behavior of Continuous and Composite Systems," Journal of Applied Mechanics, Transactions of the ASME, Sept. 1967, pp. 612-617.

4.4 Mróz, Z., "On the Description of Anisotropic Workhardening," J. Mech. Phys. Solids, 15, 1967, pp. 163-175.

4.5 Prevost, J.H., "Anisotropic Undrained Stress-strain Behavior of Clays," Journal of the Geotechnical Engineering Division, August 1978, GT8, pp. 1075-1090.

4.6 Truesdell, C. "Hypo-elasticity," Journal of Rational Mechanics Anal., 4, 1955, pp. 83-133.

Chapter V

5.1 Aboim, C.A., "Bounding-Surface Plasticity Theory Applied to Cyclic Loading of Sand," International Symposium on Numerical Models in Geomechanics, Zurich, Switzerland, Sept. 13-17, 1982.

5.2 Bardet, J.P., "Soil, a Program to Study Constitutive Equations for Soils," Report California Insitute of Technology, Pasadena, 1983.

5.3 Burlish, R. and J. Stoer, "Numerical Treatment of Ordinary Differential Equations by Extrapolation Methods," Mathematik, 1966, Vol. 8, pp. 1-13.

5.4 Chang, T.Y., H.Y. Ko, R.F. Scott and R.A. Westman, "An Integrated Approach to the Stress Analysis of Granular Materials," Report for the National Science Foundation, California Institute of Technology, Pasadena, 1967.

5.5 Dafalias, Y.F., "A Bounding Surface Plasticity Model," Proceedings of the Seventh Canadian Congress of Applied Mechanics, Sherbrooke, June 1979, pp. 89-90.

5.6 Dafalias, Y.F., "A Model for Soil Behavior Under Monotonic and Cyclic Loading Conditions," Transactions of the 5th International Conference on Structural Mechanics in Reactor Technology, Berlin, August 13-17, 1979, Session K1, pp. 1-9.

5.7 Dafalias, Y.F. and L.R. Herrmann, "Bounding Surface Formulation of Soil Plasticity," Soil-Mechanics - Transient and Cyclic Loads, edited by G.N. Pande and O.C. Zienkiewicz, John Wiley and Sons, Ltd., 1982, pp. 253-282.

5.8 Hewlett-Packard, HP-11C, "Owner's Handbook and Problem-Solving Guide," Feb. 1981, p. 162.

5.9 Horne, M.R., "The Behavior of an Assembly of Rotund, Rigid, Cohesionless Particles," Proceedings of Royal Society, Parts I and II, A286, 1965, pp. 62-97, Part III, A310, 1965, pp. 21-34.

5.10 Lade, P.V., "Elasto-Plastic Stress-Strain Theory for Cohesionless Soil with Curved Yield Surfaces," International Journal of Solids and Structures, 1977, Vol. 13, pp. 1019-1035.

5.11 Lade, P. V., "Localization Effects in Triaxial Tests on Sand," IUTAM Conference on Deformation and Failure of Granular Materials," Delft, August-September 1982, pp. 461-471.

5.12 Lee, K.L. and Seed, H.B., "Drained Characteristics of Sands," Journal of Soil Mechanics and Foundations Division, Proceedings of the ASCE, Nov. 1967, SM6, pp. 117-141.

5.13 Loret, B., "Formulation d'une loi de Comportment Elastoplastique des Milieux Granulaires," These Docteur-Ingenieur, Ecole Nationale des Ponts et Chausses, Paris, Feb. 1981.

5.14 Luong, M.P. and B. Loret, "A Rheological Model for Sand Under Various Load Paths," Comportement Rheologique et Structures des Materiaux, Compte Rendus du 15eme Colloque du Groupe Francais de Rheologie, Paris, 1980.

5.15 Luong, M.P., "Stress-Strain Aspects of Cohesionless Soils Under Cyclic and Transient Loading," International Symposium on Soils Under Cyclic and Transient Loading, Swansea, January 1980, pp. 315-324.

5.16 Momen, H. and J. Ghaboussi, "Stress Dilatancy and Normalized Work for Sands," IUTAM Conference on Deformation and Failure of Granular Materials, Delft, August-September 1982, pp. 265-274.

5.17 Nova, R., "A Constitutive Model for Soil Under Monotonic and Cyclic Loading," Soil Mechanics - Transient and Cyclic Load, Edited by G.N. Pande and O.C. Zienkiewicz, J. Wiley and Sons, 1982, pp. 343-373.

5.18 Parry, R.H.G., "Triaxial Compression and Extension Tests on Remoulded Saturated Clay," Geotechnique, 10:2, 1960, pp. 166-180.

5.19 Robinet, J.C. and M. Mokkam, "A Nonlinear Law for Sands," IUTAM Conference on Deformation and Failure of Granular Materials, Delft, August-September 1982, pp. 313-321.

5.20 Roscoe, K.H. and J.B. Burland, "On the Generalized Stress-Strain Behavior of Wet Clay," Engineering Plasticity, Edited by J. Heyman and F.A. Leckie, Cambridge University Press, 1968, pp. 535-609.

5.21 Rowe, P.W., "The Stress-Dilatancy Relation for Static Equilibrium of an Assembly of Particles in Contact," Proceedings of Royal Society, A269, 1962, pp. 500-527.

5.22 Schofield, A.N. and Wroth, C.P., Critical State Soil Mechanics, McGraw-Hill, London, 1968.

5.23 Seed, H.B. and K.L. Lee, "Undrained Strength Characteristics of Cohesionless Soils," Journal of Soil Mechanics and Foundations, Proceedings of the ASCE, SM6, Nov. 1967.

5.24 Shibata, T. and D. Karube, "Influence of the Variation of the Intermediate Principal Stress on the Mechanical Properties of Normally Consolidated Clays," Proceedings 6th International Conference SMFE, 1965, Vol. 1, pp. 359-363.

5.25 Sternberg, E., "Mathematical Theory of Elasticity," Class notes at California Institute of Technology, Pasadena, 1980.

5.26 Stroud, M.A., "The Behavior of Sand at Low Stress Levels in the Simple Shear Apparatus," Ph.D. Thesis, University of Cambridge, 1971.

5.27 Tatsuoka, H., "Dilatancy Characteristics of Soil," Soils and Foundations, Vol. 14, No. 3, Sept. 1974, pp. 13-29.

Appendix A

A.1 Tatsuoka, F. and K. Ishihara, "Yielding of Sand in Triaxial Compression, Soils and Foundations," Vol. 14, No. 2, June 1974, Japanese Society of Soils Mechanics and Foundation Engineering.

APPENDIX A

TWO EXPERIMENTS BY TATSUOKA AND ISHIHARA

A.1 FIRST EXPERIMENT BY TATSUOKA AND ISHIHARA: (A.1)

The material used in their experiment is the loose Fuji River sand. Initial samples, all of the same density, were brought to a common stress point X in the p-q space (see Fig. A.1a) through 3 different stress paths:

a) isotropic consolidation followed by an increase of axial stress at constant confining pressure σ_3; this stress path is represented by OA_0X in Fig. A.1a.

b) isotropic consolidation followed by an increase of deviatoric stress q at constant mean pressure p; the stress path is represented by OB_0X.

c) constant stress ratio test, the axial and radial stresses, σ_1 and σ_3, are increased simultaneously such that the ratio $\eta = \frac{q}{p}$ remains constant; the stress path is represented by OX.

After reaching the stress state X, "small" increments in stress, with constant amplitude but different directions, were imposed on the samples. Then the stress increments are removed so that the sample was brought back to state X. All the performed stress path and stress cycles are presented in Table A1. The volumetric and deviatoric plastic strain, denoted respectively ε_v^p and ε_q^p, which remained after this cycle

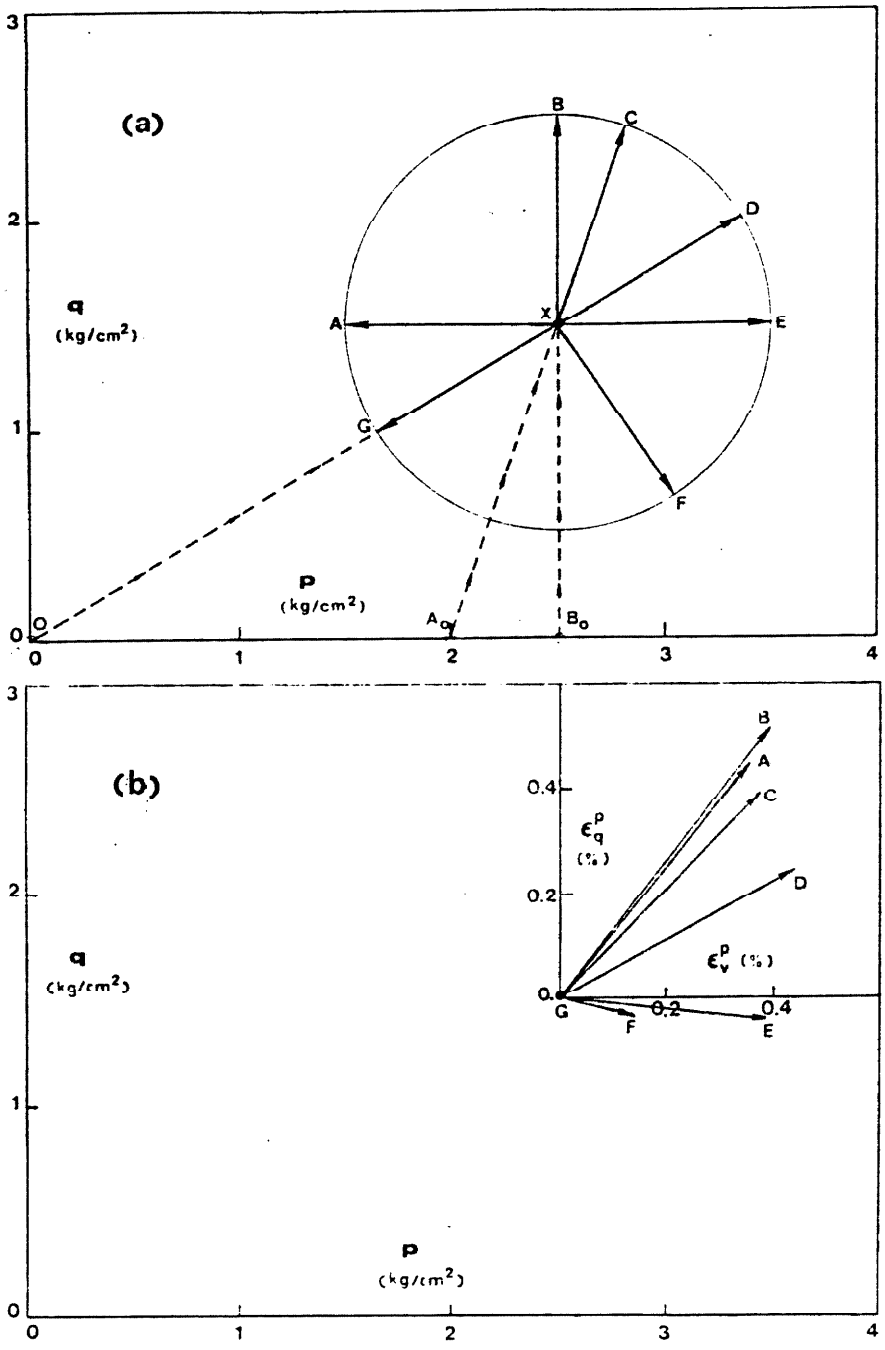

Fig. A.1. First experiment By Tatsuoka and Ishihara on the loose Fuji River sand

a) stress paths and stress increments about a common stress state X (see Table A.1)
b) measured plastic strains resulting from stress increments (see Table A.1).

TABLE A.1 SUMMARY OF LOADINGS AND TEST RESULTS FOR THE FIRST EXPERIMENT BY TATSUOKA AND ISHIHARA

Stress path to reach stress X	Increment about X	Constraint on stress increment	Relation for increment of stress in p–q space (kg/cm^2)	ε_v^p (%)	ε_q^p (%)	$\varepsilon_v^p / \varepsilon_q^p$
OA_0X	XC	constant σ_3	$dp = \frac{1}{3} dq = 0.316$	0.38	0.39	0.97
constant σ_3	XA	constant q	$dq = 0,\ dp = 1$	0.36	0.45	0.80
$\sigma_3 = 2\ kg/cm^2$	XE	constant q	$dq = 0,\ dp = -1$	0.40	−0.04	9.21
	XF	constant σ_1	$dp = -\frac{2}{3} dq$	0.15	−0.04	4.03
OB_0X	XB	constant p	$dp = 0,\ dq = 1$	0.4	0.52	0.77
constant p						
$p = 2.5\ kg/cm^2$						
OX	XG	constant η	$dq = \eta dp = -0.514$	0	0	
constant $\eta = \frac{q}{p}$	XD	constant η	$dq = \eta\ dp = +0.514$	0.44	0.24	1.83
$\eta = 0.6$						

were measured and plotted in Fig. A.1b in the form of vectors. A summary of test results represented in Fig. A.1 is found in Table A1.

A.2 SECOND EXPERIMENT BY TATSUOKA AND ISHIHARA: (A.1)

The material is still the loose Fuji River sand. The sample is subjected to the stress path represented in Fig. A.2a. The measured values of volumetric and deviatoric strain are plotted in Figs. A.2b and A.2c versus the stress ratio $\eta = \frac{q}{p}$. The sample, consolidated under a confining pressure of 2.0 kg/cm^2, was sheared to the stress ratio represented by point 2; and after further consolidation to point 4 following partial removal of the shear stress q, the sample was again subjected to a cycle of shear stress. Figs. A.2b and A.2c show that, during this reloading, both the volume and shear strains change little until a certain stress ratio is reached, whereupon appreciable increase occurs subsequently in each strain component. The stress ratio at which the appreciable strains begin to take place was determined on the diagram and designated by the point 5 in Figs. A.2b and A.2c. This point is defined as the yield point. The sample was subjected to further cycles of consolidation and shear stress according to the scheme of stress paths indicated in Fig. A.2a. In each reloading path, strains were examined and yield points at each stage were determined as indicated by the points 9, 13, and 17.

From these tests, two successive yield points located at different portions of the same yield surface are recorded. For instance, the

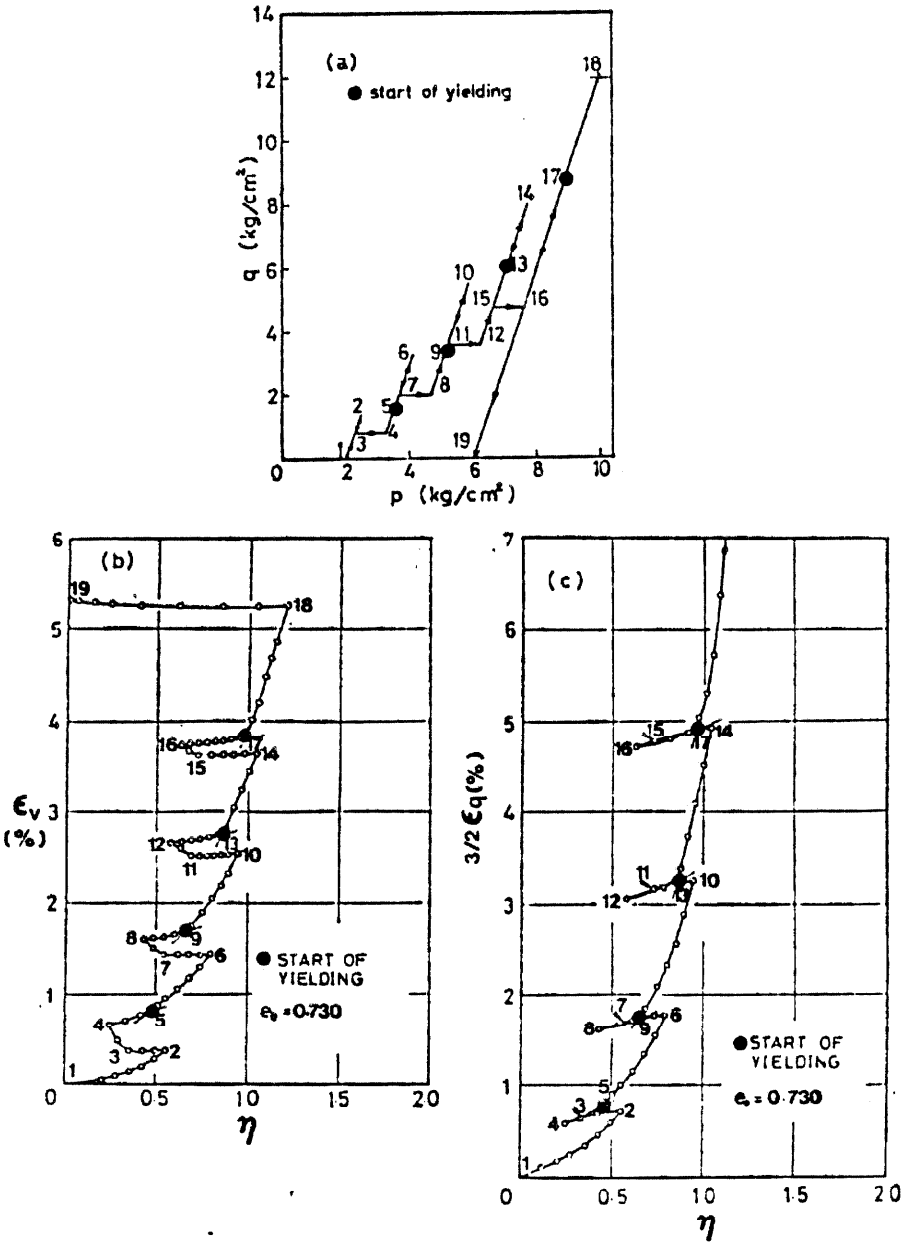

Fig. A.2. Second experiment by Tatsuoka and Ishihara on the loose Fuji River sand

a) stress path followed during the test
b) measured volumetric strain versus q/p
c) measured deviatoric strain versus q/p.

points 2 and 5 of Fig. A.3a belong to the same surface, since they are connected by a stress path in the elastic domain (namely, 2,3,4,5). Each of these points is represented by the coordinates: p_A, η_A and p_B, η_B.

With a trial and error approach, Tatsuoka and Ishihara plotted the following quantities (see Fig. A.3).

$$(\eta_B - \eta_A) \,/\, (p_B - p_A) \qquad \text{versus} \qquad (p_A + p_B)/2$$

If the yield points were close enough, the following quantities respectively represent limits:

$$d\eta \,/\, dp \quad \text{and} \quad p$$

Then the relationship established in Fig. A.3 can be expressed as:

$$d\eta/dp = f(p) \tag{A.1}$$

where f(p) is an analytical function, which describes the curve of Fig. A.3. By arbitrarily setting reference stresses p_0 and η_0, the relation (1) yields by integration the yield surface equation

$$\eta - \eta_0 = \int_{p_0}^{p} f(p)dp \tag{A.2}$$

The results obtained from relation A.2 are compared with the experimental data in Fig. A.4.

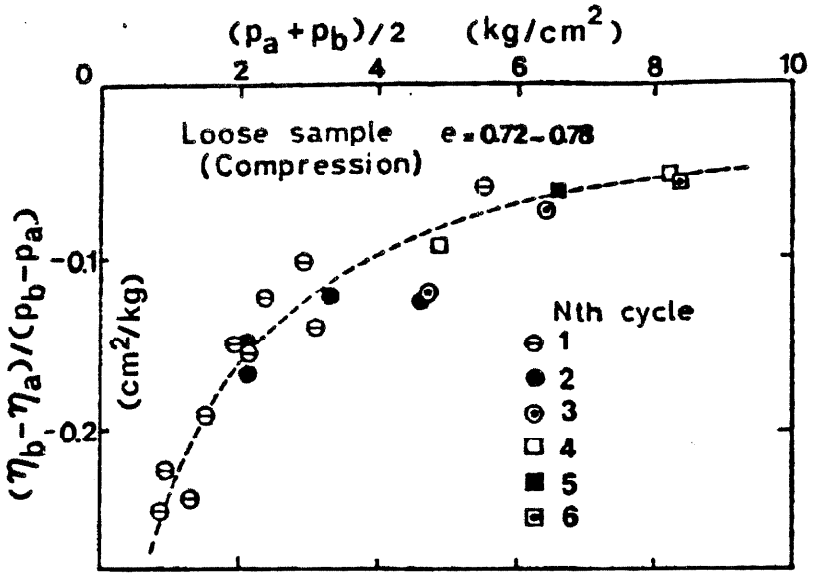

Fig. A.3. Yield characteristic of the loose Fuji River sand.

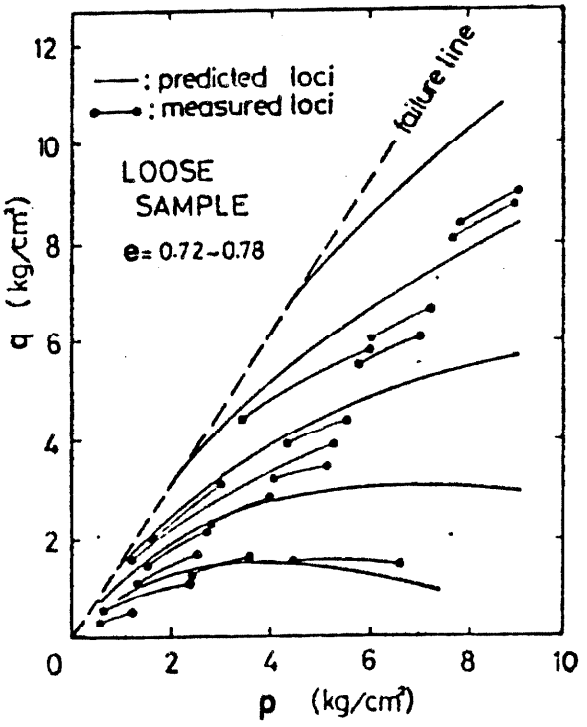

Fig. A.4. Predicted yield loci as compared with measured loci.

APPENDIX B

DRUCKER's POSTULATE

Consider a material element, which is in a certain initial state of stress σ^o. An external agency applies additional stresses to this element and then removes them. It is assumed that the changes are slow enough for the process to be isothermal. Drucker's postulate may be enunciated in the following way:

(i) During loading the additional stresses do positive work.

(ii) During the complete cycle of additional loading and unloading the additional stresses do positive work if plastic strains are produced.

Figure B.1 shows a schematic representation in stress space of the cycle of loading and unloading imposed by the external agency. Consider a loading path with the following stress steps: σ^o, σ and $\sigma + d\sigma$. From the stress σ, the infinitesimal added stress $d\sigma$ produces the corresponding elastic strain $d\varepsilon^e$ and the plastic strain $d\varepsilon^p$. The stress returns from $\sigma + d\sigma$ to σ^o by an arbitrary path. According to Drucker's postulate (ii), the work done by the additional stresses during the complete cycle is positive, i.e.,

$$\int_{\text{cycle}} (\tau_{ij} - \sigma^o_{ij}) d\varepsilon_{ij} > 0 \qquad \text{(sum on } i,j=1,2,3) \qquad \text{(B.1)}$$

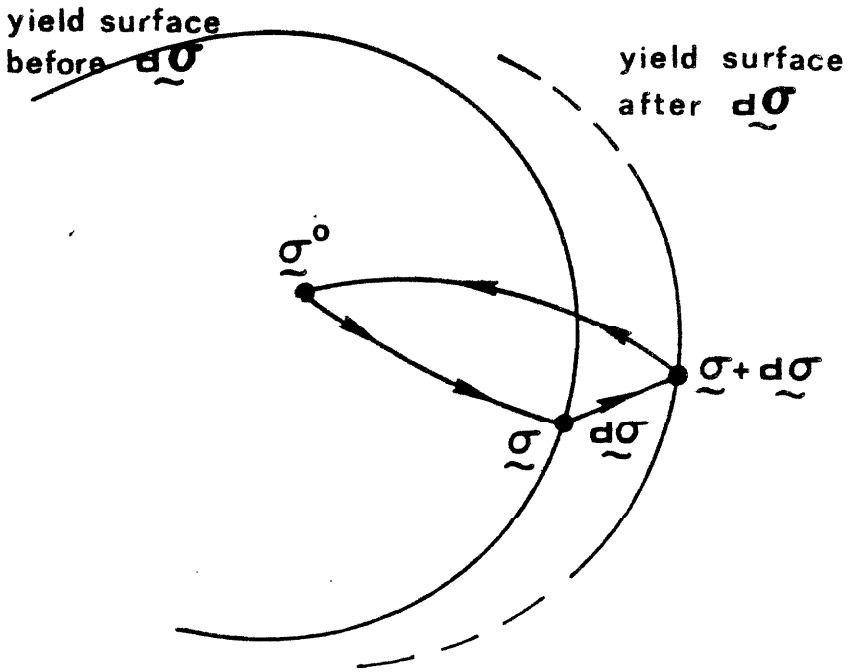

Fig. B.1. Cycle of loading-unloading for Drucker's postulate.

where τ_{ij}'s represent the variable stresses during the cycle.

For the closed path, the work done by the additional stresses and the elastic strains is zero, hence

$$\int_{\text{cycle}} (\tau_{ij} - \sigma^{o}_{ij}) d\varepsilon^{e}_{ij} = 0 \qquad \text{(sum on i,j=1,2,3)} \qquad \text{(B.2)}$$

But since strains are the sum of elastic and plastic strains from (B.1), it is concluded that

$$\int_{\text{cycle}} (\tau_{ij} - \sigma^{o}_{ij}) d\varepsilon^{p}_{ij} > 0 \qquad \text{(sum on i,j=1,2,3)} \qquad \text{(B.3)}$$

Plastic deformation takes place only in the infinitesimal part $\mathfrak{q}\ \mathfrak{a} + d\mathfrak{a}$. The following equality holds

$$\int_{\text{cycle}} (\tau_{ij} - \sigma^{o}_{ij}) d\varepsilon^{p}_{ij} = \int_{\mathfrak{q}}^{\mathfrak{a}+d\mathfrak{a}} (\tau_{ij} - \sigma^{o}_{ij}) d\varepsilon^{p}_{ij} \qquad \text{(B.4)}$$

$$\text{(sum on i,j = 1,2,3)}$$

Applying the mean value theorem, and assuming that $d\sigma_{ij}$ is small compared to σ_{ij} for any i,j, then relations (B.3) and (B.4) yield

$$(\sigma_{ij} - \sigma^{o}_{ij}) d\varepsilon^{p}_{ij} > 0 \quad \text{(sum on i,j = 1,2,3)} \qquad \text{(B.5)}$$

Consider now another cycle, where $\mathfrak{q}^{o}$ is equal to $\mathfrak{q}$. By virtue of the Drucker's postulate (i) for the loading process $\mathfrak{q}$ to $\mathfrak{q} + d\mathfrak{q}$, relation (B.4) becomes

$$d\sigma_{ij} \cdot d\varepsilon_{ij} > 0 \quad (\text{sum on } i,j = 1,2,3) \tag{B.6}$$

From the second part of the postulate, for the following cycle $\underline{\sigma}$ to $\underline{\sigma} + d\underline{\sigma}$ back to $\underline{\sigma}$, relation (B.6) becomes

$$d\sigma_{ij} \cdot d\varepsilon_{ij}^{(+)} + d\sigma_{ij} d\varepsilon_{ij}^{(-)} > 0 \quad (\text{sum on } i,j = 1,2,3) \tag{B.7}$$

when $d\underline{\varepsilon}^{(+)}$, $d\underline{\varepsilon}^{(-)}$ correspond respectively to $d\underline{\sigma}$ and $-d\underline{\sigma}$; but using relation (B.2) it follows that

$$d\sigma_{ij} \cdot d\varepsilon_{ij}^{e(+)} + d\sigma_{ij} \cdot d\varepsilon_{ij}^{e(-)} = 0 \quad (\text{sum on } i,j = 1,2,3) \tag{B.8}$$

Therefore it is concluded that

$$d\sigma_{ij} \cdot d\varepsilon_{ij}^{p} > 0 \quad (\text{sum on } i,j = 1,2,3) \tag{B.9}$$

APPENDIX C

LIST OF SYMBOLS

The symbols are ordered in the following groups.

C.1. Kinematics

C.2. Kinetics

C.3. Elastic–plastic models

C.4. Elastic model

C.5. von Mises' model

C.6. Lade's model

C.7. New sand model.

Each symbol is related to the section where it is first introduced. Some quantities related to kinematics or kinetics and starting with the letter "d" are not defined in the list of symbols: they refer to an increment of the quantities defined without a "d", e.g., $d\varepsilon_v$ is the increment of volumetric strain ε_v.

C.1. Kinematics

NOTATION	MEANING	SECTION
$\underline{x}, x_i$ (i=1,2,3)	position of a material particle	2.1
$\underline{u}, u_i$ (i=1,2,3)	displacement of a particle	2.1
$u_{i,j}$ (i,j=1,2,3)	displacement gradient $\frac{\partial u_i}{\partial x_j}$	2.1
$\bar{u}_{i,j}$ (i,j=1,2,3)	average displacement gradient	2.1
V	volume	2.1
$\underline{\varepsilon}, \varepsilon_{ij}$ (i,j=1,2,3)	infinitesimal strain tensor	2.2
$\varepsilon_1, \varepsilon_2, \varepsilon_3$	principal strains	2.2
$\varepsilon_v, \varepsilon_q$	volumetric and deviatoric strain	2.2
$\varepsilon, \varepsilon^e, \varepsilon^p$	total, elastic and plastic uniaxial strain	3.1
$\underline{\varepsilon}^e, \varepsilon^e_{ij}$ (i,j=1,2,3)	elastic strain tensor	3.2
$\underline{\varepsilon}^p, \varepsilon^p_{ij}$ (i,j=1,2,3)	plastic strain tensor	3.2
$\varepsilon^e_v, \varepsilon^p_v$	elastic and plastic volumetric strain	3.3
$\varepsilon^e_q, \varepsilon^p_q$	elastic and plastic deviatoric strain	3.3
θ_ε	direction of plastic strain increment	3.5.3
e, e_o	void ratio and initial void ratio	5.3.1, 5.4.1
e^e, e^p	elastic and plastic void ratio	5.4.1
$\|\|d\underline{\varepsilon}\|\|$	norm of $d\underline{\varepsilon}$	3.2
$\|\|d\underline{\varepsilon}^p\|\|$	norm of $d\underline{\varepsilon}^p$	3.2.2

C.2. Kinetics

NOTATION	MEANING	SECTION
$\underline{\tau}, \tau_{ij}$ (i,j=1,2,3)	Cauchy stress tensor	B
$\underline{\sigma}, \sigma_{ij}$ (i,j=1,2,3)	Cauchy stress tensor	2.3
$\bar{\underline{\sigma}}, \bar{\sigma}_{ij}$ (i,j=1,2,3)	stress tensor at image point	4.2
$\underline{\sigma}^0, \sigma^0_{ij}$ (i,j=1,2,3)	initial stress	B
s_{ij} (i,j=1,2,3)	deviatoric stress tensor	3.2.1
p,q	mean pressure and deviatoric stress	2.3
σ^*	yield stress	4.1
η, η_o	η = q/p and its initial value	5.3.3
I,J,S	first, second and third stress invariant	3.4.1
θ	Lode's angle	3.4.1
$\bar{I}, \bar{J}, \bar{S}$	first, second and third stress invariant at image point	5.8.2
$\bar{\theta}$	Lode's angle at image point	5.8.2
W	work	2.3
W^p	plastic work	3.3
$\underline{t}(\underline{n},t)$	traction vector	2.1
θ_σ	direction of stress increment in p-q space	3.5.3
$\sigma_1, \sigma_2, \sigma_3$	principal stress	2.3
u	pore pressure	5.7

C.3. Elastic-plastic Models

NOTATION	MEANING	SECTION
$\underline{n}, n_{ij}$ (i,j=1,2,3)	unit vector to yield or bounding surface	3.2.1
$\underline{m}, m_{ij}$ (i,j=1,2,3)	unit vector to plastic potential surface	3.2.2
$f(\underline{\sigma},\underline{n}) = 0$	yield surface equation	3.2.1
$\underline{r}, r_i$ (i=1,n)	parameters of yield surface	3.2.1
$\underline{s}, s_i$ (i=1,m)	parameters of potential surface	3.2.2
$g(\underline{\sigma},\underline{s})$	plastic potential function	3.2.2
H	plastic modulus	3.2.3
$H_e(x)$	Heaviside's function	3.2.3
$\langle\ \rangle$	Macaulay's function	3.2.3
$f^*(p,q,\underline{r}) = 0$	yield surface in the p-q space	3.3
n_p, n_q	unit vector to yield or bounding surface in p-q space	3.3
m_p, m_q	unit vector to plastic potential surface in p-q space	3.3
ζ	scalar	3.3
S	slope in uniaxial test	4.1
S_B	slope of bound in uniaxial test	4.1
$f(\bar{\underline{\sigma}},\underline{\varepsilon}^p) = 0$	bounding surface equation	4.2
δ	distance between stress state and image point	4.2

C.3. Continued

NOTATION	MEANING	SECTION
δ_{min}	minimum distance δ	4.2
δ_{ij} (i,j=1,2,3)	Kronecker symbol	3.1
x	scalar	4.2
H*	plastic modulus in p-q space	3.3
H_B	plastic modulus on bounding surface	4.2

C.4. Elastic Models

NOTATION	MEANING	SECTION
ν, ν_o	Poisson's ratio	3.53, 5.2
B	bulk modulus	3.5.3
G	shear modulus	3.5.3
E	Young's modulus	5.2
λ	Lame's constant	5.2
B_o	elastic model constant	5.2
n		5.2

C.5. von Mises' Model

NOTATION	MEANING	SECTION
α_{ij} (i,j=1,2,3)	center of yield surface	3.2.1
k	model parameter	3.2.1
q_c	yield stress in compression	3.2.1
q_t	yield stress in tension	3.2.1
R	yield surface radius	3.2.1

C.6. Lade's Model

NOTATION	MEANING	SECTION
I_3	third stress increment	3.2.1
χ	yield surface parameter	3.2.1
K_2	potential surface parameter	3.2.2
ξ		3.2.2
A	material constant	3.2.2
f_t		3.2.3
a		3.2.3
d		3.2.3
r_f		3.2.3
K_1		3.2.1
M		3.2.3
ℓ		3.2.3

C.7. New Sand Model

NOTATION	MEANING	SECTION
M_c, M_e	slope of critical state for positive and negative q	5.3.1
M^*_c, M^*_c	slope of characteristic state for positive and negative q	5.3.2
Γ, Γ_p	critical state parameters	5.3.1, 5.4
λ, λ_p	critial state parameters	5.3.1, 5.4
ϕ_μ	interparticle friction angle	5.3.3.a
μ	scalar	5.3.3.b
A	size of bounding surface	5.3.4
α	slope of bounding surface	5.3.4
y	scalar	5.3.4
z	$z = \frac{q}{Mp}$	5.3.4
ρ	aspect ratio for bounding surface	5.3.4
M	slope of critical state	5.3.4
h	scalar	5.3.4
$h(\delta)$	$H = H_B + h(\delta)$	5.5.2
$\bar{H}_B$	normalized plastic modulus on bounding surface	5.5.2
$\bar{H}$		5.5.2
$\bar{\delta}$	normalized distance	5.5.2
$\bar{\delta}_{max}$	normalized maximum distance	5.5.2
$\bar{\delta}_{min}$	normalized minimum distance	5.5.2

C.7. Continued

NOTATION	MEANING	SECTION
$a(\eta)$	function of η for relation between H, H_B, δ	5.5.2
η_p	model constant	5.5.2
a_o, a_1		5.5.2
$b(\bar{\delta})$	function of $\bar{\delta}$ for relation between H, H_B, δ	5.5.2
b_1, b_2	model constants	5.5.2
$g(\theta,\beta)$	function of Lode's angle θ and β	5.8.1
β	model constant $\beta = M_e/M_c$	5.8.1
N, N_p	model constants	5.8.2

CALIFORNIA INSTITUTE OF TECHNOLOGY

Reports Published

by

Earthquake Engineering Research Laboratory*
Dynamics Laboratory
Disaster Research Center

Note: Numbers in parenthesis are Accession Numbers assigned by the National Technical Information Service; these reports may be ordered from the National Technical Information Service, 5285 Port Royal Road, Springfield, Virginia, 22161. Accession numbers should be quoted on orders for reports (PB --- ---). Reports without this information either have not been submitted to NTIS or the information was not available at the time of printing. An N/A in parenthesis indicates that the report is no longer available at Caltech.

1. Alford, J.L., G.W. Housner and R.R. Martel, "Spectrum Analysis of Strong-Motion Earthquakes," 1951. (Revised August 1964). (N/A)

2. Housner, G.W., "Intensity of Ground Motion During Strong Earthquakes," 1952. (N/A)

3. Hudson, D.E., J.L. Alford and G.W. Housner, "Response of a Structure to an Explosive Generated Ground Shock," 1952. (N/A)

4. Housner, G.W., "Analysis of the Taft Accelerogram of the Earthquake of 21 July 1952." (N/A)

5. Housner, G.W., "A Dislocation Theory of Earthquakes," 1953. (N/A)

6. Caughey, T.K., and D.E. Hudson, "An Electric Analog Type Response Spectrum," 1954.(N/A)

7. Hudson, D.E., and G.W. Housner, "Vibration Tests of a Steel-Frame Building," 1954. (N/A)

8. Housner, G.W., "Earthquake Pressures on Fluid Containers," 1954. (N/A)

9. Hudson, D.E., "The Wilmot Survey Type Strong-Motion Earthquake Recorder," 1958. (N/A)

10. Hudson, D.E., and W.D. Iwan, "The Wilmot Survey Type Strong-Motion Earthquake Recorder, Part II," 1960. (N/A)

---

* To order directly by phone the number is 703-487-4650.

11. Caughey, T.K., D.E. Hudson, and R.V. Powell, "The CIT Mark II Electric Analog Type Response Spectrum Analyzer for Earthquake Excitation Studies," 1960. (N/A)

12. Keightley, W.O, G.W. Housner and D.E. Hudson, "Vibration Tests of the Encino Dam Intake Tower," 1961. (N/A)

13. Merchant, Howard Carl, "Mode Superposition Methods Applied to Linear Mechanical Systems Under Earthquake Type Excitation," 1961. (N/A)

14. Iwan, Wilfred D., "The Dynamic Response of Bilinear Hysteretic Systems," 1961. (N/A)

15. Hudson, D.E., "A New Vibration Exciter for Dynamic Test of Full-Scale Structures," 1961. (N/A)

16. Hudson, D.E., "Synchronized Vibration Generators for Dynamic Tests of Full-Scale Structures," 1962. (N/A)

17. Jennings, Paul C., "Velocity Spectra of the Mexican Earthquakes of 11 May and 19 May 1962," 1962. (N/A)

18. Jennings, Paul C., "Response of Simple Yielding Structures to Earthquake Excitation," 1963. (N/A)

19. Keightley, Willard O., "Vibration Tests of Structures," 1963. (N/A)

20. Caughey, T.K. and M.E.J. O'Kelly, "General Theory of Vibration of Damped Linear Dynamic Systems," 1963. (N/A)

21. O'Kelly, M.E.J., "Vibration of Viscously Damped Linear Dynamic Systems," 1964. (N/A)

22. Nielsen, N. Norby, "Dynamic Response of Multistory Buildings," 1964. (N/A)

23. Tso, Wai Keung, "Dynamics of Thin-Walled Beams of Open Section," 1964. (N/A)

24. Keightley, Willard O., "A Dynamic Investigation of Bouquet Canyon Dam," 1964. (N/A)

25. Malhotra, R.K., "Free and Forced Oscillations of a Class of Self-Excited Oscillators," 1964.

26. Hanson, Robert D., "Post-Elastic Response of Mild Steel Structures," 1965.

27. Masri, Sami F., "Analytical and Experimental Studies of Impact Dampers," 1965.

28. Hanson, Robert D., "Static and Dynamic Tests of a Full-Scale Steel-Frame Structure," 1965.

29. Cronin, Donald L., "Response of Linear, Viscous Damped Systems to Excitations Having Time-Varying Frequency," 1965.

30. Hu, Paul Yu-fei, "Analytical and Experimental Studies of Random Vibration," 1965.

31. Crede, Charles E., "Research on Failure of Equipment when Subject to Vibration," 1965.

32. Lutes, Loren D., "Numerical Response Characteristics of a Uniform Beam Carrying One Discrete Load," 1965. (N/A)

33. Rocke, Richard D., "Transmission Matrices and Lumped Parameter Models for Continuous Systems," 1966. (N/A)

34. Brady, Arthur Gerald, "Studies of Response to Earthquake Ground Motion," 1966. (N/A)

35. Atkinson, John D., "Spectral Density of First Order Piecewise Linear Systems Excited by White Noise," 1967. (N/A)

36. Dickerson, John R., "Stability of Parametrically Excited Differential Equations," 1967. (N/A)

37. Giberson, Melbourne F., "The Response of Nonlinear Multi-Story Structures Subjected to Earthquake Excitation," 1967. (N/A)

38. Hallanger, Lawrence W., "The Dynamic Stability of an Unbalanced Mass Exciter," 1967.

39. Husid, Raul, "Gravity Effects on the Earthquake Response of Yielding Structures," 1967. (N/A)

40. Kuroiwa, Julio H., "Vibration Test of a Multistory Building," 1967. (N/A)

41. Lutes, Loren Daniel, "Stationary Random Response of Bilinear Hysteretic Systems," 1967.

42. Nigam, Navin C., "Inelastic Interactions in the Dynamic Response of Structures," 1967.

43. Nigam, Navin C. and Paul C. Jennings, "Digital Calculation of Response Spectra from Strong-Motion Earthquake Records," 1968.

44. Spencer, Richard A., "The Nonlinear Response of Some Multistory Reinforced and Prestressed Concrete Structures Subjected to Earthquake Excitation," 1968. (N/A)

45. Jennings, P.C., G.W. Housner and N.C. Tsai, "Simulated Earthquake Motions," 1968.

46. "Strong-Motion Instrumental Data on the Borrego Mountain Earthquake of 9 April 1968," (USGS and EERL Joint Report), 1968.

47. Peters, Rex B., "Strong Motion Accelerograph Evaluation," 1969.

48. Heitner, Kenneth L., "A Mathematical Model for Calculation of the Run-Up of Tsunamis," 1969.

49. Trifunac, Mihailo D., "Investigation of Strong Earthquake Ground Motion," 1969. (N/A)

50. Tsai, Nien Chien, "Influence of Local Geology on Earthquake Ground Motion," 1969. (N/A)

51. Trifunac, Mihailo D., "Wind and Microtremor Induced Vibrations of a Twenty-Two Steel Frame Building," EERL 70-01, 1970.

52. Yang, I-Min, "Stationary Random Response of Multidegree-of-Freedom Systems," DYNL-100, June 1970. (N/A)

53. Patula, Edward John, "Equivalent Differential Equations for Nonlinear Dynamical Systems," DYNL-101, June 1970.

54. Prelewicz, Daniel Adam, "Range of Validity of the Method of Averaging," DYNL-102, 1970.

55. Trifunac, M.D., "On the Statistics and Possible Triggering Mechanism of Earthquakes in Southern California," EERL 70-03, July 1970.

56. Heitner, Kenneth Leon, "Additional Investigations on a Mathematical Model for Calculation of the Run-Up of Tsunamis," July 1970.

57. Trifunac, Mihailo D., "Ambient Vibration Tests of a Thirty-Nine Story Steel Frame Building," EERL 70-02, July 1970.

58. Trifunac, Mihailo and D.E. Hudson, "Laboratory Evaluations and Instrument Corrections of Strong-Motion Accelerographs," EERL 70-04, August 1970. (N/A)

59. Trifunac, Mihailo D., "Response Envelope Spectrum and Interpretation of Strong Earthquake Ground Motion," EERL 70-06, August 1970.

60. Keightley, W.O., "A Strong-Motion Accelerograph Array with Telephone Line Interconnections," EERL 70-05, September 1970.

61. Trifunac, Mihailo D., "Low Frequency Digitization Errors and a New Method for Zero Baseline Correction of Strong-Motion Accelerograms," EERL 70-07, September 1970.

62. Vijayaraghavan, A., "Free and Forced Oscillations in a Class of Piecewise-Linear Dynamic Systems," DYNL-103, January 1971.

63. Jennings, Paul C., R.B. Matthiesen and J. Brent Hoerner, "Forced Vibrations of a 22-Story Steel Frame Building," EERL 71-01, February 1971. (N/A) (PB 205 161)

64. Jennings, Paul C., "Engineering Features of the San Fernando Earthquake of February 9, 1971," EERL 71-02, June 1971. (PB 202 550)

65. Bielak, Jacobo, "Earthquake Response of Building-Foundation Systems," EERL 71-04, June 1971. (N/A) (PB 205 305)

66. Adu, Randolph Ademola, "Response and Failure of Structures under Stationary Random Excitation," EERL 71-03, June 1971. (N/A) (PB 205 304)

67. Skattum, Knut Sverre, "Dynamic Analysis of Coupled Shear Walls and Sandwich Beams," EERL 71-06, June 1971. (N/A) (PB 205 267)

68. Hoerner, John Brent, "Modal Coupling and Earthquake Response of Tall Buildings," EERL 71-07, June 1971. (N/A) (PB 207 635)

69. Stahl, Karl John, "Dynamic Response of Circular Plates Subjected to Moving Massive Loads," DYNL-104, June 1971. (N/A)

70. Trifunac, M.D., F.E. Udwadia and A.G. Brady, "High Frequency Errors and Instrument Corrections of Strong-Motion Accelerograms," EERL 71-05, 1971. (PB 205 369)

71. Furuike, D.M., "Dynamic Response of Hysteretic Systems with Application to a System Containing Limited Slip," DYNL-105, September 1971. (N/A)

72. Hudson, D.E. (Editor), "Strong-Motion Instrumental Data on the San Fernando Earthquake of February 9, 1971," (Seismological Field Survey, NOAA, C.I.T. Joint Report), September 1971. (PB 204 198)

73. Jennings, Paul C. and Jacobo Bielak, "Dynamics of Building-Soil Interaction," EERL 72-01, April 1972. (PB 209 666)

74. Kim, Byung-Koo, "Piecewise Linear Dynamic Systems with Time Delays," DYNL-106, April 1972.

75. Viano, David Charles, "Wave Propagation in a Symmetrically Layered Elastic Plate," DYNL-107, May 1972.

76. Whitney, Albert W., "On Insurance Settlements Incident to the 1906 San Francisco Fire," DRC 72-01, August 1972. (PB 213 256)

77. Udwadia, F.E., "Investigation of Earthquake and Microtremor Ground Motions," EERL 72-02, September 1972. (PB 212 853)

78. Wood, John H., "Analysis of the Earthquake Response of a Nine-Story Steel Frame Building During the San Fernando Earthquake," EERL 72-04, October 1972. (PB 215 823)

79. Jennings, Paul C., "Rapid Calculation of Selected Fourier Spectrum Ordinates," EERL 72-05, November 1972.

80. "Research Papers Submitted to Fifth World Conference on Earthquake Engineering, Rome, Italy, 25-29 June 1973," EERL 73-02, March 1973. (PB 220 431)

81. Udwadia, F.E. and M.D. Trifunac, "The Fourier Transform, Response Spectra and Their Relationship Through the Statistics of Oscillator Response," EERL 73-01, April 1973. (PB 220 458)

82. Housner, George W., "Earthquake-Resistant Design of High-Rise Buildings," DRC 73-01, July 1973. (N/A)

83. "Earthquakes and Insurance," Earthquake Research Affiliates Conference, 2-3 April, 1973, DRC 73-02, July 1973. (PB 223 033)

84. Wood, John H., "Earthquake-Induced Soil Pressures on Structures," EERL 73-05, August 1973. (N/A)

85. Crouse, Charles B., "Engineering Studies of the San Fernando Earthquake," EERL 73-04, March 1973. (N/A)

86. Irvine, H. Max, "The Veracruz Earthquake of 28 August 1973," EERL 73-06, October 1973.

87. Iemura, H. and P.C. Jennings, "Hysteretic Response of a Nine-Story Reinforced Concrete Building During the San Fernando Earthquake," EERL 73-07, October 1973.

88. Trifunac, M.D. and V. Lee, "Routine Computer Processing of Strong-Motion Accelerograms," EERL 73-03, October 1973. (N/A) (PB 226 047/AS)

89. Moeller, Thomas Lee, "The Dynamics of a Spinning Elastic Disk with Massive Load," DYNL 73-01, October 1973.

90. Blevins, Robert D., "Flow Induced Vibration of Bluff Structures," DYNL 74-01, February 1974.

91. Irvine, H. Max, "Studies in the Statics and Dynamics of Simple Cable Systems," DYNL-108, January 1974.

92. Jephcott, D.K. and D.E. Hudson, "The Performance of Public School Plants During the San Fernando Earthquake," EERL 74-01, September 1974. (PB 240 000/AS)

93. Wong, Hung Leung, "Dynamic Soil-Structure Interaction," EERL 75-01, May 1975. (N/A) (PB 247 233/AS)

94. Foutch, D.A., G.W. Housner, P.C. Jennings, "Dynamic Responses of Six Multistory Buildings During the San Fernando Earthquake," EERL 75-02, October 1975. (PB 248 144/AS)

95. Miller, Richard Keith, "The Steady-State Response of Multidegree-of-Freedom Systems with a Spatially Localized Nonlinearity," EERL 75-03, October 1975. (PB 252 459/AS)

96. Abdel-Ghaffar, Ahmed Mansour, "Dynamic Analyses of Suspension Bridge Structures," EERL 76-01, May 1976. (PB 258 744/AS)

97. Foutch, Douglas A., "A Study of the Vibrational Characteristics of Two Multistory Buildings," EERL 76-03, September 1976. (PB 260 874/AS)

98. "Strong Motion Earthquake Accelerograms Index Volume," Earthquake Engineering Research Laboratory, EERL 76-02, August 1976. (PB 260 929/AS)

99. Spanos, P-T.D., "Linearization Techniques for Non-Linear Dynamical Systems," EERL 76-04, September 1976. (PB 266 083/AS)

100. Edwards, Dean Barton, "Time Domain Analysis of Switching Regulators," DYNL 77-01, March 1977.

101. Abdel-Ghaffar, Ahmed Mansour, "Studies on the Effect of Differential Motions of Two Foundations upon the Response of the Superstructure of a Bridge," EERL 77-02, January 1977. (PB 271 095/AS)

102. Gates, Nathan C., "The Earthquake Response of Deteriorating Systems," EERL 77-03, March 1977. (PB 271 090/AS)

103. Daly, W., W. Judd and R. Meade, "Evaluation of Seismicity at U.S. Reservoirs," USCOLD, Committee on Earthquakes, May 1977. (PB 270 036/AS)

104. Abdel-Ghaffar, A.M. and G.W. Housner, "An Analysis of the Dynamic Characteristics of a Suspension Bridge by Ambient Vibration Measurements," EERL 77-01, January 1977. (PB 275 063/AS)

105. Housner, G.W. and P.C. Jennings, "Earthquake Design Criteria for Structures," EERL 77-06, November 1977. (PB 276 502/AS)

106. Morrison, P., R. Maley, G. Brady, R. Porcella, "Earthquake Recordings on or Near Dams," USCOLD, Committee on Earthquakes, November 1977. (PB 285 867/AS)

107. Abdel-Ghaffar, A.M., "Engineering Data and Analyses of the Whittier, California Earthquake of January 1, 1976," EERL 77-05, November 1977. (PB 283 750/AS)

108. Beck, James L., "Determining Models of Structures from Earthquake Records," EERL 78-01, June 1978. (PB 288 806/AS)

109. Psycharis, Ioannis, "The Salonica (Thessaloniki) Earthquake of June 20, 1978," EERL 78-03, October 1978. (PB 290 120/AS)

110. Abdel-Ghaffar, A.M. and R.F. Scott, "An Investigation of the Dynamic Characteristics of an Earth Dam," EERL 78-02, August 1978. (PB 288 878/AS)

111. Mason, Alfred B., Jr., "Some Observations on the Random Response of Linear and Nonlinear Dynamical Systems," EERL 79-01, January 1979. (PB 290 808/AS)

112. Heimberger, D.V. and P.C. Jennings (Organizers), "Strong Ground Motion: N.S.F. Seminar-Workshop," SL-EERL 79-02, February 1978.

113. Lee, David M., Paul C. Jennings and George W. Housner, "A Selection of Important Strong Motion Earthquake Records," EERL 80-01, January 1980. (PB 80 169196)

114. McVerry, Graeme H., "Frequency Domain Identification of Structural Models from Earthquake Records," EERL 79-02, October 1979.

115. Abdel-Ghaffar, A.M., R.F. Scott and M.J. Craig, "Full-Scale Experimental Investigation of a Modern Earth Dam," EERL 80-02, February 1980.

116. Rutenberg, Avigdor, Paul C. Jennings and George W. Housner, "The Response of Veterans Hospital Building 41 in the San Fernando Earthquake," EERL 80-03, May 1980.

117. Haroun, Medhat Ahmed, "Dynamic Analyses of Liquid Storage Tanks," EERL 80-04, February 1980.

118. Liu, Wing Kam, "Development of Finite Element Procedures for Fluid-Structure Interaction," EERL 80-06, August 1980. (PB 184078)

119. Yoder, Paul Jerome, "A Strain-Space Plasticity Theory and Numerical Implementation," EERL 80-07, August 1980.

120. Krousgrill, Charles Morton, Jr., "A Linearization Technique for the Dynamic Respone of Nonlinear Continua," EERL 80-08, September 1980.

121. Cohen, Martin, "Silent Boundary Methods for Transient Wave Analysis," EERL 80-09, September 1980.

122. Hall, Shawn A., "Vortex-Induced Vibrations of Structures," EERL 81-01, January 1981, PB-

123. Psycharis, Ioannis N., "Dynamic Behavior of Rocking Structures Allowed to Uplift," EERL 81-02, August 1981, PB-

124. Shih, Choon-Foo, "Failure of Liquid Storage Tanks Due to Earthquake Excitation," EERL 81-04, May 1981, PB-

125. Lin, Albert Niu, "Experimental Observations of the Effect of Foundation Embedment on Structural Response," EERL 82-01, May 1982, PB-

126. Botelho, Dirceau L.R., "An Empirical Model for Vortex-Induced Vibrations," EERL 82-02, August 1982, PB-

127. Ortiz, L. Alexander, "Dynamic Centrifuge Testing of Cantilever Retaining Walls," SML 82-02, August 1982, PB-

128. Iwan, W.D., Editor, "Proceedings of the U.S. National Workshop on Strong-Motion Earthquake Instrumentation, April 12-14, 1981, Santa Barbara, California," California Institute of Technology, Pasadena, California, 1981.

129. Rashed, Ahmed, "Dynamic Analysis of Fluid-Structure Systems," EERL 82-03, July 1982, PB-

130. National Academy Press, "Earthquake Engineering Research-1982."

131. National Academy Press, "Earthquake Engineering Research-1982, Overview and Recommendations."

132. Jain, Sudhir Kumar, "Analytical Models for the Dynamics of Buildings," EERL 83-02, May 1983, PB-